

SIMULATION OF THE INDIVIDUAL CARDIOVASCULAR SYSTEM

- A PILOT STUDY -

by

Rune Aaslid



UNIVERSITETET I TRONDHEIM
NORGES TEKNISKE HØGSKOLE
INSTITUTT FOR TEKNISK KYBERNETIKK

THE UNIVERSITY OF TRONDHEIM
THE NORWEGIAN INSTITUTE OF TECHNOLOGY
Division of Engineering Cybernetics

TRONDHEIM, NORWAY

May 1974

*Il faudra donc toujours, apres avoir
practiquē l'analyse des phenomenes,
refraire la synthese physiologique,
afin de voir l'action rēunie de
toutes les parties que l'on avait
isolēes.*

Claude Bernard 1865

To my parents

P R E F A C E

The study presented in this report was mainly carried out together with Alf O. Brubakk, M.D. from the Section of Cardiology, The Regional Hospital in Trondheim. The intention was to develop a realistic model of the circulation and to use it in the clinical situation. I was then attached to the Division of Engineering Cybernetics at The University of Trondheim. During the years 1970 - 1972 the model and the estimator were developed there.

From 1973 I have been attached to the Department of Surgical Research at Rikshospitalet, Oslo, continuing the work on this project.

The clinical data presented in this study came from the Surgical Department A, Rikshospitalet, Oslo and from the Section of Cardiology at the Regional Hospital, Trondheim.

Oslo, May 4, 1974

Rune Aaslid

A C K N O W L E D G E M E N T S

During the course of this investigation I have received support, advise and assistance from many sources. I hereby express my sincere gratitude to:

Dr. Alf O. Brubakk for his eager interest and close cooperation.

Professor Jens G. Balchen at the Division of Engineering Cybernetics, Trondheim, for his advise and support, particularly during the first phase of the project. I am also grateful for the opportunity to study and work in his stimulating atmosphere.

Professor Egil Amundsen at the Department of Surgical Research, Oslo. His support has been a valuable contribution to the continuation of this project. I have also been given very good working facilities at his department.

Associate professor Lars Walløe, University of Oslo, for wise guidance during this study and for helpful criticism of the manuscript.

The team of Surgical Department A, Rikshospitalet, for the cooperation and for the essential data they provided.

Dr. Jarle Holen, Oslo, for the stimulating discussions on various aspects of arterial hemodynamics.

Dr. R.D. Bradley of St. Thomas Hospital, London for his hospitality and for the opportunity to use his recorded material.

Mrs. Ingrid Pettersen for expertly typing the entire manuscript and Mr. Kåre Pettersen for his skilful layout.

Mr. Martin Riha, Håkon Solum, Erik Gjelstad, Øyvind Teig, Hans Bakken and Øivind Ellingsen for technical assistance in building the model.

The University of Trondheim, The Norwegian Council of Cardiovascular Diseases, The Royal Norwegian Council for Scientific and Industrial Research, SINTEF and AUTRONICA A/S for financial support.

Last, but not least, I thank Forenede Liv A/S who generously donated the means necessary to construct a clinically useful version of the model.

C O N T E N T S

	Page
PREFACE	V
ACKNOWLEDGEMENTS	VII
ABSTRACT	XI
Chapter 1. INTRODUCTION	1
Models reported in the literature	1
Outline of the present study	4
Chapter 2. THE LEFT VENTRICULAR MODEL	7
Introduction	7
The fibre length - volume relation	9
The shape factor	11
The muscle model	16
Ultrastructural basis of heart muscle and choice of model structure	17
The external series elastic element	19
The "intrasarcomere" series elastic element	20
The contractile element (CE) force-velocity relation	23
CE maximum velocity	24
Sarcomere tension-length relation	26
Tension active state	29
Duration of active state	30
Resting value of active state	31
The parallel elastic element PE	31
Block diagram of the muscle fibre model	32
Chapter 3. THE ARTERIAL MODEL	36
Introduction	36
Pressure and flow pulses in the ascending aorta and the femoral artery	36
Mathematical representation of the segment	39
Inertance and resistance effects	40
Pressure-volume relation of arteries	41
Block diagram of an arterial segment	45
Electrical analogue of a vessel segment	46

	Page
Input impedance	47
The arterial tree and its representation in the model	49
The aortic and arterial segmentation	51
The aortic valve model	55
The peripheral resistance	57
Chapter 4. MODELS OF MEASUREMENT PROCESSES	59
Introduction	59
Model of the catheter-manometer system	61
Chapter 5. SIMULATION METHODS	64
Chapter 6. PARAMETER ESTIMATION	66
Introduction	66
Summary of B, C and M parameters	68
Activation synchronization	70
Estimation of left ventricular end-diastolic volume	71
Automatic estimation of parameters	74
Estimation of aortic compliance	78
Estimation of peripheral damping	80
Estimation of catheter-manometer dynamic parameters	82
Errors in the estimates	83
Chapter 7. METHODS FOR TESTING THE ABILITY OF THE MODEL TO SIMULATE THE LEFT VENTRICLE AND AORTA	90
Introduction	90
The method of "good curvefit"	90
The method of independent measurements	91
The method of perturbations (the experimental method)	91
Choice of comparison criteria	91
Chapter 8. SIMULATION OF THE LEFT VENTRICLE	92
Introduction	92
The left ventricular volume-muscle fibre length relation. Comparison with data from the dog heart	92

The response of the left ventricular model to changes in end-diastolic volume and left ventricular peak pressure. Comparison with data from the dog heart	95
Simulation of changes in the contractile properties of the dog heart	102
Simulation of the human left ventricle	105
Discussion	112
Chapter 9. SIMULATION OF THE ARTERIAL SYSTEM	119
Introduction	119
Frequency domain comparisons	119
Time domain comparisons	122
Simulation of a group of 24 patients	125
Discussion	128
Chapter 10. CONCLUSIONS AND SUMMARY	133
REFERENCES	135
APPENDIX 1. THE VENOUS SYSTEM, THE RIGHT HEART, THE PULMONARY CIRCULATION AND THE LEFT ATRIUM .	146
Introduction	146
The models of the venous system, the atria and the pulmonary circulation	146
The right ventricle model	151
APPENDIX 2. DIAGRAMS OF THE MODEL	154

ABSTRACT

A simulation model of the left ventricle and aorta is described. 6 L-C-R segments are used to describe the aortic dynamics. The arterial system beyond the aorta is represented by impedance approximations. The description of the left ventricle is based upon a muscle model representing the "average" muscle fibre, and a geometrical model relating ventricular and muscle variables. The model is realized as a special purpose analog computer.

The behaviour of the model may be changed by varying its parameters. It is possible to simulate the individual cardiovascular system if we can find a set of parameters that matches the courses of the variables in the model to the measurements. The maximum velocity, and the maximum active tension of the muscle fibre, the systolic duration, the peripheral resistance and the left ventricular filling is controlled by feedback circuits so that the mean errors over a chosen set of intervals are close to zero. The aortic compliance and the peripheral damping are adjusted manually to satisfy visual criteria.

The model is tested against data from the dog and the human heart. It is found that the influence of changes in the filling of the ventricle, and in the load against ejection are realistically represented in the model. Also the influence of changes in the inotropic state of the myocardium is simulated with good agreement. This evidence suggest that the model may be used as a tool for the analysis of cardiovascular behaviour.

The application of this model to clinical data is briefly investigated. 12 patients undergoing openheart surgery and a group of 24 patients undergoing aortic catheterization are simulated. The results of this application indicate that the model and the estimator may be useful in the clinical environment for on-line analysis of the cardiovascular state.

Chapter 1.

INTRODUCTION

The present study started out as an attempt to develop a circulatory model for clinical applications. This report should be regarded as a pilot study which is intended to give experience with the application of simulation methods in cardiovascular physiology, and to find out if the behaviour of the left ventricle and aorta may be simulated with an acceptable degree of similarity by a relatively simple model.

We may consider the model as a quantitative hypothesis of the system under study.[☆] Physiological knowledge and earlier hypotheses are included in the model, and one should always keep in mind that it is a simplified description of the real system. The model has a value in as much as its ability to represent the real system can be documented. As any other hypothesis, the simulation model needs supporting experimental evidence to be considered seriously. Although quite a few authors have reported simulation studies on the left ventricular and aortic dynamics, it was felt that a systematic comparison between observations on the real system and the results of the simulations was lacking.

Models reported in the literature

The subsequent literature review does not claim to be covering the whole field of cardiovascular modelling, as we find a recent review by Beneken (1972). The emphasis will be on left ventricular-aortic models and applications of parameter estimation in this area.

A possible way of modelling the left ventricle is to regard this chamber as a time-varying compliance (Warner 1959, Beneken 1965, Snyder & al 1968 and others). Likewise the models reported by Robinson (1965) and Grodins & Buoncristiani (1967) are based on approximations of the ventricular input-output relations. These approaches may give good results as far as the dynamic waveforms and the input-output relations are concerned, but they do not in our opinion, give as much insight into the dynamics of ventricular

[☆] The analogy between a simulation model and a hypothesis was suggested to me by dr. D. L. Franklin, La Jolla, USA.

contraction as models based on muscle mechanics.

The latter approach has been used by Beneken (1965) and later improved (Beneken & de Wit 1967) to simulate the human closed loop circulation. The present model is essentially based upon their concept, using an "average" muscle fibre to represent the entire myocardium, and a geometrical model to relate muscle variables to ventricular variables. We have, however, used a different type of muscle model and different functional relationships.

The muscle model is based upon the concept of Hill (1938) for skeletal muscle, which has been carried into heart muscle physiology by Abbot & Mommaerts (1959) and Sonnenblick (1962). Although evidence is reported against the ability of this model to represent heart muscle under quick stretch and release conditions (Noble & al 1972 and Pollack & al 1972), the model may still be used as an adequate analogue for normal contractions of a ventricle.

Dyken (1970) also used this approach in the simulation of the dog left ventricle, but his choice of contractile element velocity as input variable (instead of tension or velocity active state) can be questioned.

Recently Hanna (1973) proposed a spherical model, where the wall was divided into 10 layers, each represented by a separate muscle model. But his model was not tested against experimental data except for one example of human left ventricular pressure and flow time courses which were in good accordance with literature data. From a simulation viewpoint his model is quite complex, but his approach may be fruitful for future simulations and efforts.

Donders & al (1973) report a parameter estimation study of the left ventricle in the pig. Measurements were left ventricular pressure and volume and aortic pressure. The model was basically the same as in Beneken (1965). A reasonable agreement in the simulated time courses of pressure and volume was demonstrated. The solution was, however, not unique, and a sensitivity analysis was undertaken. Although only partially successful, the study indicated that parameter estimation may be a useful research tool in this area.

We may also mention the model proposed and used by Vadot (1963) for the analysis of valvular and septal defects. This model was,

however, of a nonpulsatile type, and probably too simple for realistic simulations.

Arterial hemodynamics has enjoyed much interest over the last years. The subject was reviewed recently by Mc Donald (1968) and Noordergraf (1969). In the present study, a detailed representation of the arterial tree is not sought, and we may therefore use a simpler representation than de Pater (1966) who divided the arteries into more than 200 segments.

Snyder & al (1968) simulated the aorta, dividing it into equal-volume segments. The present study use a model quite similar to this, but we prefer dividing the system into equal transmission time segments. Beyond the anatomical points where a representation of the pulse transmission properties is unnecessary, we have terminated the model by impedance approximations. This approach is as also used by Chang (1973).

In 1961, Spencer & al published a simple electrical analogue of the dog aorta. The input to the model was a flow signal obtained by an electromagnetic flow probe around the ascending aorta. The parameters were adjusted manually, and the simulated pressure waveforms were in reasonable agreement with the measurements.

Rothe & Nash (1968) obtained estimates of renal arterial compliance using parameter estimation techniques.

Sims (1970) estimated 13 parameters in the dog aorta from two flow and three pressure measurements. The time courses of the simulated variables were not, however, in good agreement with the measurements. Recently his work has been followed up by Chang (1973) who demonstrated a successful application of parameter estimation to the dog aorta.

Wesseling & al (1973) estimated parameters in an arm arterial model on the basis of noninvasive measurements. Parameters were adjusted manually on the bases of a display of the error criterion (integrated square error over the heart cycle).

Szücs & al (1973) estimated 8 parameters in a 4. order "black box model" of the pressure transfer characteristics of the dog aorta, using different estimation procedures.

In the aforementioned studies, the model and the methods were only sparingly applied to and compared with measurements from the cardiovascular system. As this is essential in physiology, we have placed the main emphasis of the present study on a model-reality comparison and discussion.

Outline of the present study

The pulsatile dynamics of the left ventricle and the aorta are in the main focus in this study. The model proposed in chapter 2 and 3 was developed early in this project. Some of the assumptions may seem arbitrary, and in some instances the data found in the literature was contradictory. When it was felt that a particular functional relationship, or a parameter value could not be given enough evidence in light of available data, it was given a "reasonable assumption". This approach is justified by testing the model as a whole against cardiovascular data. The new features of this model compared with previous efforts are mainly: A different and simple new method for the deduction of the relationship between left ventricular pressure and muscle fibre tension (or stress), and the assumption that the developed tension is dependent upon the muscle length instead of contractile element length.

To express the model a block diagram representation was chosen. In physiology this approach has been used extensively by Guyton (Guyton & Coleman 1967).

It was preferred to use analog computer techniques for the simulation study. Because of limited computing facilities, special purpose analog computing circuits were synthesized (figure 1.1) on the basis of block diagrams resulting in a special purpose analog computer.

The model is a closed loop description, but the venous, right heart and pulmonary sections are not tested against experimental data and are only briefly described in Appendix 1.

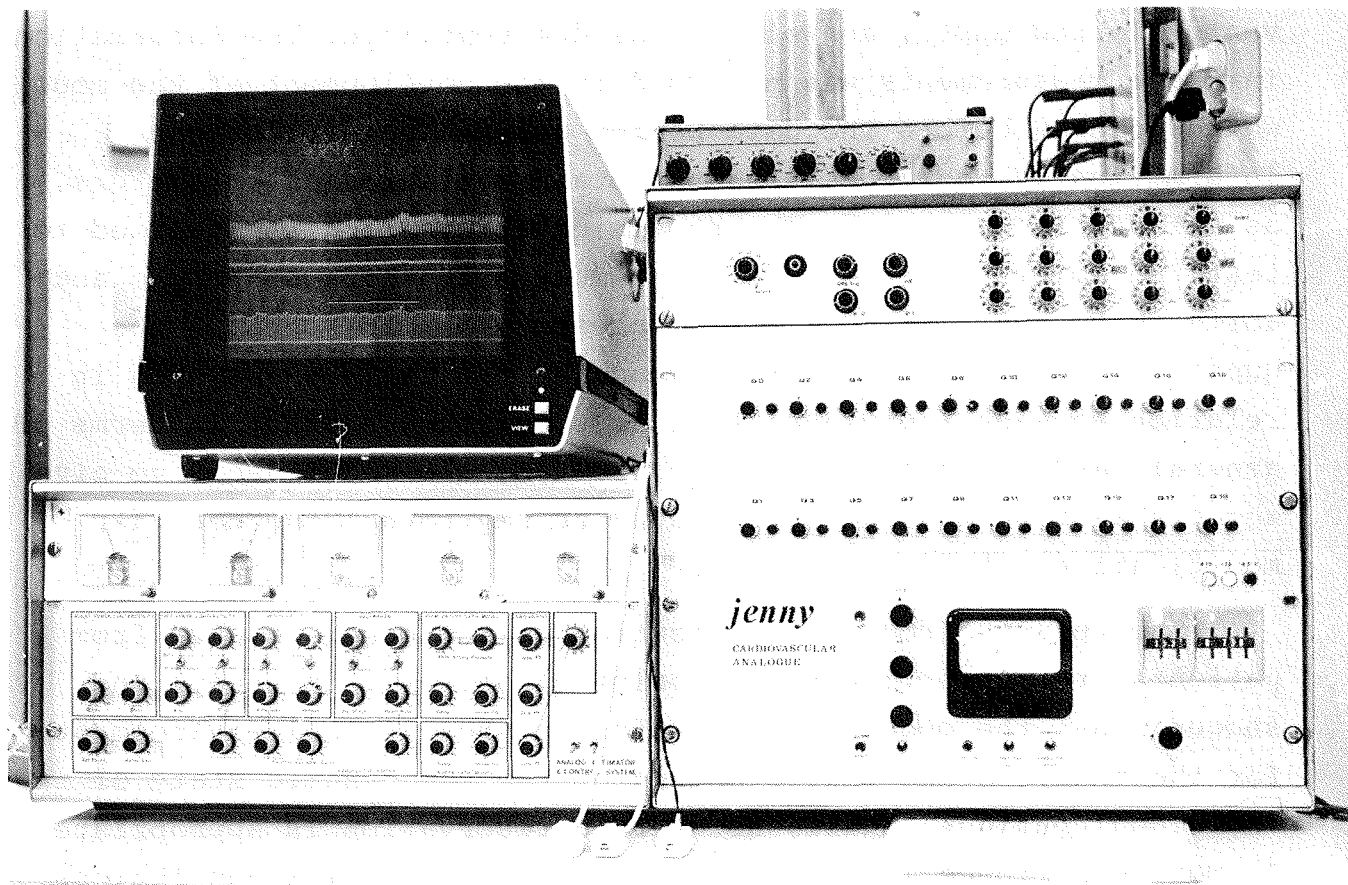


Figure 1.1. The special purpose analog computer developed for simulation of the closed-loop model.

The model contains a number of parameters.* Some of these are assumed to be constant from one individual to another. Their assumed values are listed in chapter 2 and 3. Others may vary from one individual to another (stationary parameter), and in the same individual over time (varying parameter). These must be determined for each individual we intend to simulate. The stationary parameters are estimated manually as described in chapter 6. The varying parameters are estimated by direct feedback circuits synthesized from simple considerations on the properties of the system. This study is not intended a thesis on estimation theory, and the simple and direct estimation methods seem to be adequate for the present purpose. The model is then used in simulation studies of the human left

*The term parameter is used for quantities that describe properties of the system. The term variable is used for quantities that are pulsatory. Variables are pressures, volumes, flows, tensions, lengths and velocities (and some dimensionless quantities).

ventricle and aorta, as well as the dog ventricle. The information in these measurements was not used in the development of the model, which occurred before the data became available. Part of the information is, however, used to obtain estimates of parameters, as defined in chapter 6. The remaining information is utilized to test the ability of the model to simulate the left ventricle and aorta. With the limited material presented in this study, the question: "How realistic is the model?" can only be answered in relation to each individual that is simulated, and not in terms of general cardiovascular behaviour. So far, the model seems to give acceptable results, but future studies may reveal the need for modifications of this approach.

The results from the application of the model to data from patients are supporting the underlying goal of this study, and suggest that the model may be useful in the clinical environment for the analysis and understanding of the hemodynamic state of the individual patient. Again, however, a reservation is appropriate as more experience is necessary before more definite conclusions can be drawn.

Chapter 2.

THE LEFT VENTRICULAR MODEL

Introduction

The major mechanical work in the circulation is done by the left ventricle. In the normal resting individual, this chamber delivers a mean output of 4 - 5 l/min. against a pressure of 80 - 120 mmHg. The ventricular wall consists primarily of heart muscle tissue which develops contractile force (and velocity) during systole.

If we intend to describe left ventricular performance in terms of muscle behaviour, it is necessary to relate variables such as pressure, volume and flow relevant to the ventricle, to muscle variables as tension, length and velocity. The simplest conceptual model of this type consists of only one muscle, representing the behaviour of an "average myocardial fibre". Thus, spatial differences in tension and velocity within the myocardium are disregarded. In physiological literature we find a widespread use of this approach to interpret left ventricular performance. The model adopted in this study is illustrated in figure 2.1 A.

Input variables are mitral and aortic valve flows, q_{mi} and q_{av} . The symbol represented by the circle, (including the + and - sign) performs the operation: $\Delta q = q_{mi} - q_{av}$. The output of this operator is the "net flow" Δq . In a ventricle with non-leaking valves, $\Delta q = q_{mi}$ in diastole and $\Delta q = -q_{av}$ in systole. The left ventricular volume at any instant, t , is given by the integrated net flow:

$$V_{1V} = \int_0^t \Delta q dt + V_{1V}(t = 0)$$

We disregard the "initial condition" $V_{1V}(t = 0)$, as the effect of this has vanished when the model is in steady state. Block 2

performs the integration, its output is V_{lv} . In order to simulate ventricles of different size, it is necessary to derive a normalized ventricular volume, V_{lvn} , from V_{lv} . The reference volume is V_m (see later in this chapter), and block 3 divides V_{lv} by V_m .

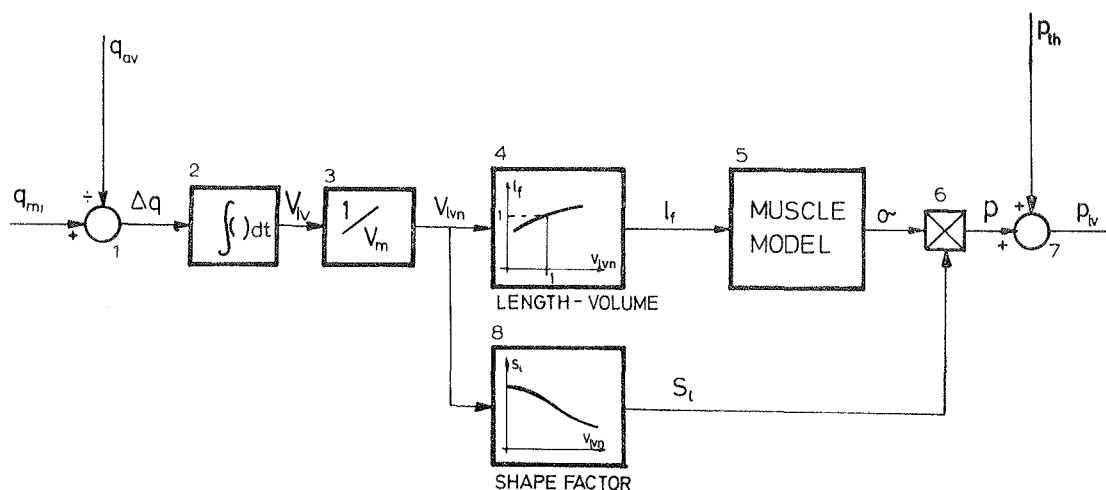


Figure 2.1. Block diagram of the left ventricular model. See text for explanation. Muscle model block diagram on p.33 figure 2.16. For symbols we refer to text.

Block 5 symbolically represent the muscle model. The static and dynamic characteristics of this is described by the block diagram in figure 2.16, and the functional relationships are discussed in the text. At the present stage, we regard the muscle model as a unit with fibre length l_f as input variable, and muscle tension σ as output. The fibre length is computed by block 4 from the normalized volume. The transmural pressure (differential pressure over the ventricular wall) is directly proportional to the muscle tension for a constant volume. Thus we may write: $p = S_1 \cdot \sigma$. The shape factor S_1 (Beneken 1965) is a function of normalized left ventricular volume, as computed by block 8. Block 6 symbolizes the multiplication of σ with S_1 .

Adding the intrathoracic pressure, p_{th} , to the transmural pressure p , the output of "block" 7, is left ventricular pressure p_{lv} . In the subsequent sections of this chapter, the functions represented by blocks 4, 8 and 5 will be derived.

The fibre length - volume relation

We shall now derive a function $l_f(V_{lvn})$ valid for two assumed shapes - a cylinder and a sphere. The volume of a sphere of radius r is:

$$V = 4\pi r^3/3$$

The relative volume change is dV/V and the relative radius change is dr/r . Differentiation of the first equation gives:

$$dV = 4\pi r^2 dr$$

Dividing by volume:

$$\frac{dV}{V} = 3\frac{dr}{r}$$

For a cylinder of radius r and length h we perform the same calculations:

$$V = \pi r^2 h$$

$$dV = 2\pi h r dr + \pi r^2 dh$$

$$\frac{dV}{V} = \frac{2dr}{r} + \frac{dh}{h}$$

Recent observations on the shape of the human left ventricle indicate a symmetrical contraction (Mc Donald 1970) in which we have $dr/r = dh/h$. Using this assumption the expression reduces to that of the sphere:

$$\frac{dV}{V} = 3\frac{dr}{r}$$

Since both a sphere and a cylinder give the same relation, we feel justified to use this for the model.

Let us use as volume reference V_m - the volume of the wall material of the ventricle. A normalized ventricular volume of 1 then means that the volumes of the cavity and of the ventricular wall are equal. Likewise the fibre length is normalized, using a reference the length of this equal volume ventricle fibre. It is now trivial to calculate the fibre length as a function of the volume for the two cases that the muscle is situated at the inner (l_i) and outer (l_o) surface of a sphere, and the results are shown graphically in figure 2.2.

The length-volume relations of muscle fibres located at various intermediate positions in the myocardium will lie between these curves.

A multilayer model would, however, be of much greater complexity, and would need many additional (presently unavailable) pieces of physiological information to give distinct advantages. Therefore a $l_f(V_{lvn})$ relation corresponding to a muscle fibre situated midway between the outer and inner surface is assumed to be representative of the average muscle behaviour.

The $l_f(V_{lvn})$ relation actually used is shown graphically in figure 2.2.

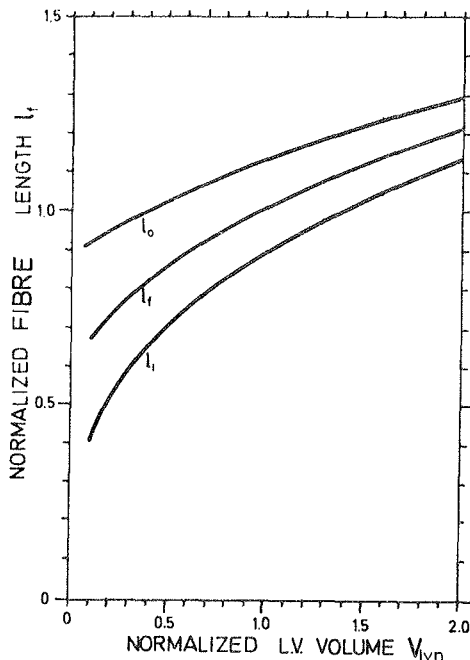


Figure 2.2.

The fibre length-volume relation. The upper and lower curves signify muscle fibres situated at the outer and inner boundaries of the ventricular wall respectively. The middle curve is an approximation for the "average" muscle fibre.

The shape factor

The assumption that an "average fibre" is representative of the entire myocardium implies that the transmural pressure p of the ventricle is a function only of its normalized volume $V = V_{lvn}$ and the tension, σ , in the average muscle fibre. This relation can be described as:

$$p = S_1(V)\sigma$$

where the shape factor S_1 is a function of left ventricular normalized volume. The formulae used by most authors are valid only for thickwalled spheres with isotropic homogeneous wall material. The structure of the myocardium is not isotropic and homogeneous. A typical property of a fibre of this material is the ability to develop stress in mainly one direction - parallel to the myofibrils. Hence we base the deduction of the shape factor upon the following assumptions:

- 1) The wall material is incompressible.
- 2) A muscle fibre develops tension in one direction only.
- 3) Shear stresses between adjacent fibres are neglected.
- 4) The fibre tension is equal throughout the wall thickness.
- 5) The right ventricle does not influence the left.

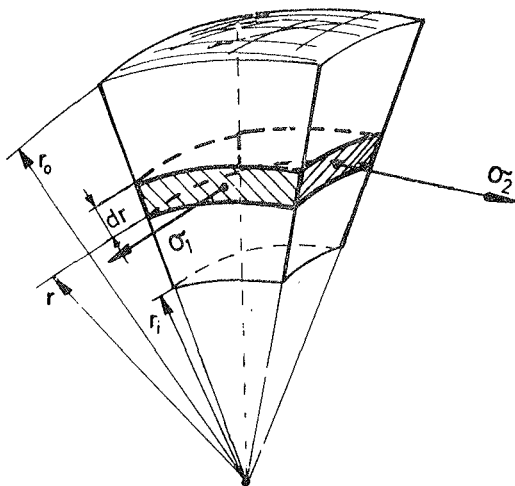


Figure 2.3. Section of a spherical wall. Symbols explained in the text.

Let us consider an infinitesimal segment (shaded) located a distance r from the centre of the sphere. The thickness of this segment is dr . Let us further assume a pressure p on the inside of the segment, and a transmural pressure dp . The pressure on the outside (at a radius $r + dr$) is $p - dp$. Since dr is infinitesimal small, we may

use "Laplace's law" to derive the wall stress σ_1 (and σ_2)

$$\sigma_1 = \sigma_2 = \frac{1}{2} \frac{r}{dr} dp$$

We assume that half of the fibres occupying the segment volume are running in the σ_1 direction, the other half in the σ_2 direction. The tension* σ in a muscle fibre is then twice the wall stress:

$$\sigma = 2\sigma_1 = 2\sigma_2$$

Using this expression in the first equation and solving for dp gives:

$$dp = \sigma \frac{dr}{r}$$

We consider the ventricular wall to be composed of thinwalled spheres of thickness dr , each giving a contribution dp to the total transmural pressure. We assume that there is no friction between these spheres (assumption 3) and we arrive at the total transmural pressure by integration:

$$p = \sigma \int_{r_i}^{r_o} \frac{dr}{r} = \sigma \ln \frac{r_o}{r_i} = \sigma \ln \sqrt[3]{\frac{V+1}{V}} = \frac{\sigma}{3} \ln \frac{V+1}{V}$$

where r_i and r_o are inner and outer radii of the ventricle and V is the normalized volume (with reference to the wall volume) of the ventricle. The shape factor according to this deduction is:

$$S_1 = \frac{1}{3} \ln \frac{V+1}{V}$$

If one accepts as reasonable the assumptions made in the start, the appropriate formula to use for computing left ventricular muscle tension then would be:

$$\sigma_{lv} = 3 \frac{P_{lv}}{\ln \frac{V_{lv} + V_m}{V_{lv}}}$$

* tension we define as force/cross-section area of parallel muscle fibres.

Assuming a cylindrical model as shown in figure the stress in the tangential direction is:

$$\sigma_t = \frac{r}{dr} dp$$

and in the direction of the longitudinal axis:

$$\sigma_l = \frac{r}{2dr} dp$$

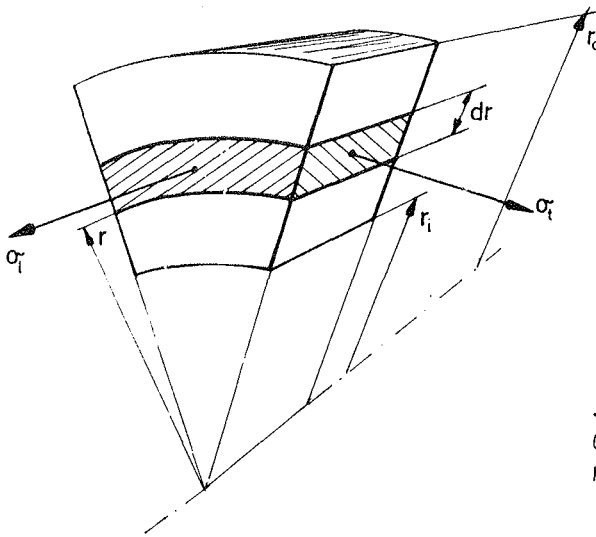


Figure 2.4.
Section of a cylindrical wall. See text for the meaning of symbols.

An equal fibre tension will now be achieved if 1/3 of the muscle fibres runs in the σ_l direction and 2/3 in the σ_t direction. The fibre tension is then:

$$\sigma = \frac{3}{2} \sigma_t = 3\sigma_l$$

We proceed analogously with the sphere:

$$dp = \frac{2}{3} \sigma \frac{dr}{r}$$

$$p = \frac{2}{3} \sigma \int_{r_1}^{r_0} \frac{dr}{r} = \frac{2}{3} \sigma \ln \frac{r_0}{r_1} = \frac{2}{3} \sigma \ln \sqrt{\frac{V+1}{V}} = \frac{1}{3} \sigma \ln \frac{V+1}{V}$$

$$S_l = \frac{1}{3} \ln \frac{V+1}{V}$$

The assumptions (1 - 5) have the rather surprising result that a sphere and an openended cylinder give the same shape factor S_1 when normalized to wall volume. Consequently it seems justifiable to infer that intermediate shapes as an ellipsoid, a cylinder ended by a sphere, will, if not yield equal shape factors, certainly be close to the relation deducted here.

It is important to distinguish between stress and muscle tension as defined in this section. Tension is the force per unit area crosssection of the parallel bundle of myocardium. This implies that the (muscle fibre) tension, σ is twice the stress observed in a sphere and 1.5 times the circumferential stress in a cylinder.

It is of interest to compare the formula developed for the shape factor with "in vivo" measurements. The recent contribution by Mc Hale and Greenfield (1973) report on measurements of circumferential stress in the dog ventricle using an auxotonic force transducer. In control state and in response to phenylephrine they found peak systolic l.v. pressures of 116 and 153 mmHg, end-diastolic outer radius of 2.59 and 2.75 cm and wall thicknesses of 1.12 and 1.14 cm respectively. Using this data we may calculate circumferential wall stresses of 2.57 and 3.71 g/cm² using a cylindrical model, while the authors measured 2.15 and 3.30 g/cm² in the same states. A spherical model gives 1.30 and 1.92 g/cm² respectively, and is clearly not so appropriate. If we assume an ellipsoid we might obtain results that were even closer to their findings than the cylinder, but the authors did not publish the ratios of the major/minor radius, so that a comparison will not be exact.

The shape factor relating muscle fibre tension (vs. wall stress) to l.v. pressure show potential of being less sensitive to assumptions in left ventricular geometry. We shall therefore use the muscle fibre tension rather than wall stress. This will inevitably have as a result that the maximum tension experienced during a contraction, and the maximum

tension parameter of the muscle model (σ_{\max}) will exhibit larger numerical values than usually found in the literature on papillary muscle and myocardial mechanics. But the favourable comparison with the results of Mc Hale and Greenfield above is, at least, some justification for these assumptions.

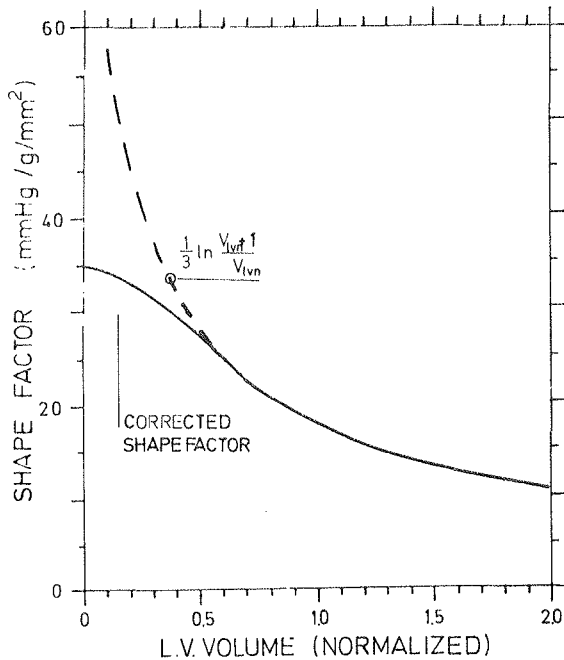


Figure 2.5.

The shape factor. Broken line indicates theoretical value based on the deduction in the text. Unbroken line signify shape factor corrected for "ineffective inner myocardium" as implemented in the preset description.

The unit for tension is chosen as g/mm^2 , while pressure is in mmHg, so that the shape factor is expressed in $mmHg/gmm^{-2}$. The uncorrected shape factor (the broken line in the figure) becomes very large for small volumes. This is due to the small radius of the inner layers. For this situation, the "average" muscle fibre does not represent the inner muscle fibres, as these become rather short and develop only very small, or even negative (elastic recoil) tensions. We might divide the myocardium into an "effective" outer portion, V_o , and a less effective or inner portion, $V_i = 1 - V_o$. V_i increases when the ventricular volume V decreases. This will give rise to a lower value of S_1 than the uncorrected value.

In figure 2.5 we have made a correction on the basis that this effect starts to influence the ventricle shape factor at normalized volumes of 0.5.

The muscle model

Originally proposed by A. V. Hill (1938) for skeletal muscle, two or three element muscle models are now widely used to describe the behaviour of cardiac muscle. The simple two element model is shown in figure 2.6 A. The series elastic component or element (SE) is described by passive tension-length curves.* The contractile element (CE) is characterized by a force-velocity-length-time-function. This element actively develops force when activated and is thought of as being freely extensible during relaxation.

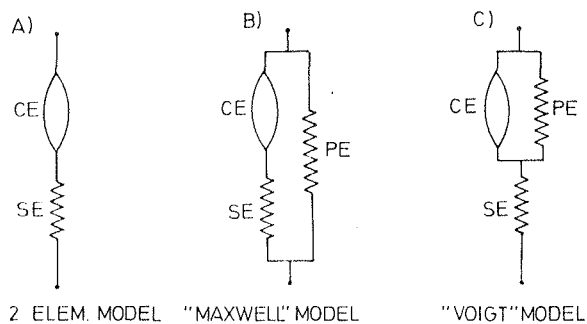


Figure 2.6.

Different conceptual models of heart muscle.

According to this model, the phenomena occurring during a normal ejecting heart beat are:

- a) Isovolumic contraction phase. The CE is activated and starts to contract. It then stretches the SE, while total fibre length is constant.
- b) Ejection phase. The fibre length is reduced. In a normal ejecting beat muscle tension will not be constant, but for an isotonic contraction as in experiments on isolated cardiac muscle, the muscle force and the length of the SE is constant.
- c) Isovolumic relaxation phase. The CE relaxes and lengthens due to the elastic energy stored in the SE.

*in accordance with the vocabulary of muscle physiology, the term force or tension is used, and thus means force/unit area or g/mm^2 .

- d) Filling phase. The fibre length is increased. For an isotonic relaxation, the length of the SE is constant in this phase.

It may be remarked that in the normal ejecting beat, phase d follows after phase c, while in an isotonic contracting muscle fibre, phase d will follow phase b, and c after d.

To account for the diastolic passive force-length relation of cardiac muscle, a parallel elastic element PE is often incorporated in the muscle model. This may be placed parallel to the combination of CE and SE, (Maxwell model figure 2.5 B) or parallel to the CE only (Voigt model figure 2.5 C).

Before we proceed to a detailed treatment of the model elements it is of relevance to review briefly the theory of muscle contraction.

Ultrastructural basis of heart muscle and choice of model structure

The myocardial cells are $10 - 15\mu$ in diameter and $30 - 60\mu$ in length (Braunwald & al 1967). This cell or fibre contains multiple crossbanded myofibrils which run the length of the fibre. The myofibrils in turn are composed of a serially repeating structure, the sarcomere schematically illustrated in figure 2.7 A. This is the fundamental function unit of contraction. It is delimited by two dark lines termed z-lines, the distance between these normally vary from 1.5 to 2.2μ depending on the muscle length. The contractile substance of the sarcomere is an array of partially overlapping myofilaments, built up of contractile proteins. The thicker myofilaments (myosin) are 100\AA in diameter and $1.5 - 1.6\mu$ in length, and the thinner (actin) are 50\AA in diameter and 1μ in length.

According to the sliding filament theory proposed by Huxley and Hanson (1954) and by Huxley and Niedergerke (1954), activation of the muscle causes an interaction between the actin and myosin filaments, and force-generating cross bridges are created between these. During the contraction, the length of

the myofilaments is thought to be constant - the length change of the sarcomere (the z-lines are moving towards each other) is accounted for by the actin filaments sliding further into the A-band (in the middle of the sarcomere), and partially overlapping when the length is below 2.0μ .

To compare different physiological experiments and to proceed from these to a general description it is necessary to use a reference for muscle length, in this case we shall use the sarcomere length in μ as the length unit in the muscle model. We may then think of the sarcomere model as having a cross section of 1 mm^2 and a length of one sarcomere unit. The different sarcomeres within this cross-section are assumed to behave identically.

We find no direct counterparts of the muscle model elements in this ultrastructural description, and they should not be thought of as distinct entities, but as distributed properties of the muscle (Hill 1970). An important question to ask in this connection is: Is the sarcomere length constant, or does it shorten during an isometric (or isovolumetric) contraction? If the elastic properties due to fibrous tissues, necrotic or ischemic areas of the muscle tissue or heart valves are the chief determinants of the series elastic effects, then the Voigt model is the most appropriate to use, and sarcomere length clearly will diminish during the isovolumic part of a contraction.

In any ventricle, no matter how homogenous, some elastic effects of this type will be present. On the other hand, recent investigations (Nilsson 1972) demonstrate that the Maxwell model is the most appropriate analogue. There is evidence that some of the series elasticity resides inside the sarcomere for skeletal muscle (Hill 1970, p. 108), and it is thus reasonable to assume that this also applies to heart muscle. Thus we divide the series elasticity into an intrasarcomere elastic element SE and an additional series element SE_0 residing outside the functional contractile unit, as illustrated in figure 2.7 B.

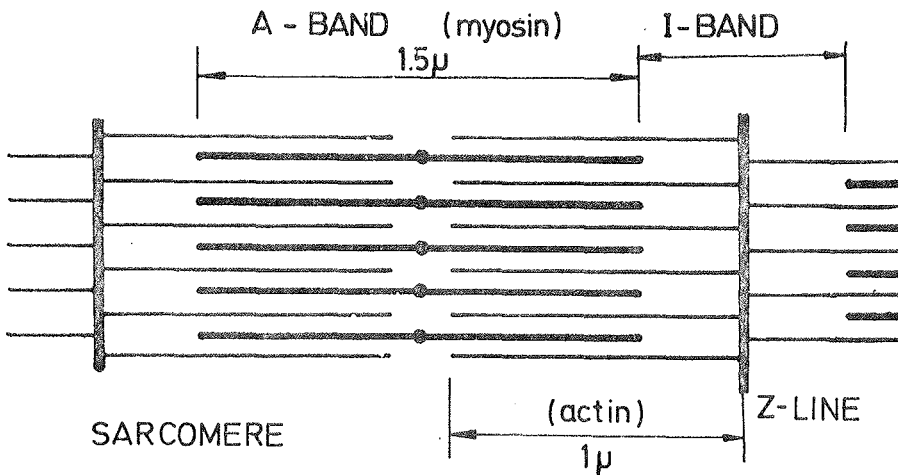


Figure 2.7 A.

Ultrastructural model of a sarcomere. When the muscle is activated, force-generating links are thought to develop between the actin and myosin filaments which then start sliding into one another.

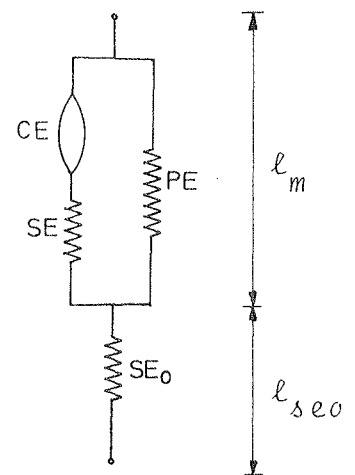


Figure 2.7 B.

The muscle model configuration used in the present study.

We regard the circumferential fibre as composed of two components in series - purely passive elasticities and sarcomeres, and the lengths of these are l_{seo} and l_m respectively.

We must take into account that ventricles having the same l_m (normalized, p. 10) may differ with regard to the length of the average sarcomere l_{sac} (Gatch & al 1972). The parameter k_{sac} relates these two lengths:

$$l_{sac} = l_m \cdot k_{sac}$$

(see block diagram p. 33). Thus two factors may cause a ventricle to be considered dilated - either it has an abnormally compliant SE_0 , or it has a low value of k_{sac} (needing a longer fibre to give the necessary stretch of the sarcomeres).

The external series elastic element SE_0

This element has in block diagram representation (figure 2.16) fibre tension σ as the input variable, and

length l_{seo} as the output variable. Since most biological tissue exhibit length-tension curves that are closer to logarithmic functions than to linear, it seems natural to use the former for this element. The length of the additional series elastic element is given by the function shown in figure 2.8.

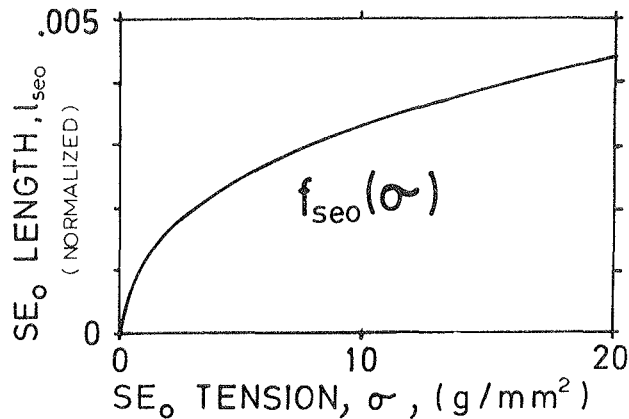


Figure 2.8. The length-tension relation of the external series elastic element. l_{seo} is normalized with the same reference as l_f .

The "intrasarcomere" series elastic element SE

Let us briefly recapitulate two widely used approaches for determination of the SE-tension-extension relation, the presentation here disregards the PE (parallel elastic element):

- a) In the incremental quick stretch (or release) method, the muscle is first activated, and allowed to develop force isometrically until the desired level is reached. Then an incremental step, Δl , in length is made, and the corresponding step in force, $\Delta \sigma$, is recorded (Brady 1971, Nilsson 1972). Thereby the stiffness $\Delta \sigma / \Delta l$ can be computed as a function of series elastic element tension, σ , and is rectilinearly dependent on this. This in turn, means that the tension-extension relation of the SE is approximately exponential, and

the coefficient $k_{se} = \frac{\Delta\sigma}{\sigma} \left[\frac{1}{\text{unit length}} \right]$ was found to be in the range from 52 - 115 with a mean of 76 for rabbit papillary muscle (Nilsson 1972). This is including any external series compliance.

- b) The other method (see for ex. Parmley & Sonnenblick 1967) is to let the muscle perform afterloaded contractions with varying loads. Assuming that the contractile element velocity is not significantly affected by the transition from the isometric to the isotonic state, the SE stiffness can be calculated from:

$$\frac{d\sigma}{dl} = \frac{d\sigma/dt \text{ (before transition)}}{dl/dt \text{ (after transition)}}$$

Values obtained by this method for k_{se} are 24 - 30/unit length (Parmley and Sonnenblick 1967).

Their value of k_{se} measured by large quick releases was of the order of 50 - 60/unit length).

The discrepancy between these observations is of such magnitude that it is not caused by measurement errors and variation in the preparations. A. V. Hill (1970, p. 95) finds that SE stiffness for skeletal muscle is dependent upon the previous history of contraction - and when this is made identical, the extension-tension curves determined by the two methods are compatible.

This may be the cause of the discrepancy. We must bear in mind, however, that the two-element muscle model is a conceptual simplification, and that the reality underlying muscle behaviour may be such that different relations and parameters must be used in our model to make it describe the effects observed by different experimental environments (as quickstretch equipment).

Heart muscle in vivo is not subject to quick stretches or releases - the nearest usual in vitro analogue is the afterloaded contraction. It seems justifiable, therefore, to use the series elastic element characteristics found in this experimental environment in a model intending to represent a normal ejecting heart beat.

The SE $\sigma_{se} - l_{se}$ curve determines together with the SE_0 and the force-velocity relation* of the CE the timecourse for the buildup of isovolumetric pressure in the intact ventricle.

The force-velocity relation is chosen primarily to be representative of the conditions during ejection, but we assume that the postulated $\sigma_{ce} - v_{ce}$ curves are representative during the pre-ejection (and after-ejection) periods of systole, and do not include in the description a hypothetical increase in v_{max} when the transition from isometric to isotonic (or auxotonic) takes place. This hypothesis is given by Parmley and Sonnenblick (1967) to explain the discrepancy in SE stiffness estimates using the two methods outlined above.

We summarize this section by showing the SE tension-extension $f_{se}(l_{se})$ actually used in our model (figure 2.9). The SE tension is given as:

$$\sigma_{se} = e^{k_{se} \frac{l_{se}}{2.0}} - 1 \left[g/mm^2 \right]$$

$l_{se}/2.0$ is the normalized SE length and k_{se} is a stiffness parameter.

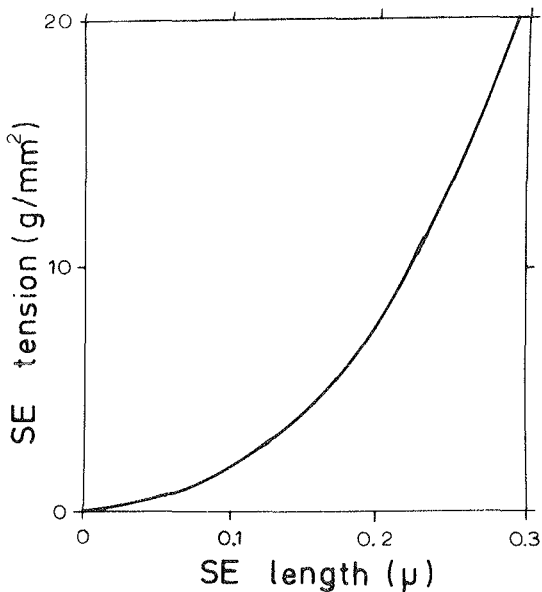


Figure 2.9.

The length-tension relation of the series elastic element as implemented in the present description. The curve is plotted for a stiffness factor (k_{se}) of 24/unit length.

* the f.v. curve is a function of the state of activation and muscle length as described on page 23, therefore the effect of these variables are included in the statement above.

For reasons given on p. 28 the absolute length of the SE is unimportant, and may be chosen freely, only its extension is of interest.

Any possible viscous effects that can be ascribed to the SE (Hill 1970, p. 103) are not modelled here, as these probably have relatively short time constants, and therefore do not affect a normal contraction.

The contractile element (CE) force-velocity relation

The contractile element CE changes its characteristics when the muscle is activated. The concept of activation is perhaps most easily explained in conjunction with a force-velocity curve ($\sigma_{ce} - v_{ce}$ -curve) of the CE shown in figure 2.10 which depicts the dynamic property that the velocity of shortening, v_{ce} , is dependent on the load, σ_{ce} , of the element. The velocity is normalized to sarcomere lengths (2.0 μ)/sec. The basis of the curve shown is Hill's equation in a slightly modified form:

$$v_{ce} = v_{max} \frac{\sigma_0 - \sigma_{ce}}{\sigma_0 + k_{hyp} \sigma_{ce}}$$

For negative shortening velocities, available data are scarce, and this portion of the curve is assumed. The steepness of the negative f.v. curve is independent of v_{max} .

If k_{hyp} , a parameter determining the curvature of the hyperbolic relation, is considered constant, we are left with two parameters: v_{max} - the velocity at zero load, and σ_0 - the tension at zero velocity, to determine the force-velocity relation. σ_0 is considered to be a function of sarcomere length and activation:

$$\sigma_0 = \sigma_{max} \cdot f_{\sigma}(l_{sac}) \cdot a_{\sigma}(t)$$

When the intensity of the active state (a_{σ}) changes, we interpret this as changes in the force-velocity relation, described

by the equation above. a_{σ} and f_{σ} are normalized functions having maximum values of 1, so that the parameter σ_{\max} represents the value of σ_0 when the muscle is fully activated and optimum (with regard to f_{σ}) length.

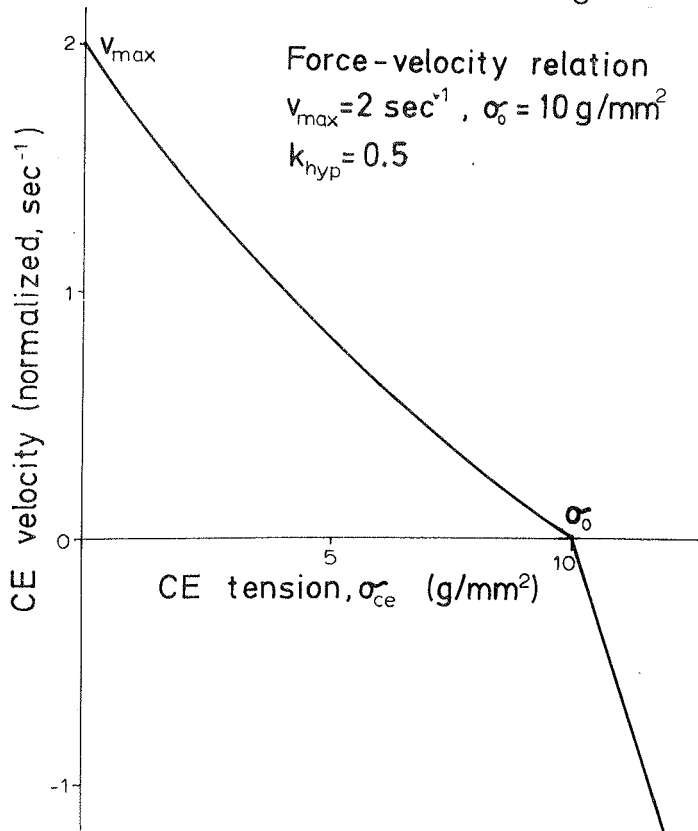


Figure 2.10.

The force-velocity relation of the Hill's equation (positive velocities) and the assumed relation (for negative velocities).

CE maximum velocity

In figure 2.10 we used the term v_{\max} to denote the interception point of the force-velocity curve with the v_{ce} axis. There is evidence (Nilsson 1972, Pollack 1970) that v_{\max} is length and activation dependent, but the literature is controversial as to whether this dependency is of such a magnitude that it is of significance in this model.

Brusaert and Sonnenblick (1971), using an unloading technique for continuously adjusting the preload so that it corresponds to the passive tension at the instantaneous muscle length, conclude that for normal sarcomere lengths, v_{\max} is relatively constant, whereas for smaller lengths ($<1.7\mu$) the velocity at zero CE load (Maxwell model) is progressively reduced. At these minute loads, the choice of muscle model influences the results considerably (Pollack 1970) and the statistical distribution of intrinsic speeds among different

muscle fibres is not "averaged" as the fastest fibres will tend to dominate (Hill 1970).

Recent investigations by Nilsson (1972) using quick-release techniques indicate that v_{\max} is proportional to σ_0 over the entire ascending portion of the active developed force relation. An objection to quick releases has been the postulated uncoupling effect of the sudden movement. Even if the "damped quick release" used by Nilsson is claimed not to affect the intensity of the active state, the type of contraction performed is not similar to the normal physiological behaviour of cardiac muscle, and the afterloaded isotonic determination of the f.v. curve is a better analogue.

It is assumed that contractile element velocity at zero load, hereafter denoted by v_0 , is dependent on v_{\max} and σ_0 only. The length and activation influence is taken care of by the way these variables influence σ_0 . Our equation for the CE shortening velocity is modified:

$$v_{ce} = v_{\max} \frac{\sigma_0 - \sigma_{ce}}{\sigma_0 + k_{\text{hyp}} \frac{\sigma_{ce}}{\sigma_0} + \Delta\sigma_0}$$

Thus for any positive $\Delta\sigma_0$, v_{\max} can never be reached, not even hypothetically. Even so, it is a meaningful parameter as the velocity for any load less than σ_0 is proportional to v_{\max} . Here we assume $\Delta\sigma$ to be 1 g/mm^2 , and f.v. curves as implemented the model are shown in figure 2.11 A for some values of σ_0 .

The shortening velocity is normalized to sarcomere length of 2.0μ , a v_{ce} of 1 sec^{-1} means a sarcomere CE velocity of $2.0\mu/\text{sec}$. This is close to the widely used unit for this velocity: muscle lengths/sec. In panel B, the dependency of v_0 on muscle length is indicated, and we observe that it resembles the relation found by Brusaert and Sonnenblick (1971). The proposed equation should only be interpreted as a convenient way of representing this observed decline of v_0 with σ_0 .

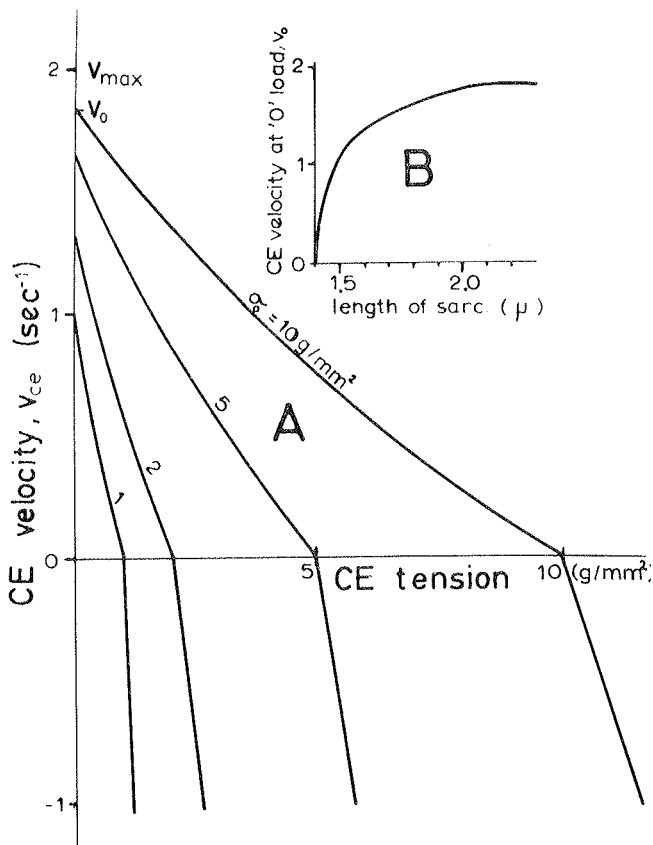


Figure 2.11.

A: The force-velocity relation of the model is shown for an assumed v_{max} of 2 sec^{-1} and for 4 different values of σ_0 .

B: The CE velocity, v_0 , at zero load, is shown for the case that $\sigma_{max} = 10 \text{ g/mm}^2$ and $v_{max} = 2.0 \text{ sec}^{-1}$.

Sarcomere tension-length relation $f_{\sigma}(l_{sac})$

In literature on cardiac muscle mechanics it is often implied that the ability to develop tension depends upon CE length which may differ from muscle length due to the extension of the SE.

When assuming a compliant SE, this difference becomes significant. In a study by Brusaert and Sonnenblick (1969), it is assumed that the shortening of the CE (during the isometric phase) is responsible for the deviation of the measured force-velocity relation from Hill's equation. The CE is then assumed to operate on the ascending limb of its developed tension-length relation (sarcomeres are shorter than 2.2μ). They show (figure 6) a method of obtaining a true hyperbola, but in this procedure they do not use the actual force-length relation of the SE.

The deviation of the measured force-velocity curve from the hyperbola is most prominent for greater loads, where the SE is

quite stiff (Parmley and Sonnenblick 1967) and then we should not expect any significant change in length distribution among the CE and SE.

Based on the data given in a contribution by the same authors (1971) a f.v. curve is reconstructed from their data using the method illustrated and explained in figure 2.12.

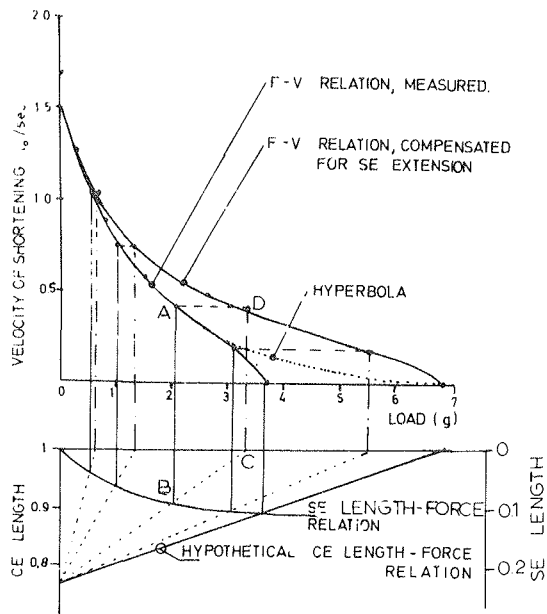


Figure 2.12.

Modification of the f.v. relation by a hypothetical compensation for SE elongation. Lengths are normalized to l_0 - the optimum length of the muscle. We assume that the SE length-force curve is as shown in the lower part of the figure. Furthermore we assume a linear length-force relation of the CE so that zero developed force occur at $l_{ce} = 0.75$. We take as an example a contraction where muscle length $l_f = l_{ce} + l_{se} = 1$. The lower force-velocity curve is obtained experimentally.

Let us start with point A on this curve. B is the corresponding point on the SE length-force curve. We observe that

$l_{se} = 0.1$ and $l_{ce} = 0.9$. The dotted line signifies the CE length force curve at max value of active state. C represent the hypothetical force if the SE was perfectly stiff. And thus D is the point on the force-velocity curve for constant CE length (=1). The other points on this curve are determined the same way.

We see that the f.v. curve corrected for SE elongation does not resemble a hyperbola significantly more than the uncorrected.

This use of their data leads to two conclusions:

- a) The deviation of the measured f.v. curve at greater loads from Hill's equation is not primarily due to the change in length distribution among the SE and CE.
- b) The findings by Brusaert and Sonnenblick (1969) can not be used to conclude that the developed tension is

dependent on CE length and not on sarcomere length. If sarcomere length corresponds to the CE length (i.e. the series elasticity is found outside the sarcomeres) then their assumption becomes justified.

This controversy cannot be properly resolved until more is known about the nature and location of the SE. But even if it is demonstrated that the SE is located mainly in the sarcomere, this does not necessarily refute the assumption made in the present model that the actively developed force is dependent on sarcomere length and not on a conceptual CE length.

Another reason for making this choice is that, as long as the stiffness of the SE tension-extension curve remain controversial and as the objective is mainly to use this to represent the dynamics of isometric force buildup, it seems unjustified to base any more confidence in the 2 or 3 element muscle model and in controversial results from papillary muscle experiments than necessary.

The relation between f_{σ} and sarcomere length used in the model is shown in figure 2.13.

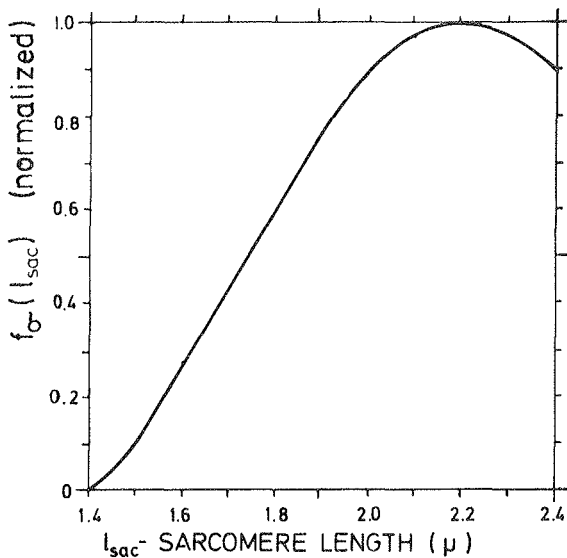


Figure 2.13.

Tension-length relation of sarcomere. Tension is normalized so that a maximum of 1 occurs at an optimum sarcomere length of 2.2μ .

It has a maximum at $l_{sac} = 2.2\mu$ (when the myofilaments are supposed to overlap maximally), beyond this length, it declines. For lengths less than 2.0μ it is assumed to be approximately linear, with zero developed force occurring at 1.4μ .

The measured actively developed force - fibre length relation of papillary muscle has a more curved relation at lower length (Donders and Beneken 1971). These lengths do not usually occur "in vivo" (Braunwald & al. 1967, p. 28).

Tension active state $a_{\sigma}(t)$

The time course of tension active state $a_{\sigma}(t)$ is not independent of how the muscle contracts, a longer initial length gives a longer duration (Edman and Nilsson 1971), the isometric active state declines slower than the isotonic (Sonnenblick 1965) and a constant velocity contraction lasts longer than an isotonic (Brusaert, Claes and Donders 1972).

There seems to be evidence (Hill 1970, p. 70) that active state in skeletal muscle reaches a plateau at 20% of the time to peak isometric tension (for a single twitch). For cardiac muscle a plateau in active state is inferred from experiments where isotonic velocity is displayed as function of length (see for example Brusaert and Sonnenblick 1969). The observation that these phase-plane trajectories meet in a common pathway are indicative of a plateau in the active state. Furthermore the simulations by Donders and Beneken (1971) are indirect evidence for this, as a time course of active state not having a pronounced plateau does not give common pathways in the phase-plane.

When we regard the time course of an isometric contraction (see for example Sonnenblick 1965) we observe no plateau in developed tension, the summit of this curve has a continuously rounded shape. This may be due to the active state starting to decrease before maximum isometric tension is developed, as found in single twitches of skeletal muscle (Hill 1970, p. 73). Further evidence for this explanation are the experiments of Brusaert and Sonnenblick (1969, fig. 2) where in an isotonic beat with almost maximal afterload, the muscle started to lengthen after 285 msec., while the time to peak isometric tension was 320 msec. It then becomes clear that the tension reached in an isometric contraction is less than the true maximum at this muscle length and that, in a force-velocity relation measured by normal afterloaded isotonic

contractions, the obtained curve will deviate from the true f.v. relation as figure 2.12 clearly demonstrates.

If the force-velocity curve is measured at a fixed time after the start of activation, an activation-independent f.v. relation should be obtained, and the published curves of Nilsson (1972) show a nearly hyperbolic relation - also for tensions approaching σ_0 (or P_0).

The time course of tension active state, $a_\sigma(t)$, used in the model is shown in figure 2.14 and is assumed to be applicable to a normal ejecting heart beat. We use the parameter T_{sys} to signify the time duration of activation. A plateaulike phase is assumed on the basis of the aforementioned experiments (Brusaert and Sonnenblick 1971) and simulations (Donders and Beneken 1971).

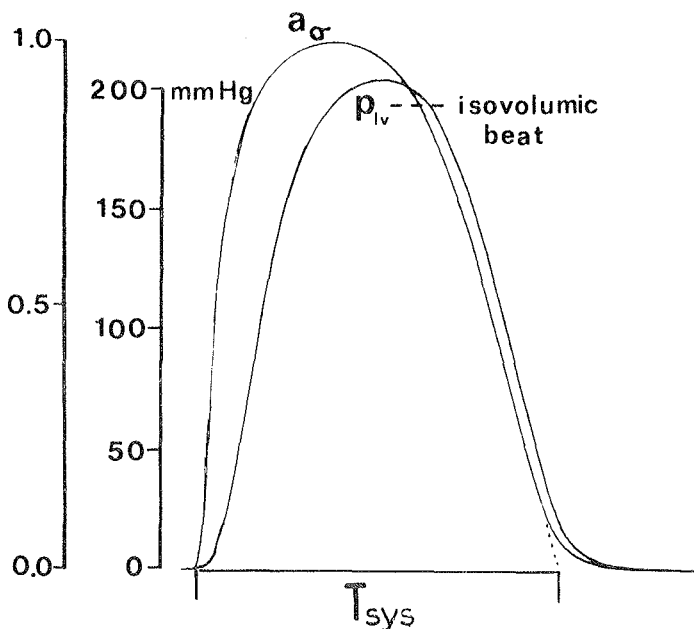


Figure 2.14.

Time course of tension active state $a_\sigma(t)$ normalized so that maximum is 1. For comparison purposes, the time course of l.v. pressure is an isovolumic contraction is also shown. We observe that peak isovolumic pressure is reached when active state has started to decline.

The gradual rise of the time course is supposed to reflect the gradual rise in active state (Brady 1971) as well as the nonsynchronous activation of different fibres.

Duration of active state

The time course of active state is length-dependent, it seems that a stretching of the muscle prolongs the duration (see for example Edman and Nilsson 1971), and that a movement (shortening) has the effect that the level of active state starts to fall

earlier and steeper.

Since available quantitative data on this subject are scarce, this relation is not incorporated in the description. The best value of T_{sys} is estimated for each simulation by the method outlined in chapter 6.

Resting value of active state

In the models of Beneken (1965, p. 96) and Donders and Beneken (1970) a minimum value of active state, δ , is assumed to be present when the muscle is relaxed, and to account for "passive" tension-length properties of heart muscle at low and intermediate lengths. Here we assume that $a_{\sigma} \rightarrow 0$ in diastole, and ascribe all passive elastic effects to the parallel elastic element, PE.

The parallel elastic element PE

As defined in figure 2.7 B, the PE is in parallel with the combination of the SE and the CE. Its input variable is l_{sac} - (sarcomere length) and the output variable is σ_{pe} (the parallel elastic element tension). It is supposed to represent the length-tension relation of resting heart muscle, as well as non-muscle elastic tissue, recoil effects etc. of the ventricle.

Considerable passive tension is present in heart muscle at sarcomere lengths of 2.2μ where skeletal muscles are almost freely extensible. It seems reasonable to assume that this passive elasticity is located elsewhere than the contractile machinery.

Again, different experimental methods will yield different estimates of the PE tension-length curve. Dynamic measurements (incremental stretches) give stiffer curves than static (Nilsson 1972). In the present context the static curves are the most appropriate, and figure 2.15 depicts the PE tension-length

model as used in the description. At the present stage we assume that all heart muscles exhibit the same PE length-tension curve, although recent evidence suggest that it may vary considerably in the diseased heart (Gaatch & al 1972).

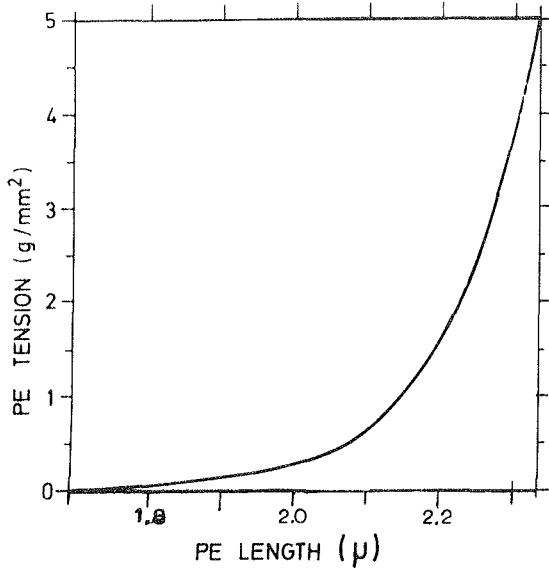


Figure 2.15.

Tension-length relation of the parallel elastic element (PE) as implemented in the present model.

Block diagram of the muscle fibre model

So far we have discussed the various elements in the muscle fibre model, a summary of this is given in block-diagram form, figure 2.16.

Input variable is the l_f -fibre length (from ventricular geometry model) and the output variable is muscle fibre tension σ (to ventricular geometry model, figure 2.1).

From l_f is subtracted l_{seo} - the length of the external series elasticity, derived from the tension-length relation of this element (upper part of the figure). Then we are left with the muscle length, l_m , multiplying this with k_{sac} yields l_{sac} , the sarcomere length. Let us assume that the CE submodel

The course of tension active state, $a_o(t)$ is synthesized (figure 2.14) from a generator symbolically represented by the block a_o . This is multiplied with the parameter σ_{max} (the maximum tension) and the output f_o from the tension-length relation of the sarcomere. Having now determined both σ_o and σ_{ce} , we may use the modified Hill's equation to calculate the shortening velocity of the CE, v_{ce} . Simple integration of v_{ce} yields CE length with a minus sign.

The block diagram is necessarily quite complicated due to the strong interaction of the variables in a 3-element muscle model.

In this chapter, a left ventricular model is described which is based upon the assumption that an "average" myocardial fibre model in conjunction with some, rather simple, geometrical considerations may account for the behaviour of the left ventricle. The geometrical relations are based upon a spherical shape of the chamber, but it is shown that an open-ended cylinder will give the same numerical results. Thus, the actual choice of geometry is probably not the crucial factor in this approach.

The description of the muscle fibre is based upon a modified Hill muscle analogue. The following parameters are assumed to have fixed numerical values:

$$k_{se} = 24 \frac{1}{\text{unit length}} \text{ series elastic element stiffness}$$

$$k_{sac} = 2.2 \frac{\mu\text{m}}{\text{normal length}} \text{ relates sarcomere length to muscle fibre length}$$

$$k_{hyp} = 0.5 \text{ (dimensionless) curvature of CE force-velocity relation}$$

$$\Delta\sigma = 1 \text{ g/mm}^2 \text{ "offset" of the CE force-velocity curve}$$

Besides, the functional relations indicated on the block-diagrams are fixed.

The performance and characteristics of the model may be changed by varying the following parameters:

V_m [ml] myocardial volume

T_{sys} [msec] duration of active state

v_{max} [sec^{-1}] maximum velocity of CE

σ_{max} [g/mm^2] maximum active tension

In chapter 6 we shall consider methods to obtain estimates of these parameters.

Chapter 3.

THE ARTERIAL MODEL

Introduction

The main role of the arterial system is to receive the stroke volume from the left ventricle and deliver a smooth flow to the various systemic capillaries. The number of arterial branches is large, and a detailed model of the entire system would be of prohibitive complexity. We must concentrate on those parts where we want a faithful reproduction of pressure and flow pulses - the aorta and some larger vessels, and use a simplified representation of the complex branching beyond these.

In order to achieve a qualitative understanding of the pressure-flow dynamics, we shall first look at some representative waveforms of pressure and flow pulses, then the general structure of the mathematical model and an electrical analogue of a vessel segment are postulated, and the division of the arterial system into spatial segments is discussed. The mathematical representation of the aortic valve is also included in this chapter and finally the model of the arteriolar and capillary peripheral resistances is presented.

Pressure and flow pulses in the ascending aorta and the femoral artery

The flow and pressure recordings shown in the subsequent figures are recorded from the model using the "standard" parameters (listed in table 6.1).

Figure 3.1 depicts the time courses of pressure and flow in the ascending aorta.

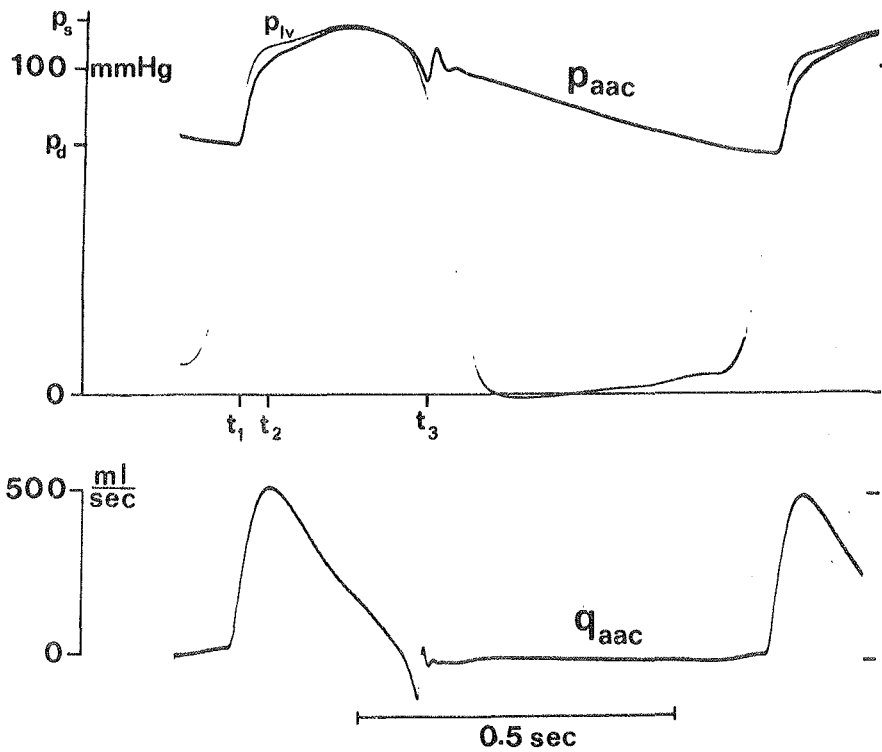


Figure 3.1.

Pressure (p_{aac}) and flow (q_{aac}) in the ascending aorta.

t_1 - start of ejection

t_2 - peak aortic flow

t_3 - end of ejection

p_s - systolic pressure

p_d - diastolic pressure

Left ventricular pressure (p_{lv}) is superimposed.

At t_1 the left ventricular pressure exceeds the aortic diastolic pressure p_d and causes the aortic valve to open. This marks the beginning of the ejection phase, and a sharp rise in both pressure and flow tracings follows immediately after this event.

Peak flow (at t_2) is reached relatively early after t_1 , and the flow tracing then declines in a curvilinear manner. The pressure tracing continues to rise some time longer until systolic pressure (p_s) is reached. When the flow becomes negative, aortic valve closure starts, and at t_3 the valve cusps have floated together and suddenly interrupts the backflow causing a marked oscillation in both pressure and flow tracings.

The left ventricular pressure tracing is also vaguely included in the figure. In accordance with the findings of Spencer and Greiss (1962) the pressure gradient over the valve is positive during the first portion of ejection (when the blood flow is accelerated) but becomes almost zero, or even negative during the later parts, when the flow is decelerated.

After closure of the valve cusps, the flow through the aortic valve remains close to zero, the only aberration is caused by the small volume necessary to fill (or empty) the compliant valvular membranes when the pressure across the closed valve changes.

From t_3 until the next ejection begins, the arterial system is autonomous, i.e. it is not driven by any input flow and the time courses of its variables are determined solely by the intrinsic dynamics and the values of the state variables (pressures and flows) at t_3 .

If we use the simple "Windkessel" approximation, the pressure curve in diastole will be an exponential decay. In our case, the diastolic pressure timecourse is more linear than exponential due to the rather complicated dynamics of the multisegment approximation of the distributed system.

In our "normal", cardiac output is 5 l/min and the pulse pressure is 40 mmHg, values which may be considered average for young human arterial systems.

If we proceed towards the periphery and observe the pressure and flow waveforms in the femoral artery (figure 3.2) we find mainly the same patterns as for the central aortic curves.

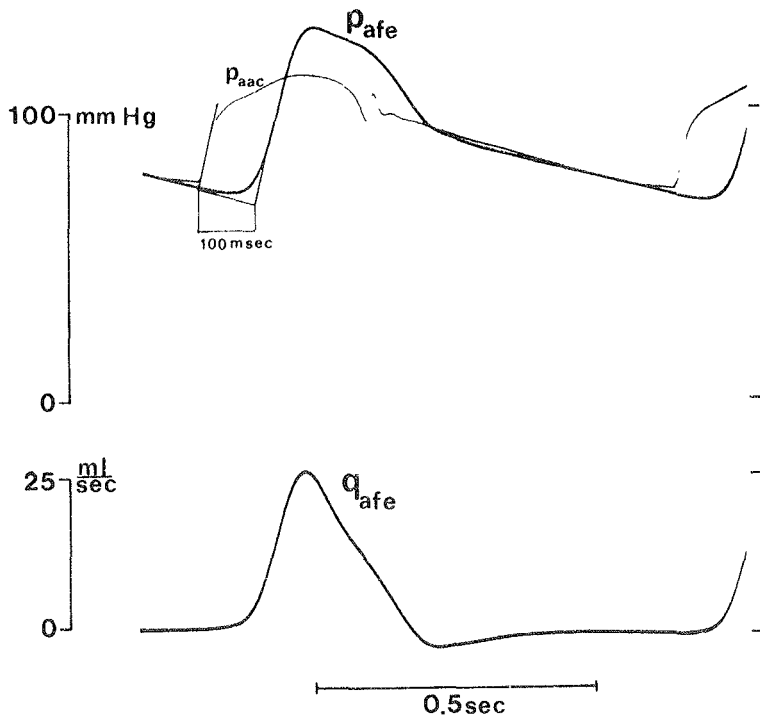


Figure 3.2.

Pressure (p_{afe}) and flow (q_{afe}) in the femoral artery. Ascending aortic pressure (p_{aac}) is superimposed. Parameters as in table 6.1.

There is, however, a longer delay before the upstroke of the tracings, due to the transmission line characteristics of the elastic aortic tube. We may calculate a "transmission time" of 100 msec, corresponding to a foot to foot wave-velocity of 5 m/sec. As would be expected, the maximum amplitude as well

as the mean value of the flow are significantly less than in the ascending aorta - other branches are also sharing the cardiac output. The mean pressures are approximately the same in the two positions - as we can predict from the negligible influence of viscous resistive effects in the large vessels. The peak systolic pressure, however, is higher in the femoral artery than in the ascending aorta. This phenomena can also be measured in a human cardiovascular system. Its cause can be ascribed to the general elastic and crosssectional tapering of the arterial tree, causing reflections.

These simple considerations indicate that the proposed arterial system model may represent the "Windkessel" or volume storage effect as well as the propagation properties of the aorta. We shall now discuss various aspects of the model more in detail, and start with a simplified mathematical formulation of the pressure-flow relationships.

Mathematical representation of a segment

It is beyond the scope of this study to present a rigorous mathematical treatment of fluid flow in elastic tubes, and the pressure-volume-flow relations will be postulated directly.

We may envisage a model of a blood vessel as a series of elastic reservoirs joined by rigid tubes, illustrated in fig. 3.3.

It has been shown previously by some authors (see for example Rideout and Dick 1967, de Pater 1966) that the mathematical structure of this model may be arrived at by simplification and discretization of the Navier-Stokes equations.

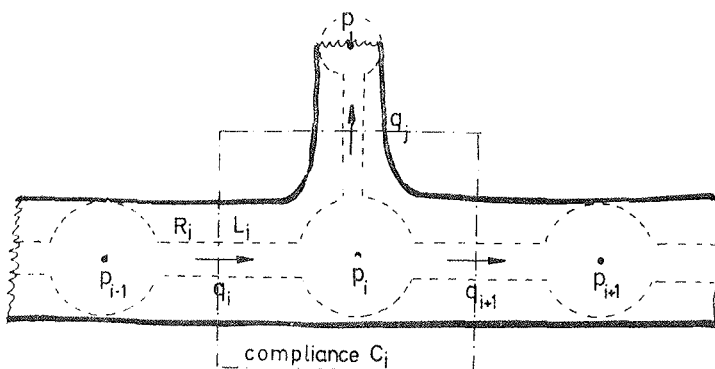


Figure 3.3.

"Hydrodynamic" model of a vessel segment. p_i - pressure at location i , q_i - flow between location $i-1$ and i . The line - - - - - indicates the region where the compliance C_i is thought to be located. For further explanation, see text.

While the pressure (and flow) in a vessel are continuous functions of both location and time, this lumped description allows the variables to be computed only at selected anatomical points. At locations between such points, the lumped model does not give any solution. As one set of differential equations describe the inertance and resistance effect of the postulated rigid tubes, and another represent the elastic properties of the "Windkessel", it is not evident that the pressures and flows are referred to the same anatomical locations. In figure 3.3 we have indicated the points where the model pressures are computed. The inertance and resistance effects are then ascribed to the column of blood between these two locations, while the elastic effect of the "Windkessel" may be thought of as belonging to the vessel as indicated in the figure. It will then be natural to envisage the anatomical locations where the flows are computed to lie between the pressure points. This is clear when we consider the left ventricle, where we assign l. v. pressure to some centre of the chamber, while flows are referred to the mitral and aortic valve openings.

In practical discussion of pressure and flow in the arterial system this difference will not cause any great difficulty, however, the calculation of the input impedance of any location will not be quite representative, especially with regard to the phase angle.

Inertance and resistance effects

The equation governing the motion of fluid from one segment (i-1) to another (i) is written in differential form:

$$p_{i-1} - p_i = R_i q_i + L_i \frac{dq_i}{dt} \quad (2.1)$$

The "driving pressure" $p_{i-1} - p_i$ is distributed among a resistive term resulting from the viscous friction created by the fluid flow, and an inertial term which is involved in accelerating the flow. For all arteries where we shall employ this description, the relative contribution of the inertial effects are larger than the resistive. The coefficients L_i and R_i are called the inertance and resistance of the segment and they may be deducted from hydrodynamic considerations. The formula used by Fry (1959), assume a nearly flat velocity profile

over the cross section, an assumption which is confirmed for larger vessels by thin film anemometry measurements by Bergel et al (1970).

$$L = \frac{1.1\rho}{\pi r^2} \Delta z \tag{2.2}$$
$$R = 1.6 \cdot \frac{8\mu}{\pi r^4} \Delta z$$

r is the radius of the vessel, Δz the length of the section considered, ρ is the density and μ the viscosity of the fluid. Arteries "in situ" exhibit very small longitudinal movement (Wetterer and Kenner 1968 p. 135), therefore Δz may be regarded as a constant over the heart cycle. Due to the elastic properties of the arterial wall, the radius will change when the pressure changes. The amount of variation is in the order in 1.2%/10mmHg for the ascending aorta in vivo (Greenfield et al 1967). A pulse pressure of 40mmHg thus corresponds to a change in radius of approximately 5%. The inertance is inversely proportional to the squared radius and the change in this coefficient will then be in the order of 10%. This is not a large deviation, but it will have some effect on the transmission of the pressure pulse, and should therefore be incorporated if a very representative model is sought. We have not included this phenomenon in the arterial model.

The resistance term of equation 2.1 is very small compared to the inertance term, and it is considered linear.

Pressure-volume relation of arteries

The volume V_i of the "Windkessel" (fig. 3.3) is found by simple integration

$$V_i = \int_0^t (q_i - q_{i+1} - q_j) dt + V_i(t = 0) \tag{2.3}$$

where q_i is flow into the vessel, q_{i+1} and q_j are flows out of it.

The initial condition may be omitted and the equation is reformulated:

$$V_i = \int_0^t (q_i - q_{i+1} - q_j) dt$$

If there is no branch at location i , then q_j is omitted.

As blood vessels have elastic wall material, they exhibit volume distensibility. We shall mean by compliance the ratio $C = \Delta V / \Delta p$, where ΔV is an incremental volume change and Δp the corresponding pressure change. If C is independent of the pressure, the system is linear - the relation between volume and pressure is a straight line. In a real arterial segment C tends to decrease with increasing pressure.

The compliance may be calculated if the elastic properties of the wall material is known, by assuming an appropriate geometrical model of the vessel wall. (Wetterer and Kenner 1968 p. 144). This method is, however, not universally applicable, as the vessel wall extensibility differ from one person to another, tending to be stiffer with increasing age and blood pressure. Indirectly we may calculate the vessel compliance from measurements of the wave velocity - defined as the distance between two points divided by the time necessary for a perturbation (usually the foot of the steep pressure upstroke) to pass between these. The simplest expression of this wave-velocity c is (Wetterer and Kenner 1968 p. 30)

$$c = \frac{1}{\sqrt{LC}}$$

where L and C are inertance and compliance of a unit length of the vessel. This formula may be rearranged so that the compliance can be calculated once the wave-velocity and inertance are known. This is demonstrated in fig. 3.4 B using a wave-velocity-pressure function measured by Anliker and coworkers (1970) by superimposing small sinusoidal perturbations on the pressure in the dog thoracic aorta. (Their results are reproduced in fig. 3.4 A).

We use the volume, compliance and inertance at 100mmHg as normalization references. The calculated compliance at 120 and 80mmHg then are 1.12 and 0.87 respectively - which means a $\pm 12\%$ change in vessel compliance caused by a "normal" periodic pressure variation. The error caused by linearization of the

pressure-volume relation should not become too excessive, as can be judged from the rather slight curvature of the volume curve of fig. 3.4B in the actual pressure range.

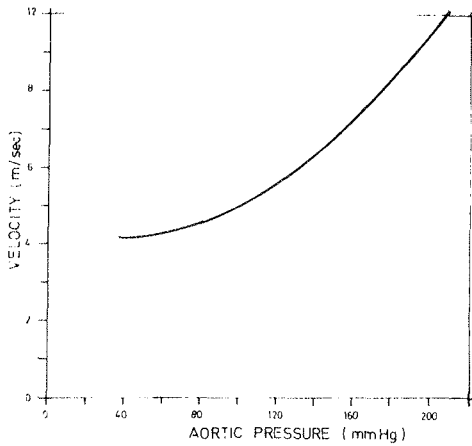


Figure 3.4A. Wave-velocity in the thoracic aorta of the dog as determined by Auliker & al (1970)

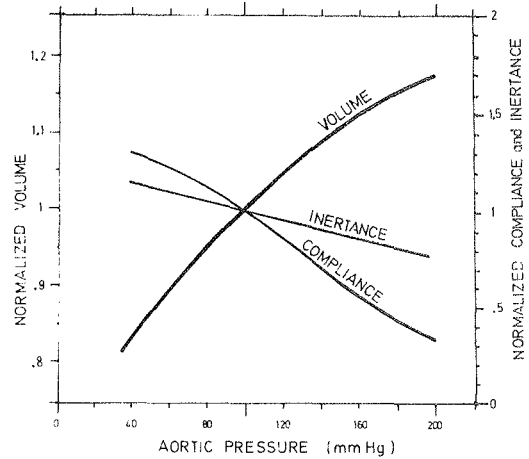


Figure 3.4B. Calculated vessel compliance and volume as functions of aortic pressure. Explained in text.

If the pulse pressure becomes large (as would be expected in older aortas), or if a large transmural pressure change (which may be the result of a Valsalva maneuver) is encountered, a linear pressure-volume relation may be too coarse an approximation.

A linear model will exhibit a wave velocity that is independent of transmural pressure - and it is only a good approximation for a limited range of mean pressures. If we can measure the wave velocity we may use this information to estimate compliances (Chapter 6 p. 78).

In the line with most previous models of the arterial system (Snyder and Rideout 1968, de Pater 1966) we have linearized the pressure volume relation. The errors caused by this approximation should become most prominent when trying to simulate elderly aortas, where the greatest nonlinearities (Wagner and Kapal 1952), as well as increased pulse pressures are found. Moreover the distal pressure pulse (femoral artery) can be expected to rise less steeply in a linear model than in a nonlinear (Anliker and coworkers 1970).

The relative change of segment volume due to a pulse pressure of 40 mmHg (fig. 3.4B) indicates a diameter excursion of 5%, a

value in accordance with the angiographic measurements by Greenfield and coworkers (1967) on the human ascending aorta.

So far we have tacitly assumed that the segment pressure is a static function of the volume. Arterial walls are, however, of a biological material that exhibit a frequency dependent modulus of elasticity. Measurements by Bergel (1961) on excised arterial and aortic strips demonstrate that the ratio dynamic/static modulus of elasticity (frequencies > 0.5 Hz) in the aorta is 1.15 - 1.2, a value which increases to 1.7 for the carotid artery. His data does not indicate that the variation of stiffness (or compliance) in the normal/harmonic frequency range (1 - 15 Hz) is of such a magnitude that it becomes an important determinant of the dynamic behaviour of arterial segments. The same can probably also be said about hysteresis effects - although these may be seen in the dynamic "in vivo" pressure diameter relations measured by Remington (1962).

Although more complicated representations may be preferred for a specialized study of arterial wall dynamics, a linear viscous model is postulated in most published models (Snyder and coworkers 1968, de Pater 1966) and is also used here:

$$p = \frac{1}{C_i} \left[\int (q_i - q_{i+1}) dt + C_i D_i (q_i - q_{i+1}) \right]$$

where D_i is a "damping factor". $C_i D_i$ has the dimension of time. The effect of this damping applied to the aorta model can be seen from figure 3.5, where panel A is a recording of ascending and abdominal aortic pressure when $D_i C_i = 5$ msec and B shows the same pressure when $D_i C_i = 2.5$ msec for all aortic segments. We observe that the viscous property hardly influences the time course and propagation of pressure pulses.

The damping term acquires another significance when applied to peripheral branches (p. 48).

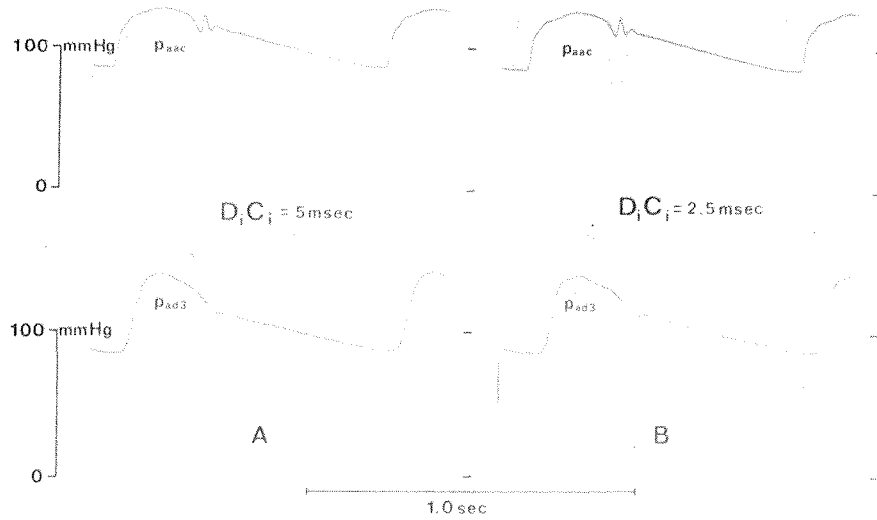


Figure 3.5. The influence of the damping terms $D_i C_i$ on pressure wave-forms in the ascending (p_{aac}) and abdominal (p_{ad3}) aorta. To the left the "normal" damping ($D_i C_i = 5$ msec), to the right reduced damping with $D_i C_i = 2.5$ msec.

Block diagram of an arterial segment

It is convenient to express the mathematical model of the vessel segment in block diagram form as shown in figure 3.6.

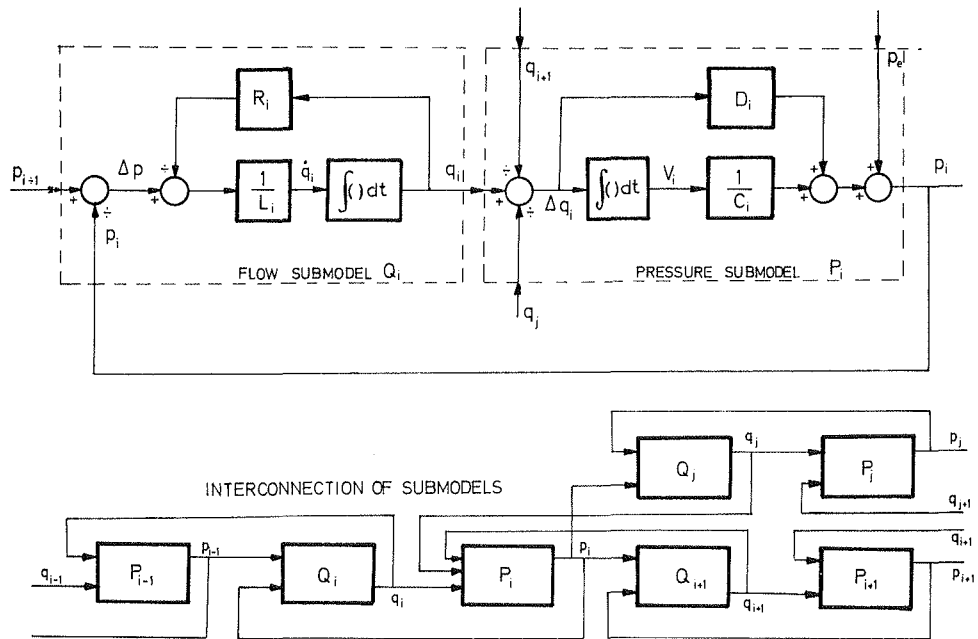


Figure 3.6. Upper panel: Block diagram of arterial segment i . The model is divided into a flow submodel Q_i and a pressure submodel P_i , see text for further discussion. Lower panel shows interconnection of such submodels to form a model of the vessel region depicted in figure 3.3.

The segment is divided into two submodels, the first having pressure as input variable and flow as the output variable (flow submodel Q_i). The second has flow and external pressure as inputs and pressure as the output variable (pressure submodel P_i).

The first subtraction yields "driving pressure" Δp . We subtract from this the product $R_i q_i$ which is the pressure drop due to the viscous flow resistance. The resulting pressure difference accelerates the column of blood. After multiplication by the inverse inertance $1/L_i$ we obtain the acceleration of flow \dot{q}_i which after integration yields q_i .

We subtract the flow(s) out of the segment, q_{i+1} (and q_j) from q_i , the result is net flow Δq_i into the segment. Integration of Δq_i gives segment volume and multiplication of this with the inverse compliance $1/C_i$ yields (static) transmural pressure of the model. Adding to this the vessel environmental pressure p_e and the damping term $D_i q_i$ we have found segment pressure p_i .

The lower half of fig. 3.7 depicts how the submodels are interconnected to represent the piece of artery shown in fig. 3.3.

Electrical analogue of a vessel segment

The same equations and block diagrams that are used to describe the pressure-flow relations of a vessel segment can also be attributed to lumped electrical transmission line model as shown in fig. 3.7. The analogy between the hydro- (or hemo-) dynamic and electrical

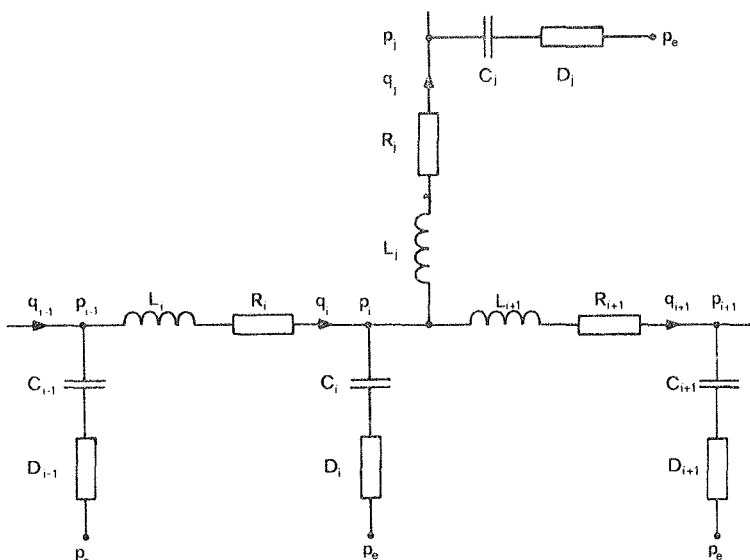


Figure 3.7.

The representation of an arterial model by electrical symbols. The figure illustrates the piece of artery shown in figures 3.3 and 3.6.

Table 3.1 - Electrical analogue variables and parameters

Hydrodynamic	Electrical
q - flow	i - current
V - volume	Q - charge
p - pressure	u - voltage
R - Resistance	R - resistance
L - Inertance	L - Inductance
C - Compliance	C - Capacitance

variables and parameters are listed in table 3.1.

The symbols used in fig. 3.7 represent a convenient shorthand notation of the block diagram shown in fig. 3.6. We may then use these electrical symbols to designate the structure of a hemodynamic model.

Input impedance

We may use the concept of impedance to describe the pressure-flow relation in the arteries. Supposing linearity and purely sinusoidal pressure variations of a variable angular frequency ω we have

$$Z(j\omega) = \frac{p(j\omega)}{q(j\omega)}$$

where $Z(j\omega)$ is the complex frequency dependent impedance. We may express $Z(j\omega)$ by its modulus $|Z|$ and its phase θ . If sinusoidal pressure and flows are present we have:

$$|Z(j\omega)| = |p(j\omega)| / |q(j\omega)|$$

where $p = |p(j\omega)| \sin(\omega t + \theta)$
and $q = |q(j\omega)| \sin(\omega t)$

Any periodic waveform may be represented by its harmonic components, and the postulated equations may be applied to these. The concept of impedance is therefore not limited to purely sinusoidal waveforms.

Beyond certain anatomical locations in the arterial tree, we are not interested in the wave transmission phenomena of the vessel(s), the important property is the input characteristic or the pressure-flow relation of the branch considered. Therefore we represent the distal parts of the arterial system by input impedance approximations. These are named terminating segments. The structure of these segments is assumed to be similar to the intermediate segments and is expressed in shorthand form in figure 3.8. But the circuit elements are not (as in the case of intermediate segments) directly deductible from geometric and hemodynamic considerations.

Thus C is not directly corresponding to the entire volume compliance of the arteries and arterioles beyond this location. As the value of R_p (the peripheral resistance) is usually an order of magnitude larger than $Z_o = \sqrt{\frac{L}{C}}$, the damping of this resistor on the resonant $L - C$ network will be quite small, and in addition we have introduced a viscous damping D . This is not only signifying the vessel wall viscosity, but also damping due to random branching (Pollack 1968), and the general characteristic impedance matching of the distal vessels. Considerable uncertainties exists in determining the terminating segment parameters and the figures listed in table 3.2 must be regarded as preliminary.

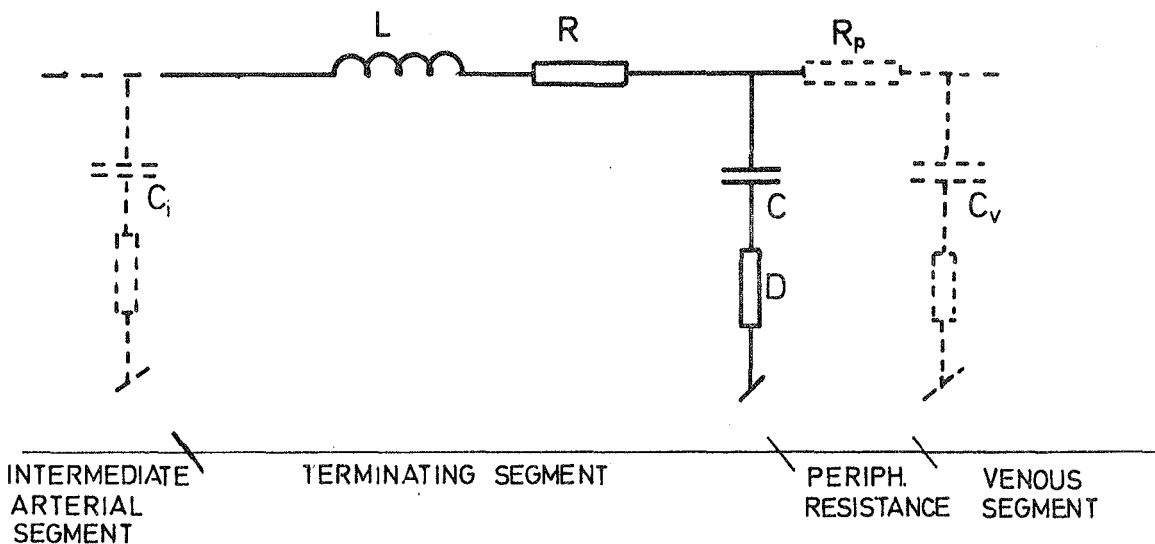


Figure 3.8. The model of a terminating segment. See text for explanation.

Impedance considerations are only justifiable when the system is linear - or fairly close to linearity. As previously noted, a large pulse pressure may exceed the limits where the linear approximation is appropriate. When introducing nonlinear pressure-volume relation of the vessel segments in order to achieve a more realistic description of arterial dynamics under varying mean- and pulse pressures conditions, impedance considerations should not be applied to evaluate the dynamic relations, and we must resort to time-domain methods of analysis.

The arterial tree and its representation in the model

The basis for deciding the arterial model structure is the choice of where we want a faithful representation of pressure and flow dynamics. As we shall compare the model with measurements from catheterizations, or from non-traumatic methods, we shall first consider where the available sites of measurement are located.

By inserting a catheter into the femoral artery (figure 3.9), and advancing this upstreams, pressure measurements from the femoral and iliac arteries, the abdominal, thoracic, and even the ascending aorta may be obtained. If the same catheter carry an electromagnetic or ultrasonic probe, flow velocity information might also be made available. Direct measurements of instantaneous blood flow in the aorta is presently not possible without surgical interventions. Recently, the development of external ultrasound doppler instrumentation shows promise of obtaining the velocity of flow in the aortic arch or the start of the decending aorta (Baker 1973, Light & Cross 1972).

Of the branches starting from the aortic arch, the common carotid arteries at both sides of the neck are coming quite near to the surface so that external measurement by pulse transducers and ultrasound velocity doppler is quite feasible.

Proceeding further downstream the aorta, passing its bifurcation, and following the external iliac artery, we come to a location at the beginning of the femoral artery where it comes quite near to the surface - and here again is a good location for external measurements (and needle puncture).

Beyond these locations, the arterial dynamics are represented by impedance approximations. It might be a question whether a model

of the wave propagation properties through the subclavian, axillary and brachial arteries is a worthwhile addition. Here again are suitable sites for external measurements and needle punctures, but since we are primarily interested in the aortic dynamics (since most of the arterial compliance is situated there), it does not seem necessary to include this branch to obtain further important information by comparing model variables with the possible measurements at this location.

In figure 3.9 A the aorta and its main branches are illustrated. It follows from this figure that the large branches are located in three main regions, corresponding to the aortic arch, the abdominal aorta and its bifurcation. Consequently we concentrate the model arterial tree into three main branches corresponding to these regions.

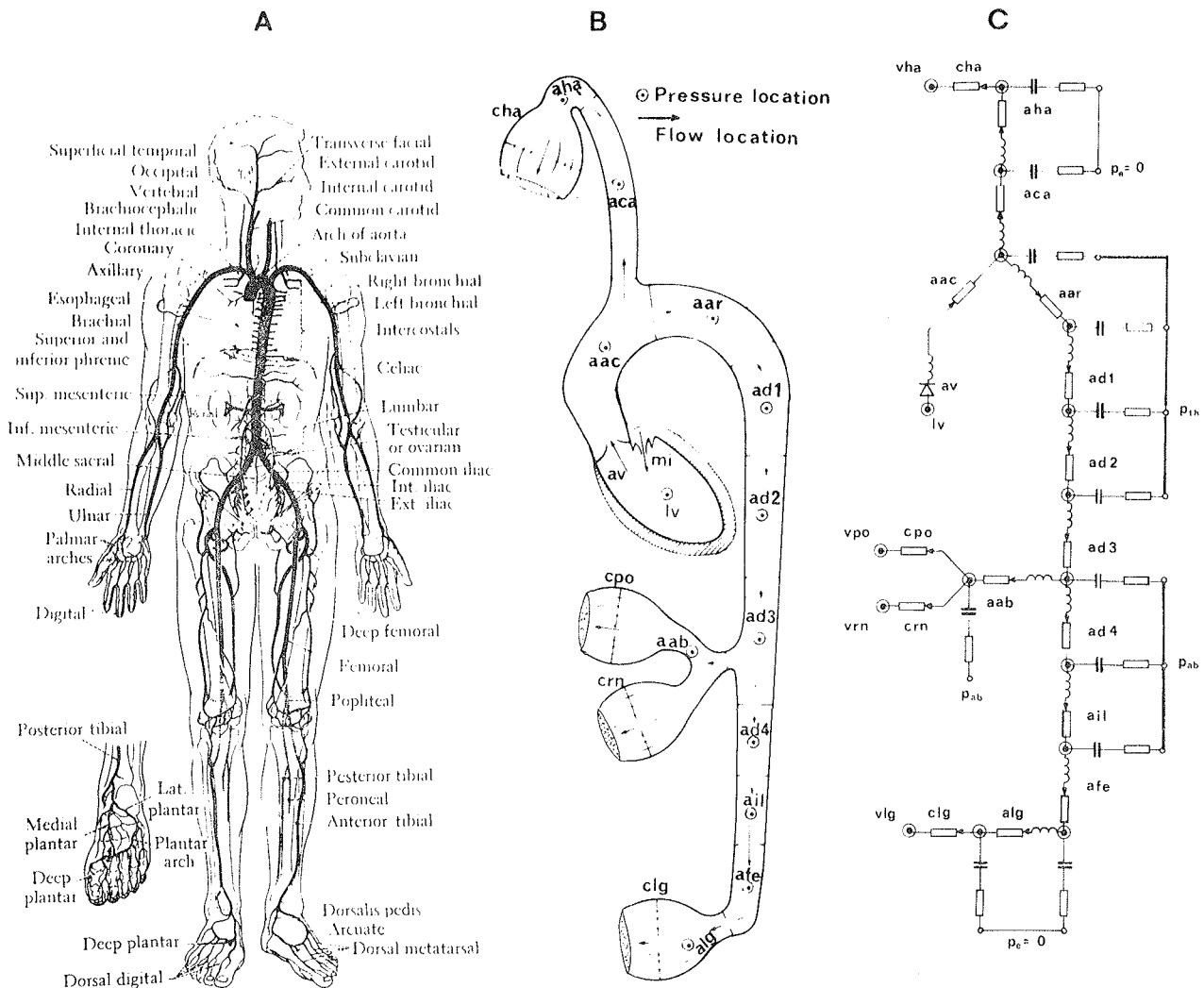


Figure 3.9.

A. An overview of the human arterial system after

B. Schematic representation of the arterial model. See table 3.2 for abbreviations.

C. The arterial model expressed in shorthand electrical symbols.

The simplification involves the use of one model branch to represent the parallel of two or more real arteries. The inertance and compliance coefficients and the input impedance of this representation do not correspond to the single arteries but to the parallel of these. Likewise the flow in the single model branch is the sum of the corresponding arteries. This way of reducing the complexity of an arterial model have been applied previously by for example Snyder and coworkers (1968).

We shall now proceed to a more detailed discussion of the segmentation of the arterial system into a discrete representation.

The aortic and arterial segmentation

The primary factor to be considered when deciding the number of segments used to represent the aorta and arteries, is the bandwidth of the lumped approximation.

For increasing frequencies the correspondance between a transmission line and its lumped approximation grows progressively less, both with regard to amplitude and phase characteristics. In the aorta, the dynamically dominant parameters are the inertance and compliance, as the viscous resistance and wall damping are small. We denote by f_0 the resonant frequency of the segment with parameters L and C .

$$f_0 = \frac{1}{2\pi\sqrt{LC}}$$

This frequency is a measure of the bandwidth of the approximation.

If the harmonic content of arterial pressure and flow pulses, is analysed, relatively small components are found beyond 10 Hz in the aorta (Dyken 1970). It may be assumed that a model having f_0 in the region of 20 Hz will be able to reproduce quite well these pulses (Snyder & al 1968). In building a model that is flexible, to allow the simulation of arterial systems exhibiting different compliance characteristics, we cannot give a general answer to which frequency the approximation is reasonable. In order to achieve a good approximation with a minimum of segments, we have chosen to divide the aorta into 6 segments having nearly the same f_0 . For the "standard" compliance $f_0 \approx 14$ Hz for the aortic segments. As the wave-velocity is:

$$c = \frac{1}{\sqrt{CL}}$$

this segmentation philosophy means that the length of a segment is proportional to the wave-velocity of the corresponding part of the aorta. As the wave velocity increases towards the periphery, probably due to an increase in stiffness of the wall material, a model segment also represent a longer portion of the vessel.

As stated previously, the pressure and flows of the lumped approximation are referred to different spatial locations. Fig.3.9 indicates the approximate anatomical localization of this representation. Segment *aac* represents the ascending aorta and the proximal portion of the aortic arch, while *aar* represents the distal portion of the arch. *ad1*, *ad2* represent the thoracic descending aorta and *ad3*, *ad4* the abdominal.

The left common carotid and subclavian arteries are together with the brachiocephalic trunk represented by one branch in the model. The segment *aca* branches from the aorta at location *aac*, and is meant to represent the transmission time and properties from the aorta to the left or right common carotid artery where external pulse measurements are readily available. The flow q_{aca} is the sum of the flows into the abovementioned arteries. We assume the flow to be $q_{aca}/2$ in the brachiocephalic trunk at the point just before this bifurcates into the right subclavian and right common carotid arteries.

aha is the head and arms terminating segment representing the parallel of the impedances seen in the common carotid and subclavian arteries.

The intercostal arteries branching from the thoracic aorta are relatively small and are omitted in the model.

The next major site of branching is just below the diaphragm in where *arteria coelica*, *arteria mesenterica cranialis* and *arteria renalis* take a major portion of the cardiac output to the intestines and kidneys. We represent the parallel of all these branches and also the minor arteries of the abdomen by a terminating segment *aab* connected to the abdominal aorta at *ad3*.

The aorta bifurcates into the 2 common iliac arteries. The abdominal aortic pressure p_{ad4} is meant to be located near this bifurcation.

To represent the wave transmission from the bifurcation to the external measurement and the needle puncture location in the femoral arteries, just before it branches into the femoris arteries, 2 intermediate segments are necessary, and are named a_{il} (iliac artery) and a_{fe} (femoral artery). The common iliac artery branches into the internal and external iliac arteries. a_{il} represents the parallel of these. Strictly we should incorporate in parallel with a_{fe} an input impedance, at the transition from the iliac to the femoral artery to account for the dynamical behaviour of the branches to the internal iliac artery. But as these branches are short and relatively narrow compared with the branches associated with the external iliac artery (supplying the leg), we shall not make a too excessive error in letting a_{fe} and the leg terminating segment a_{lg} represent all branches to the common iliac artery. The real femoral artery flow is supposed to be $0.35 \cdot q_{afe}$ (q_{afe} in the model represent the flow through all branches, including the femoral artery, of the common iliac artery).

The numerical values of the arterial model are found by comparing a variety of sources (Snyder & al 1968, de Pater 1966, Beneken & de Wit 1967). They are tabulated in table 3.2. The compliance of a certain segment is a fixed fraction of C_{ao} ("total aortic") compliance. The inertance and resistance parameters are assumed to have fixed values at the present stage. This description implies a fixed (or standard) elastic and geometrical tapering of the arterial tree - but it allows the elasticities to be varied.

Instead of tabulating the damping factor D (figure 3.9) we find it more meaningful to give the corresponding time constant CD in msec.

Another significant parameter that is important in a discussion of arterial dynamics is the characteristic impedance of a segment defined by:

Table 3.2

Index	C_i Compliance $\frac{\text{ml}}{\text{mmHg}}$	$C_i D_i$ Damping timeconst. msec	L_i Inertance $\frac{\text{mmHg}}{\text{mlsec}^{-2}} 10^{-3}$	R_i Resistance $\frac{\text{mmHg}}{\text{mlsec}^{-1}} 10^{-3}$	Z_o Charact. impedance $\frac{\text{mmHg}}{\text{mlsec}^{-1}} 10^{-3}$		P_e External pressure
aac	$0.23 C_{ao}$	10	0.6	0.2	55	Ascending aorta	} P_{th}
aar	$0.23 C_{ao}$	7	0.8	0.2	65	Aortic arch	
ad1	$0.17 C_{ao}$	5	1.3	0.4	95	} Descending aorta	
ad2	$0.17 C_{ao}$	5	1.3	0.4	95		
ad3	$0.12 C_{ao}$	5	2.1	0.8	140		} P_{ab}
ad4	$0.08 C_{ao}$	5	2.7	1.5	170		
ail	$0.032 C_{ao}$	5	5.0	6	370	Iliac arteries	} P_{ab}
afe	$0.030 C_{ao}$	10	9.0	20	510	Femoral arteries	
aca	$0.040 C_{ao}$	10	6.0	10	380	Carotide subclavian arteries	} 0
aha	$0.15+0.17 C_{ao}$	$330T_p$	13.0	40		Head & arms arteries	
aab	$0.10+0.11 C_{ao}$	$100T_p$	6.0	10		Abdominal arteries	P_{ab}
alg	$0.10+0.11 C_{ao}$	$150T_p$	13.0	40		Leg arteries	0
av	0.04	1	0.6^* } same as } aac	0.2^*		Aortic valve $V_{bak} = 2.5 \text{ ml}$	
"Standard" values: $C_{ao} = 0.87 \text{ ml/mmHg}$, $T_p = 1$, $p_{ab} = 0 \text{ mmHg}$ and $p_{th} = -4 \text{ mmHg}$							

$$z_o = \sqrt{\frac{L}{C}}$$

In the arterial system, z_o increases towards the periphery due to geometric and elastic tapering. In a lumped model the changes in impedance are represented at discrete intervals corresponding to the segment boundaries. These changes in characteristic impedance are important aspects of the dynamic transmission of pressure and flow waves. The left ventricle faces a relatively low impedance (at $f \approx 1$ Hz) in the elastic aorta, facilitating the ejection of the stroke volume, while the total peripheral resistance (the parallel of all systemic resistance) is 10 - 20 times this impedance (Patel & al 1965). The characteristic impedance for the "standard" parameters are listed in table 3.2.

At locations where the characteristic impedance changes, reflections will occur, i.e. some of the forward travelling energy is reflected in a wave travelling backwards. The waveform is the result of a superposition of many reflections from different locations. One effect we should expect of the impedance changes is an increase in the dynamic pressure components towards the periphery. This follows from simple energy considerations. An increase in impedance results in a larger pressure/flow ratio, and since the product of these variables is constant in a supposedly loss free transmission line, pulsatile pressure will increase, and the flow decrease. The increase in pulse pressure can also be interpreted in terms of reflections.

The aortic valve model

The structure of the assumed aortic valve model is shown in figure 3.10. In the open state the valve and nearest vessel segment are represented by inertance and resistance effects similar to the other arterial segments (figure 3.10 A)

In the closed state, the valve is assumed to be nonleaking. The valvular membranes are elastic and may be represented by a compliance. The flow "through" a valvular ring will distend (or relax) the closed elastic membranes. The same flow will increase (or decrease) the effective ventricular volume (i.e. that which distends the myocardial fibres).

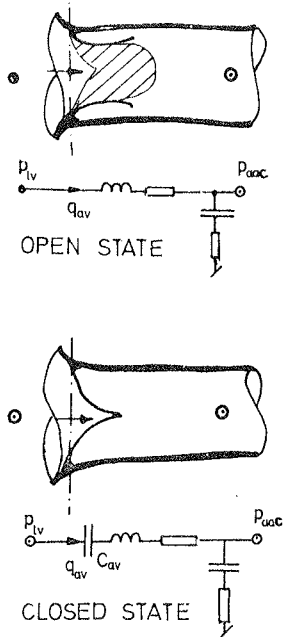


Figure 3.10.

Upper panel illustrates aortic valve in open state. The electrical analogue is as shown below, and is similar to that of an aortic segment. The blood volume indicated by the shaded area flows back into the ventricle during closure of the valve.

The lower drawing illustrates the valve in the closed state. The compliance C_{av} represent the elasticity of the valvular membranes.

The equation for "flow" through the valve in the closed state is:

$$q_{av} = C_{av} \frac{d(p_{lv} - p_{aac})}{dt}$$

The aortic valve model opens when the left ventricular pressure exceeds the ascending aortic pressure.

It can be noticed on dynamic records of ascending aortic flow (Spencer & Greiss 1962) that some back flow occurs before

the valve closes. The same authors find that the backflow volume is remarkably constant in the same animal over wide ranges of stroke volume and arterial pressure.

The model is closed when a certain volume V_{bak} (figure 3.10) has flowed back.

The parameters C_{av} , V_{bak} , as well as ascending aortic segment inertance L_{aac} and resistance R_{aac} characterize the aortic valve model. Numerical values for a "standard" cardiovascular system were given in table 3.2.

The peripheral resistance

The main resistive effects in the systemic circulation are located in the small vessels: the arterioles, precapillary sphincters, capillaries and venules. For a certain part of the body, these resistances are arranged in series, so that the peripheral resistance of this part is the sum of resistances of these different vessels. In the model we use a single element, R_p in figure 3.8, to represent the peripheral resistance, leading from the capacitance C of the terminating arterial segment over to the venous capacitance vessels, represented in the figure by C_v .

The peripheral resistances of different pathways from the arterial to the venous system are arranged in parallel. In this context it may be more convenient to use the term (total) peripheral resistance for the parallel of all branches of the systemic circulation.

Unless specifically stated otherwise in the text, a fixed distribution of the cardiac output on the various systemic bed is assumed, and the local peripheral resistances are functions of the total peripheral resistance, R_p as shown in table 3.3.

When the total peripheral resistance changes, we assume the change to be proportional in all parts of the circulation.

Table 3.3

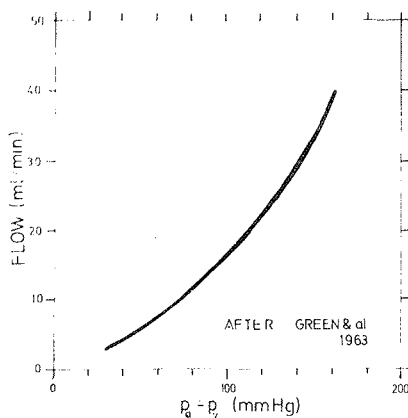
Abbr.	Anatomical location	Resistance
cha	head and arm vessels	$4 \cdot R_p$
clg	leg vessels	$10 \cdot R_p$
cpo	vessels associated with the portal system	$3 \cdot R_p$
crn	renal (and other not associated with cpo) vessels	$3.5 \cdot R_p$

"Standard" value: $R_p = 1.0 \text{ mmHg/mlsec}^{-1}$.

The application of a constant resistance to represent the peripheral pressure-flow relation is based on a linearization of this relation:

$$q_c = (p_a - p_v) / R_p$$

where q_c is the flow, p_a and p_v arterial and venous pressures. Experiments by Green and coworkers (1963) demonstrate that the peripheral pressure-flow relation is upwards curvilinear as shown in figure 3.11. This phenomenon can be explained by an increase in arteriolar and capillary diameter when the vessel is extended by an increasing transmural pressure. This nonlinear effect is



not very marked in the normal physiological range (80 - 120 mmHg), and the relation can be considered linear without introducing significant errors.

The restitutive effects of larger arteries and veins are small compared with the peripheral vessels - and we do not include these in our definition of peripheral resistance.

Figure 3.11. Peripheral pressure-flow relation after Green & al (1963).

Chapter 4.

MODELS OF MEASUREMENT PROCESSES

Introduction

A measurement system introduces noise as well as static and dynamic errors in the signals. The stochastic measurement noise is not significant in physiological pressure recordings. Proper calibration procedures may reduce the static errors to acceptable levels. We are then left with the dynamic errors, which may become serious, in particular when pressure is measured by an extracorporeal transducer connected to the measurement site through salinefilled catheters or needles.

In principle, the dynamic errors can be eliminated by an "inverse filter" as shown schematically in figure 4.1.

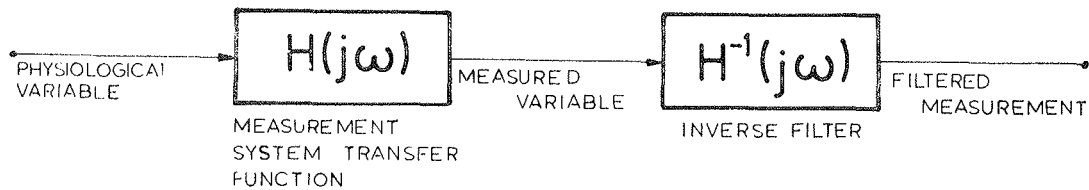


Figure 4.1. Use of an inverse filter ($H^{-1}(j\omega)$) of the measurement process $H(j\omega)$ to restore the course of the original physiological variable.

The frequency dependent measurement system transfer function is $H(j\omega)$. If this is known, a more or less accurate inverse function $H^{-1}(j\omega)$ can be used to filter the measurement signal. Theoretically, the signal processed in this manner should follow the course of the physical variable. In practical applications, this ideal is hard to achieve.

If our objective is to compare the time courses of physiologi-

cal quantities with the simulated variables, we can use the approach outlined in figure 4.2.

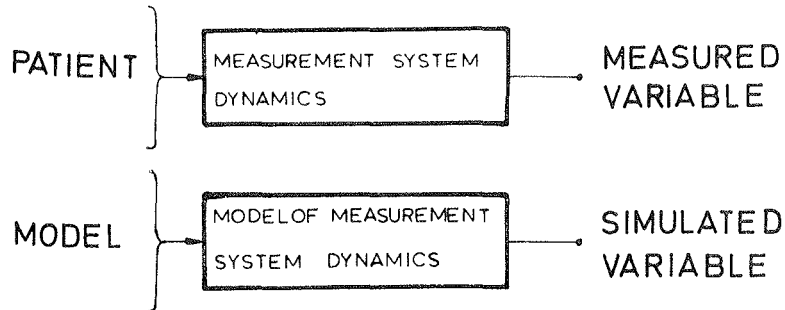


Figure 4.2. Method used in present study to minimize measurement process errors. Both variables are similarly distorted if the model of measurement system dynamics is representative.

Again, the measurement system transfer function distorts the physiological measurements. Now we process the appropriate model variable with a filter or a model corresponding to the measurement system transfer function. Ideally, similar dynamic errors are introduced in both signals. A comparison is then justifiable.

In case of the electromagnetic flowmeter, the transfer function may be approximated by the two first order lowpass filters having the transfer function:

$$\frac{1}{1 + T_1(j\omega)} \cdot \frac{1}{1 + T_2(j\omega)}$$

The numerical values of T_1 and T_2 depend upon the flow probe and the lowpass filter chosen on the flowmeter. These parameters are tabulated in table 8.2.

The shape of the "real" and the critically damped pressure curves are for all practical purposes identical.

The model of the pressure measurement system is used in all circumstances where the model pressures are compared with physiological or clinical measurements.

Chapter 5.

SIMULATION METHODS

The equations and functional relationships proposed in the previous chapters are meaningful only if we can solve them and compare the solutions with measurements obtained from the human or animal cardiovascular system. The solutions of differential or integral equations such as the proposed model is composed of, are functions of the independent variable time, and the results can be presented as the time courses of the different variables.

Of practical means to solve the differential equations in real time, we were left with analog computation techniques, as fast enough digital algorithms were not available when this study was initiated. The decision to build a special purpose analog computer was taken early in the project, as it soon became evident that a realistic model would exhaust the available general purpose analog computer by a factor of 3 for most computing elements.

The idea of using cheap modern integrated operational amplifiers for the construction of analogues of vessel segments was proposed by Rideout's group (Grewe & al 1969). As this approach seems to be accurate enough, we built the entire analogue (and estimator, see chapter 6) using in addition integrated circuit multipliers, diodes and transistors for non-linear function generation, and complementary MOS digital IC's for switching and other logic.

The design of the electronic circuits is essentially based upon the block diagrams. For each of the elements we design an electronic circuit that perform the specified operation (such as addition, multiplication or function generation) on the input

variable voltages and gives an output voltage which is analogous to the output variable of the block diagram operator. The interconnection of these circuits may be called an electronic analogue of the system; we shall, however, also use the term model to signify this special purpose analog computer. The electronic diagrams of the left ventricular and the arterial model are included in appendix 2.

In an analog computer, the variables are represented as voltages. For modern integrated circuits the range from -10 to +10 volt is most convenient to use. The scaling factors relating the units of the real variables (for example mmHg, or ml/sec) to computer variable units (volts) are listed in table 5.1.

Table 5.1. Scaling of the special purpose analog computer.

Variable	Notation	Scaling (units/10V)	Unit
pressures	p	200	mmHg
flows	q	1000	ml/sec
l.v. volume	V_{lv}	400	ml
l.v. volume	V_{lvn}	2	dimensionless
tension	σ	20	g/mm^2
length	l_f, l_{seo}, l_m	1	dimensionless
length	l_{sac}, l_{se}, l_{ce}	2.0	$\mu (= 10^{-6}m)$

If these values are exceeded by more than 20% (for example if the pressure to be simulated exceeds 240 mmHg) the operational amplifiers saturate, and errors will occur. We must therefore always check that the key variables do not go beyond their respective limits.

Chapter 6.

PARAMETER ESTIMATION

Introduction

The behaviour of the model may be modified by changing its parameters. If our purpose is to simulate an individual left ventricle and arterial system, we must find a method to determine or estimate a set of parameters that results in a correspondence between the simulated and the real cardiovascular behaviour.

The cardiovascular system is observed through the measurement system. The output of this are electrical voltages analogous to pressure, flow, velocity, volume, length etc. at different anatomical locations. The output of the model are also electrical voltages representing simulated pressure, flow etc.

The measured and the corresponding simulated variables may be compared in real time.

Some noise and distortion are invariably present in the measurements, in the recording system and in the analogue computer. Also, the model is a simplified description of infinitely complex cardiovascular phenomena. The simulated variables will therefore deviate from the measured. The difference between the measurement and the corresponding simulated variable is called the error.

The available measurements may be used to estimate model parameters. The general principle is illustrated in figure 6.1. The parameters are adjusted manually or automatically until a criterion of the errors is minimized.

Applied without appropriate considerations, such an approach may give quite erroneous results. Attempting to adjust too many parameters from the available measurements may result in nonunique solutions. In this study, the number of parameters to be estimated is deliberately reduced to a bare minimum. Thereby, uniqueness of the estimates is assured, and the approach and its limitations are more easily recognized.

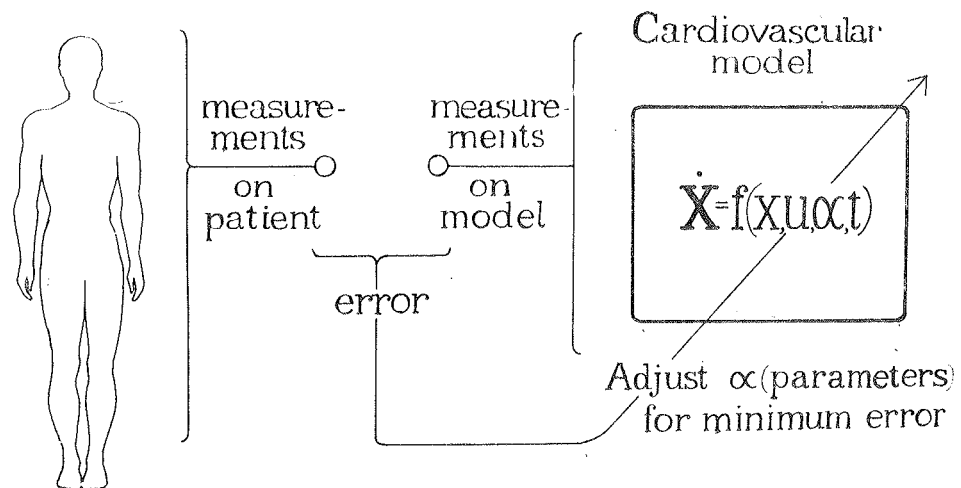


Figure 6.1. Outline of the parameter estimation approach. The measurements from the cardiovascular system are compared with the analogous "measurements" on the model. If a discrepancy, or error is found, we adjust (either manually or automatically) the parameters until a satisfactory simulation of the measured variables is obtained.

If we succeed in determining a unique set of parameters that matches the model to an observed cardiovascular behaviour, the next obvious question is: How meaningful is the individually matched model from a physiological or clinical viewpoint? If the model is too crude and based upon unrealistic assumptions, it is not appropriate to use in the interpretation of cardiovascular events. Therefore an investigation of the ability of the model to represent the real system is necessary, and a study on this is presented in chapters 8 and 9.

In addition to the parameters, it is necessary to identify the input variables to the system. When we consider the left ventricle, its degree of filling is influenced by many factors in the right heart and venous system. In order to achieve a correct return flow to the left heart model, these parts of the circulation must be realistically represented. This is impractical when the left ventricular and aortic dynamics are in the main focus of interest. Two alternatives are considered for the solution of this problem:

Estimator I: If a measurement such as left ventricular diastolic pressure, volume, or muscle length is available, this may be used to control the (model) left ventricular filling so that it corresponds to the observation.

Estimator II: No such measurement is available, and the end-diastolic volume has to be assumed. Then the estimates of the left ventricular parameters are uncertain, but the ventricular model may still be able to generate a realistic input flow to the arterial system so that the arterial parameters can be estimated with the same confidence as with estimator I.

The parameters are divided into 4 main categories (the definitions of the first 3 are similar to those of Donders & al 1973).

A (apriori) parameters, or rather constants, are listed in chapters 2 and 3. These are assumed to reflect general properties of the left ventricle and arterial system, and have the same values for all individuals.

B parameters are estimated on the basis of observations not used in the real-time estimation. These are assumed to be stationary, but may differ from one individual to another.

C (variable) parameters are estimated by automatic methods.

M (manual) parameters are estimated by the operator of the system on the bases of visual feedback from a time-mode display of the variables. These are assumed to be stationary.

The estimation procedure proposed in the following sections do not claim any optimality. In this pilot study simple and direct methods of parameter estimation has been preferred.

A brief error analysis is presented at the end of this chapter, giving an indication of the accuracy of the proposed estimator.

Summary of B, C and M parameters

The arterial model is characterized by 3 parameters. The aortic compliance C_{ao} varies with age and blood pressure, but may be considered relatively constant over the observation period if the blood pressure level does not change too much. The peripheral

damping timeconstant T_p (or impedance level) is also assumed to be relatively stationary. C_{ao} and T_p are therefore estimated manually (M-parameters). The total peripheral resistance R_p vary quite quickly in response to environmental and internal changes. An automatic feedback estimator should be considered for this parameter.

The left ventricular model is characterized by 4 parameters. The myocardial volume V_m may be roughly estimated from chest x-rays or ultrasound echo techniques (B-parameter). For the present study V_m is assumed to be 230 ml for a normal heart. The maximum velocity v_{max} and the maximum active fibre tension σ_{max} characterize the contractile properties of the myocardium. v_{max} and σ_{max} may change quickly in response to control influences. The same considerations also apply to the duration of active state T_{sys} , and these 3 parameters should be estimated by automatic methods.

Likewise, the input variable to the left ventricular model, the mitral valve flow q_{mi} change considerably on a beat to beat basis, and automatic control of this variable is preferred.

The heart rate HR is estimated by synchronization of model and patient heart beat.

The parameters are listed in table 6.1.

In addition to the left ventricular and arterial parameters, the catheter-manometer system characteristics must be estimated. This is achieved by a manual curvefitting procedure (M-parameters).

First, the estimation methods for the C-parameters will be described. It is assumed that the M-parameters have realistic estimates obtained by methods described later in this chapter.

Symbol	Name	Category	"Standard" value	Unit
v_{max}	CE max. velocity	C	2.2	sec^{-1}
σ_{max}	CE max. tension	C	10.0	g/mm^2
T_{sys}	systolic duration	C	470	msec
EDV	l.v.end-diastolic volume	C	150	ml
V_m	l.v.myocardial volume	B	230	ml
R_p	peripheral resistance	C	1.0	$mmHg/mlsec^{-1}$
C_{ao}	aortic compliance	M	0.87	ml/mmHg
T_p	peripheral damping timeconst.	M	1	dimentionless
HR	heart rate	(C)	72	min^{-1}

Table 6.1. Summary of parameters and input variables to be estimated.

Activation synchronization

The first step in the estimation procedure is to synchronize the patient and model heart beats. An ECG trigger circuit reacts to the steep upstroke of the QRS complex, and initiates the time-course of active state in the model (figure 6.2). In the heart muscle, there is a delay from the start of electrical activation until the force generating process is turned on (Sonnenblick 1965). This phenomenon is simulated by the variable time delay T_d shown in figure 6.2.

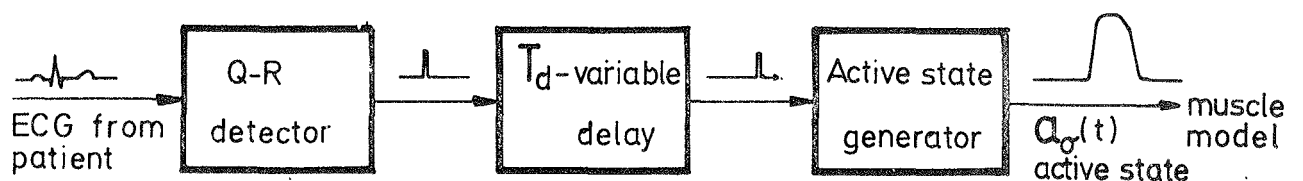


Figure 6.2. Block diagram of Activation synchronization circuit. Explained in text.

If a left ventricular pressure measurement is available, the proper value of this delay is determined by manually adjusting T_d until the foot of the model left ventricular pressure upstroke occur simultaneous with the measurement. Representative tracings are shown in figure 6.3. The point A, 10 mmHg above the left ventricular pressure at the onset of contraction is used as a comparison criteria. The delay is $T_d = 8$ msec in this simulation.

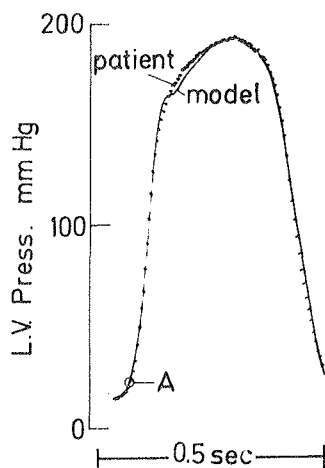


Figure 6.3.

Model and patient left ventricular pressure. Parameters as in table 8.2 pat. N.K. A indicates a point approximately 10 mmHg above the end-diastolic pressure where the comparison is made.

When a left ventricular pressure recording is not available, i.e. for estimator II, the value of T_d is chosen so that the active state is initiated on the R wave of the QRS complex.

Estimation of left ventricular end-diastolic volume

The left ventricular and arterial models described in this report are part of a closed loop model. But no individual estimation is performed on the venous, right heart and pulmonary circulation. Therefore the flow through the mitral valve will not necessarily be realistic. Given the time course of mitral valve flow, q_{mi}^0 , as predicted by the closed loop model, we may add to this an estimated incremental flow Δq_{mi} .

The total mitral valve flow is then:

$$q_{mi} = q_{mi}^o + \Delta q_{mi}$$

First, let us consider estimator I. The left ventricular pressure in diastole is a function of the ventricular filling. The error, defined here as the left ventricular pressure in the patient minus the analogous model pressure, is dependent upon the left ventricular volume in diastole. The error may be corrected if Δq_{mi} is controlled so that similar pressure courses are obtained in diastole. To this end, we design a feedback servosystem as illustrated in figure 6.4.

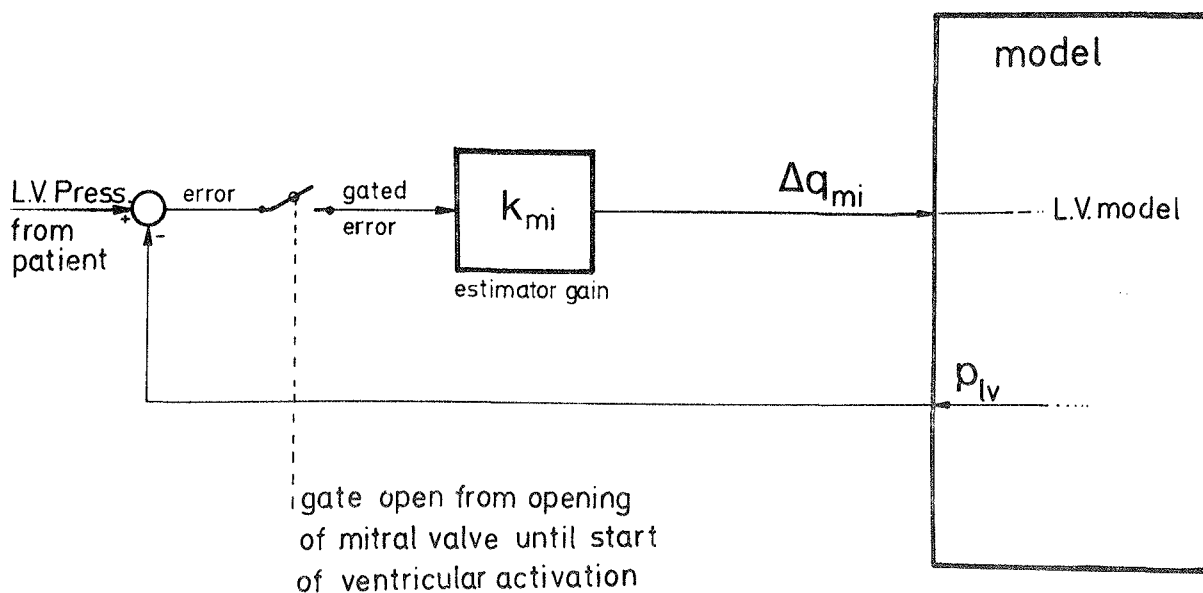


Figure 6.4. Block diagram of inflow estimator when a l.v. pressure measurement is available. The block diagram is explained in the text. The "standard" gain is $k_{mi} = 250 \text{ mlsec}^{-1} / \text{mmHg}$.

The pressure error is gated by an electronic switch and only the interval from opening of the (model) mitral valve until the onset of active state (QR detector) is used to correct left ventricular filling. The gated error is multiplied with a gain

constant, k_{mi} , and the product is the correction flow, Δq_{mi} , which is fed into the left ventricular model. If as an example, the model pressure is too low, Δq is positive, and the ventricular volume (and pressure) will increase.

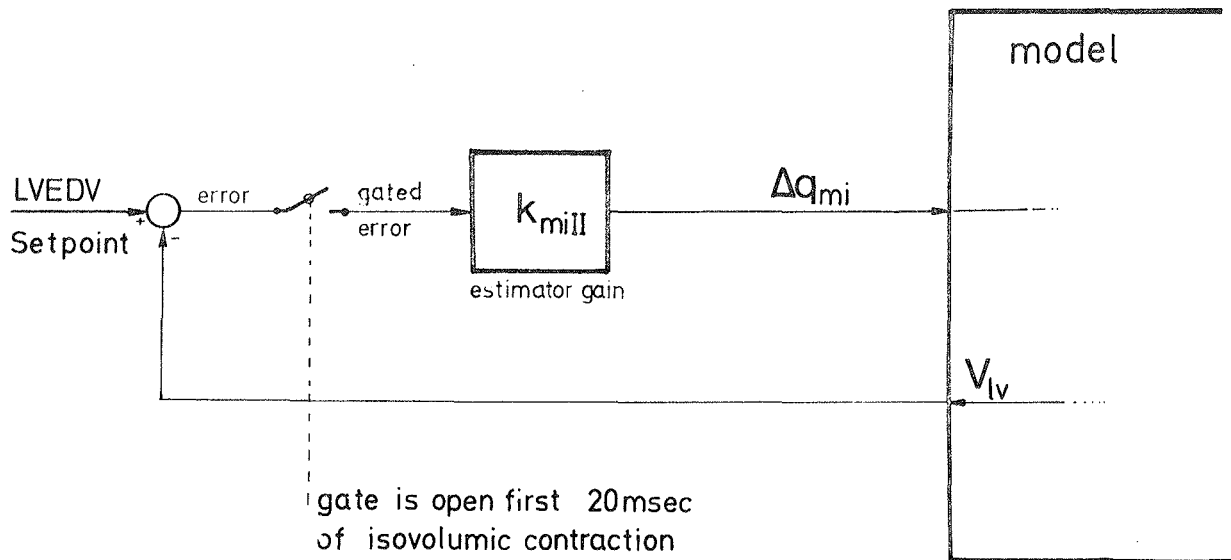


Figure 6.5. Block diagram of end-diastolic volume control system. "Standard" value of k_{miII} is 100 sec^{-1} .

The dynamic performance of this feedback system is dependent upon the gain k_{mi} . A large gain gives a short settling time.

In the estimator II configuration, no dynamic measurements of the left ventricular pressure, volume or dimensions are available. The mitral valve flow is then controlled on the basis of an assumed left ventricular end-diastolic volume using the scheme illustrated in figure 6.5.

The assumed volume is compared with the model volume, the difference is amplified, and used to adjust the corrective flow Δq_{mi} until the difference is zero. This correction is gated by the QRS trigger circuit so that only the first 20 msec of "isovolumic" contraction is used. The performance of this system is demonstrated in figure 6.16. It is clear that a high gain results in a practically constant left ventricular volume before the start of ejection.

Automatic estimation of parameters

The variables in the cardiovascular system follow characteristic patterns in each heart cycle. We may divide the courses of the variables into time intervals or windows. The error during an interval is dependent upon the parameter values. For each parameter it is prescribed an interval in which we assume that the error is particularly sensitive to the parameter under consideration. The error may exhibit both positive and negative values during an interval. We choose to design the estimator so that it estimates parameter values that result in mean errors that are close to zero during the intervals.* Thus the criterion is different from the minimum integrated squared error commonly used in estimation theory. The reason for the choice is the simplicity of the resulting estimator scheme. The method used to estimate a parameter is shown in figure 6.6. The error is the difference between the measurement and the analogous model variable. This error is gated. The gated error is zero except for the interval when the gate is activated.

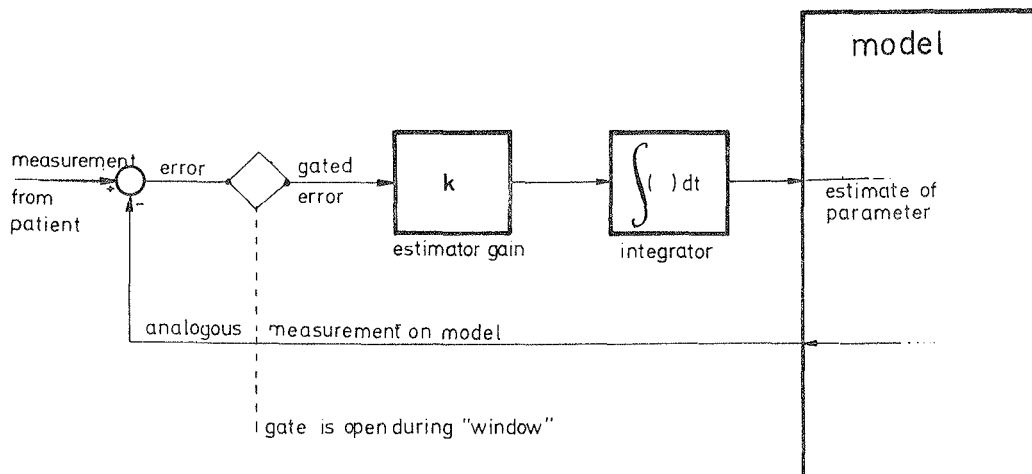


Figure 6.6. Estimation strategy used in the present study.

*The mean error may be both negative and positive. It is defined in the interval from t_1 to t_2 as $\frac{1}{t_2 - t_1} \int_{t_1}^{t_2} e dt$ where e is the error.

This interval we may envisage as a window through which the estimator observes the measurement. The gated error is multiplied with a constant, k , which is the estimator gain, and passed on to an integrator. The integrator output is the estimate of the actual parameter, and it is connected to the appropriate part of the model. If the input to the integrator is positive, its output will increase with time. The integrator will hold its value when the input is zero. If the measurement, the gate window timing and the gain constant are properly chosen, the integrator will stabilize on the value which results in zero mean error during the interval. All windows are defined and generated with respect to the model.

Let us first consider the estimator I configuration where left ventricular as well as aortic pressures are measured. On the model, we observe that a low v_{\max} gives a low rate of change of left ventricular pressure in the isovolumic contraction phase. This is in accordance with observations from experiments (figure 8.5). The v_{\max} estimator uses the time derivative of the l.v. pressure as measurement, and the isovolumic contraction phase as window.

We desire that the model ventricle faces the same aortic pressure as the real at the start of ejection. The diastolic pressure is strongly dependent upon the peripheral run-off conditions. The peripheral resistance is estimated using as measurement the aortic pressure and as window the isovolumic contraction period.

Thus the model ventricle starts its ejection against practically the same aortic pressure as the real. The pressure course in the ejection period is dependent upon the stroke volume, the rate of ejection and vascular factors. Since we have established practically the same end-diastolic pressures in the ventricles, we may now control σ_{\max} to change the stroke volume. We therefore estimate σ_{\max} using l.v. pressure as measurement and the ejection period as the window.

The remaining C parameter, T_{sys} , influences the length of ventricular systole. We use l.v. pressure as measurement and the isovolumic relaxation period as window. Estimator I is summarized in figure 6.7.

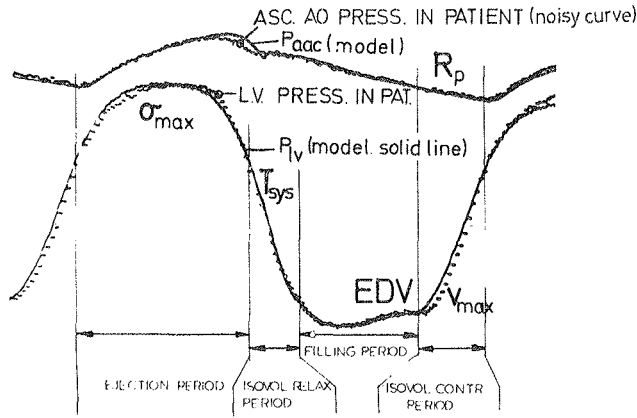


Figure 6.7.

Summary of estimator I. Measurements from patient E.T. Calibration and parameters listed on pages 110 and 111. In the table below the criterion refers to a comparison of model variable with measurement from patient.

Parameter	Interval or window	Measurement	Criterion	Estimator gain (Standard)
EDV	From start of filling period until start of next activation	l.v. press.	p_{lv} in model is equal to measured l.v. pressure during interval	$250 \text{ mlsec}^{-1}/\text{mmHg}$
v_{max}	Isovolumic contraction period	$\frac{d(\text{l.v. press.})}{dt}$	Same (mean) rate of rise of l.v. press. during interval	$5 \cdot 10^{-2} \text{ sec}^{-1}/\text{mmHg}$
σ_{max}	Ejection period	l.v. press.	Same (mean) l.v. press. during interval	$5 \text{ gmm}^{-2} \text{ sec}^{-1}/\text{mmHg}$
T_{sys}	Isovolumic relaxation period	l.v. press.	Same (mean) l.v. press. during interval	$2 \cdot 10^{-3}/\text{mmHg}$
R_p	Isovolumic contraction period	aortic pressure	Same (mean) aortic press. during interval	0.1 ml^{-1}

In the estimator II configuration, no direct information on the left ventricular pressure is available. We are then left with aortic pressure as measurement for v_{max} , σ_{max} and R_p estimation. We use the first 25 msec of the ejection phase as a window for the v_{max} integrator. We then achieve approximately synchronous start of ejections. The ejection period is used as window for σ_{max} , analogous to the estimator I. The "non-ejection" period is used as window for R_p estimation. This scheme assures that model and patient aortic pressures have the same means both in the ejection and the "non-ejection" periods. T_{sys} is estimated so that model aortic valve closure occur approximately simultaneously with the first sharp deflection of the 2. heart sound. The system explained in figure 6.8 is used. Estimator II is summarized in figure 6.9.

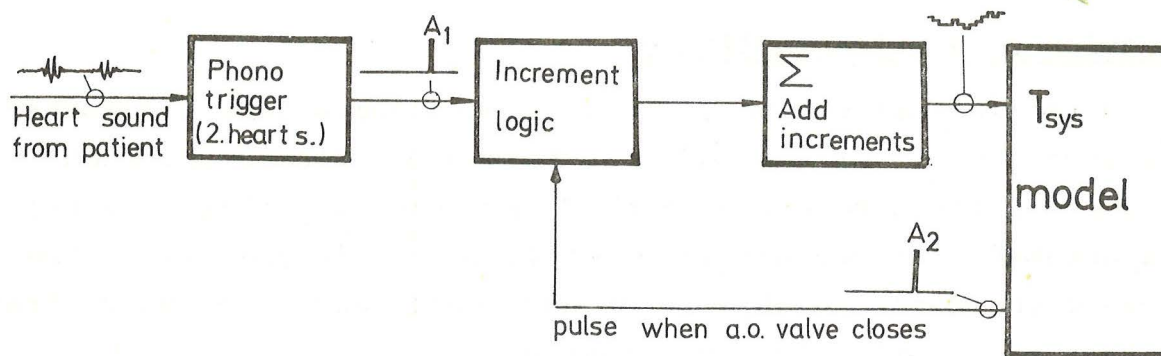


Figure 6.8. Block diagram of T_{sys} estimator when phonocardiogram is measured. The output of the Phono trigger is a short (2 msec) pulse A_1 . The model sends out a pulse A_2 (2 msec) when its aortic valve closes. The increment logic decides which of these pulses arrive first. If A_1 occur after A_2 , then an increment of 5msec is added to T_{sys} . If A_1 occur before A_2 the the same increment is subtracted from T_{sys} .

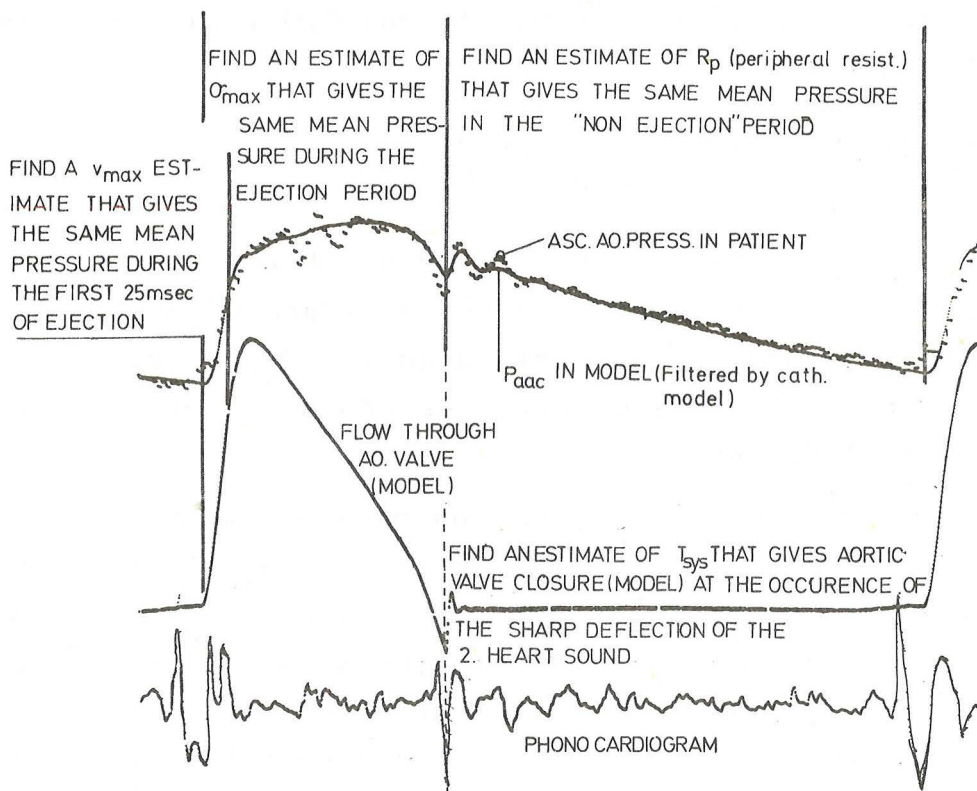


Figure 6.9. Summary of estimator II. Measurements from patient B.L. "Standard" estimator gains are:

- v_{max} : $2 \text{ sec}^{-2} / \text{mmHg}$
- σ_{max} : $4 \text{ g}(\text{mm})^{-2} \text{ sec}^{-1} / \text{mmHg}$
- R_p : 0.05 ml^{-1}

Estimation of aortic compliance

So far in this chapter, it has been assumed that the aortic compliance, C_{ao} , of the model is reasonably realistic. When discussing methods to estimate this parameter (in this section) it is assumed that the automatic estimator is in operation. The automatic estimator is able to produce model aortic pressure tracings that are similar to the measured. The estimated stroke volume (and cardiac output) is, however, critically dependent upon C_{ao} . In fact, we find that estimated stroke volume is nearly directly proportional to aortic compliance.

If the cardiac output, patient C.O., is determined by an independent method such as Fick, thermo- or dye-dilution, this may be compared with the estimated cardiac output, model C.O., defined as mean flow through the aortic valve in the model when the estimator is operating. Let $C_{ao}^{(0)}$ be the initial aortic compliance guess. If model C.O. is different from patient C.O., the new value of C_{ao} may be chosen as:

$$C_{ao}^{(1)} = C_{ao}^{(0)} \cdot \frac{\text{Patient C.O.}}{\text{Model C.O.}}$$

If necessary, this procedure may be iterated until model C.O. is within $\pm 2-3\%$ of patient C.O. The estimate of aortic compliance found by this method may be designated as $C_{ao}(\text{C.O.})$ and is based upon an independent cardiac output determination in addition to the measurements of pressure.

The propagation velocity of the pressure wavefront through the aorta is a function of the vessel wall stiffness. In conjunction with ascending aortic or arch pressure, a simultaneous measurement of femoral artery pressure will give information on the propagation properties of the aorta (and iliac arteries). An external pulse transducer of the bubble type may also give sufficient information of the pressure upstroke.

The pulse transducer cannot directly measure mean and pulse pressures. The circuit schematically illustrated in figure 6.10 adds (or subtracts) the output of an integrator to the pulse measurement. The input to this integrator is the difference between model femoral artery pressure and the "scaled" pulse measurement. The gain factor k_{puls} is chosen to let the time constant of the system be 0.5 sec.

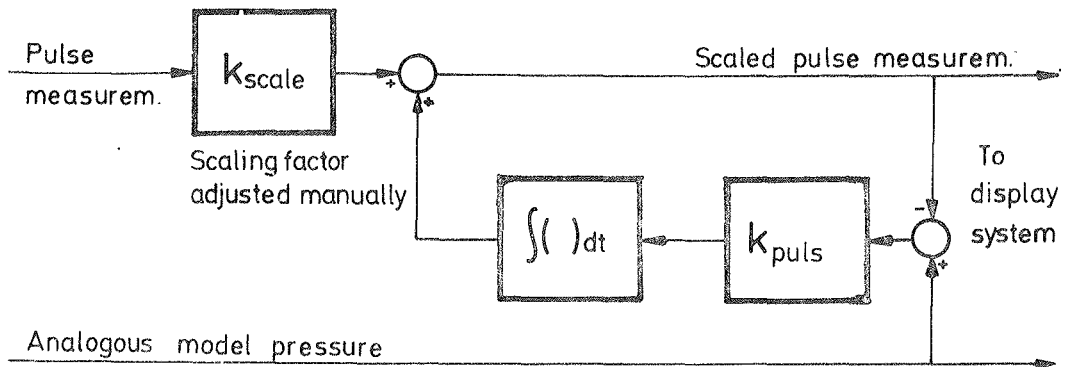


Figure 6.10. Block diagram of circuit used for scaling of external pulse measurement. "Standard" parameters are:
 $k_{puls} = 2 \text{ sec}^{-1}$, k_{scale} : variable.

This feedback system results in a mean level of the "scaled" pulse measurement which is close to the model femoral artery mean pressure. The adjustable gain is manually operated to obtain similar pulsatile components of the traces as judged by a visual comparison on the display CRT.

Representative traces are shown in figure 6.11. Due to the design of the data acquisition system, the patient measurements are sampled every 5 msec and held until the next sample. The continuous or slightly dotted (display chopper) curves represent the corresponding model variables. The high sweep rate of the display facilitates the adjustment of C_{ao} to achieve a similar transmission of the model pulse wavefront as observed in the patient. Panel B of figure 6.11 illustrates an example of a C_{ao} (pulse) estimate that satisfy a visual criteria. The first part of the nearly linear upstroke (after the foot curvature) is used for the comparison. Panel A and C shows the pressure traces when the C_{ao} (pulse) estimate is either too low or too high.

The C_{ao} (pulse) estimate is not necessarily identical with the C_{ao} (C.O.) estimate. A brief comparison of these independent determinations appear in chapter 9. If both methods are used, and a discrepancy is present, we may correct the inertances so that

C_{ao} (pulse) = C_{ao} (C.O.). The underlying principle is that the transmission time is also related to the inertance parameters. Let L_{ao} represent a normalized correction factor that modify all model inertances so that:

$$(\text{New inertance parameter}) = L_{ao} \cdot (\text{the numbers given in table 3.2}).$$

C_{ao} is now determined on the basis of a cardiac output measurement, and L_{ao} is corrected to give a correct transmission delay.

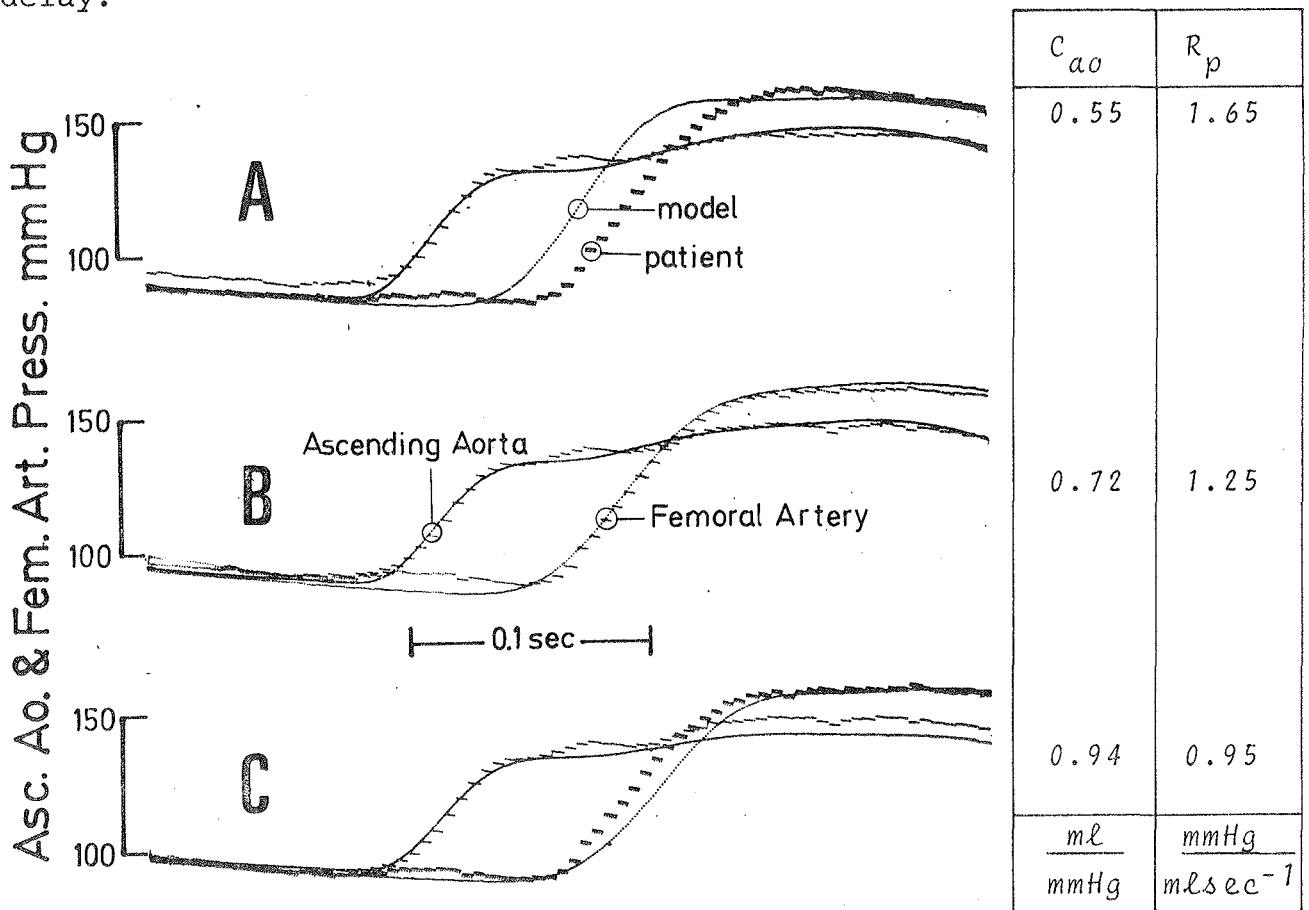


Figure 6.11. Influence on aortic transmission properties as a result of changes in C_{ao} .

Estimation of peripheral damping

The aortic pressure and flow wave-shapes are influenced by the conditions in the arterial branches and peripheral arteries. Some of the pulsatile energy is reflected into backward travelling waves. The reflection coefficients are dependent upon the degree

of matching between the characteristic impedances in the arterial tree.

In the model, the peripheral damping terms are quite influential on the pressure and flow dynamics in the aorta. This is illustrated in figure 6.12 where 3 different values of T_p are simulated. In panel A, T_p has half the "standard" value, and a marked aberration is observed in pressure course in the end of ejection and during diastole. On the other hand, increasing T_p to twice its "standard" value also causes a significant deviation in the pressure waveshape (panel C). As shown in the last section of this chapter, the estimates of the other parameters are not critically dependent upon the T_p estimate. Therefore a subjective criteria based on the "best curvefit" is used to adjust T_p . The slope of the pressure course in late ejection and the curvature of the diastolic slope are observed. Panel B represent the choice of T_p for this case.

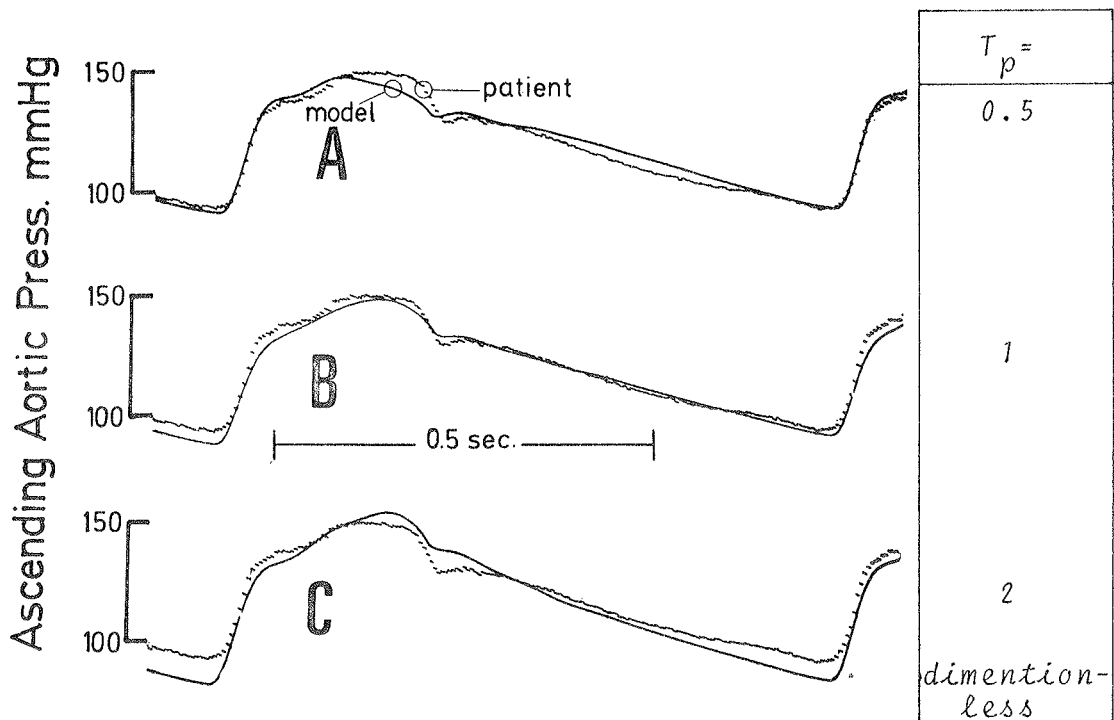


Figure 6.12. Influence of peripheral damping on aortic pressure course. Except T_p parameters are as listed on page 124. (Patient N.N.)

Estimation of catheter-manometer dynamic parameters

The catheter-manometer model described in chapter 4 is characterized by two parameters, f_0 - the undamped resonant frequency, and ξ , the damping factor. These parameters may vary with the type of catheter and the amount of air trapped inside the pressure transducer or its connections. If the damping is not too pronounced, these parameters are easily estimated from the dynamic pressure records. Figure 6.13 demonstrates an ascending aortic pressure from patient B.L. with superimposed model tracings.

In panel A, f_0 is too low, the oscillations after the aortic valve closure are seen to have a lower frequency in the model tracing. In panel B, f_0 has been adjusted to give a representative curve-fit, but the model tracing is more oscillatory than the patient measurement. Therefore, ξ is increased, and the tracings shown in figure 6.13 C are obtained. With this approach a step response test is unnecessary as long as the system is underdamped.

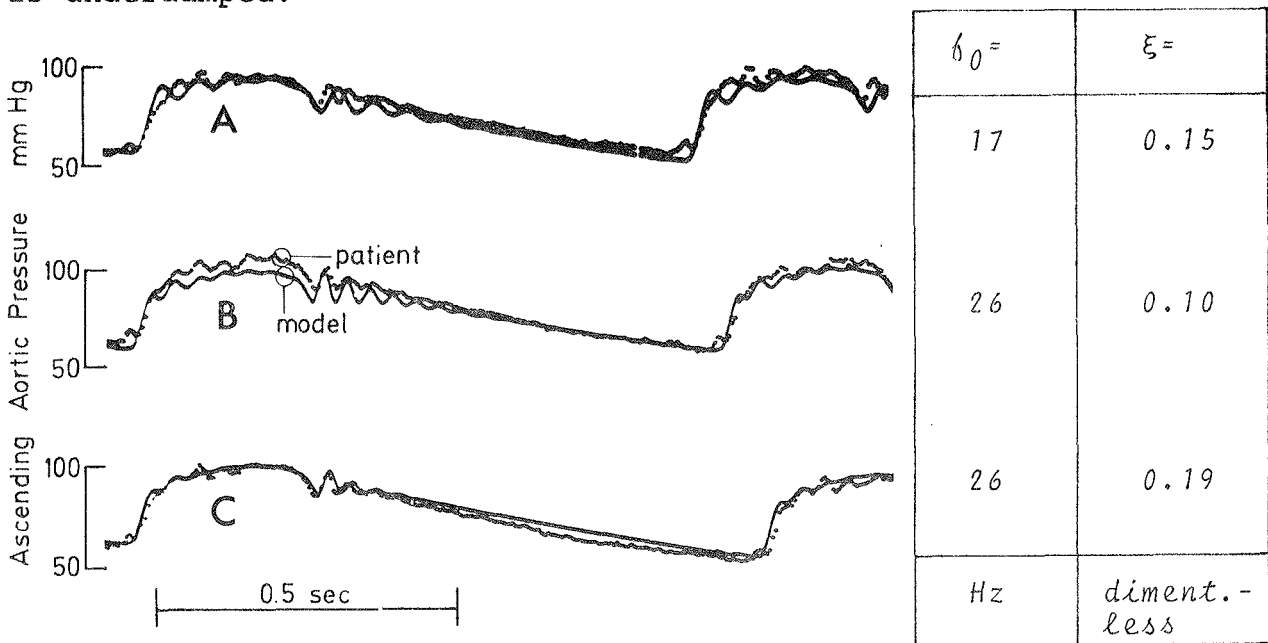


Figure 6.13. Influence of catheter parameters on aortic pressure time course. Parameters as in page 124, patient B.L.

Errors in the estimates

There are 5 main sources of errors in the parameter estimates:

- 1) Inability of the automatic estimator to follow rapid parameter variations.
- 2) The assumptions on which the model is based are unrealistic.
- 3) The A and B parameters are incorrect.
- 4) The measurements are more or less distorted and noisy (C parameters).
- 5) Observer errors in the manual estimation procedures (M parameters).

The physiological validity of the proposed model can only be investigated in light of measurements on the real cardiovascular system. Chapters 8 and 9 are devoted to this subject. An indication of the 4 other sources of error may be found in a model to model estimation study.

The proposed estimator is in its nature a multivariable feedback "servo system" with cross coupling between the different loops. As such it might be possible by control theory methods to analyse its dynamical properties and to synthesize decoupling networks. As strong nonlinearities are present, the analysis will necessarily be quite complicated. It is considered sufficient at the present stage to study the dynamic behaviour of the estimator to "artificial" and real patients.

The "artificial patient" is another model or recorded measurements from the same model. The pulse which initiates activation, left ventricular and ascending aortic pressures are recorded on magnetic tape using P.P.M. modulation (Aaslid & Brubakk 1971). During this recording, the parameters R_p , σ_{max} and v_{max} are varied as shown in figure 6.14 A. The upper tracing represent the left ventricular volume.

The measurements recorded on the tape are then utilized as input to the estimator, and the tracings shown in figure 6.14 B are the estimates of the parameters. The estimated left ventricular volume is close to the "patient" volume. The time courses of the

estimated parameters exhibit slight fluctuations. This is due to a small amount of noise inherent in the recording system. The estimator is stable, there are no overshoots or oscillations in the traces. Also the cross coupling effects are small - i.e. a change in one parameter affects the estimates of the others only little. The most noticeable crosscoupling effect is seen in the σ_{\max} estimate. There are small transient errors (for 3 beats) while R_p is changed.

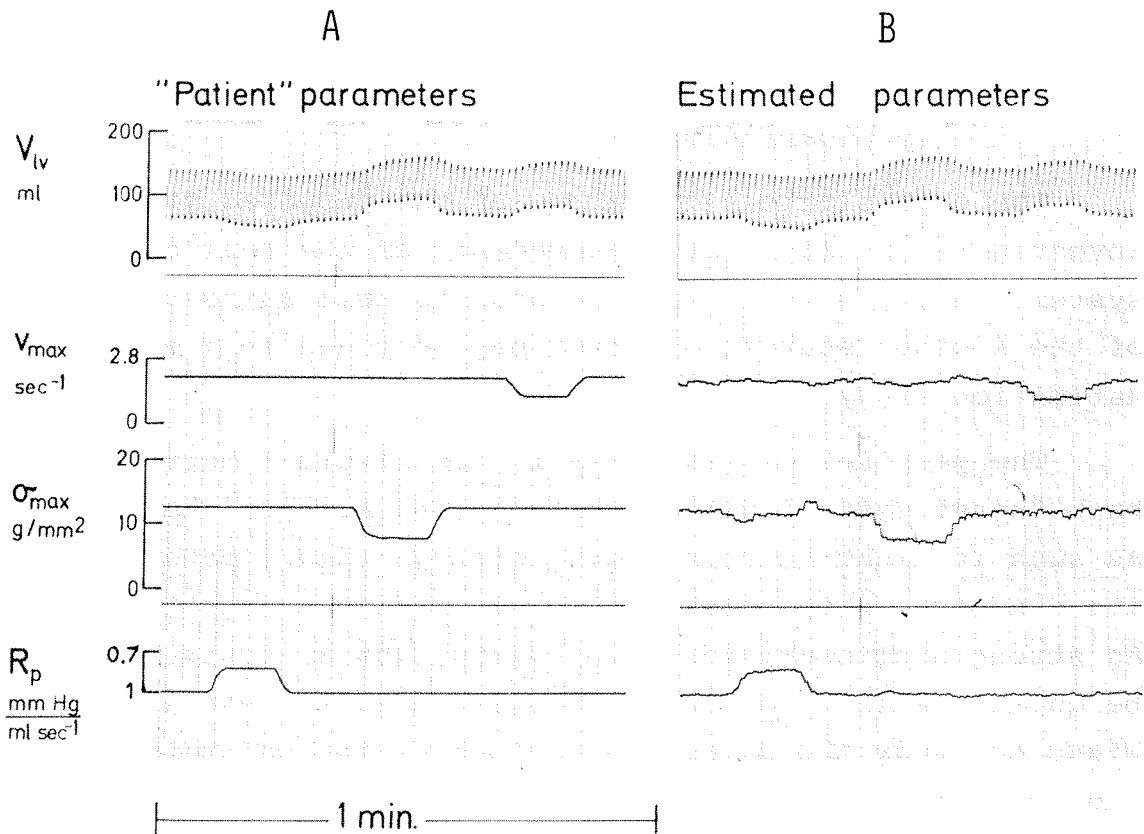


Figure 6.14. The left panel shows how parameters v_{\max} , σ_{\max} and R_p are varied when the model variables are recorded on magnetic tape. In the upper tracing, the left ventricular volume is also shown. The right panel demonstrates the response of the estimator I when the tape is used as a "substitute" for measurements from patients.

This example demonstrates the capabilities of the proposed estimator to follow quick changes in the cardiovascular function. The estimated parameters are close to the correct values one or two heart beats after the change was induced. The response of the T_{sys} parameter is not shown, and it is somewhat slower than the other parameters, requiring 2-3 heart beats to follow a step increase (Estimator I configuration).

An example demonstrating the response of the EDV estimator to measurements from the human is shown in figure 6.15, where left ventricular pressure of patient R.H. is shown. In diastole the model pressure practically tracks the measurement by means of the Δq_{mi} feedback system. The l.v. volume in the model is also shown. It looks reasonable from an physiological viewpoint, and a slight extra contribution (maybe due to atrial contraction) at the end of diastole may be discerned.

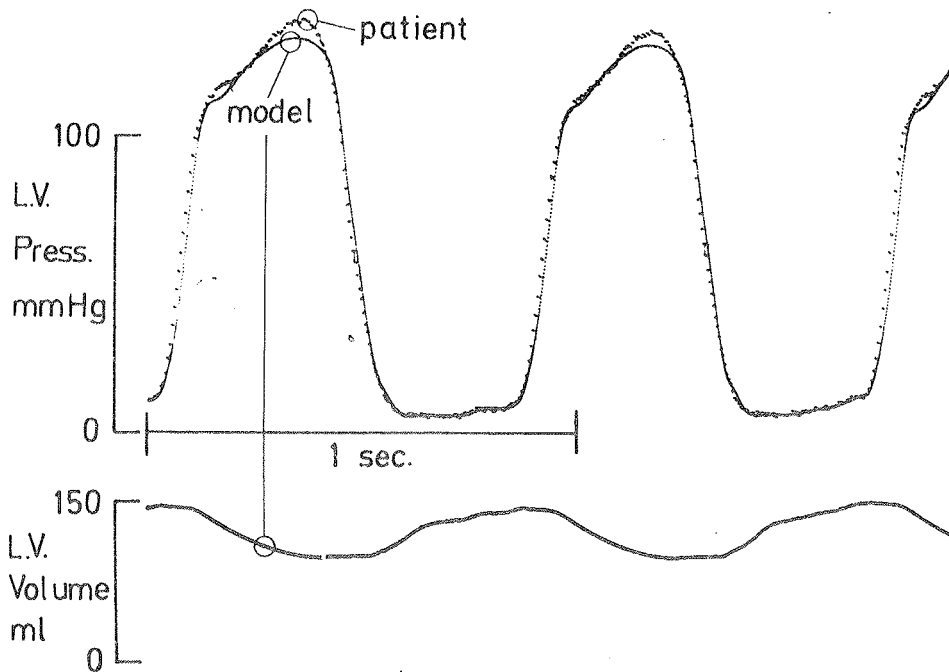


Figure 6.15.
Response of estimator I when applied to measurements from the human heart. Patient R.H. Parameters as in table 8.2.

The ascending aortic pressure of patient N.N. is shown as the upper trace of figure 6.16. We observe strong variations possibly due to respiration. The middle trace is the model aortic pressure when estimator II is in operation. The model is able to follow the variations on almost a beat to beat base. The lower trace illustrates the variations in model left ventricular volume. A constant end-diastolic volume is achieved by the feedback servo-system.

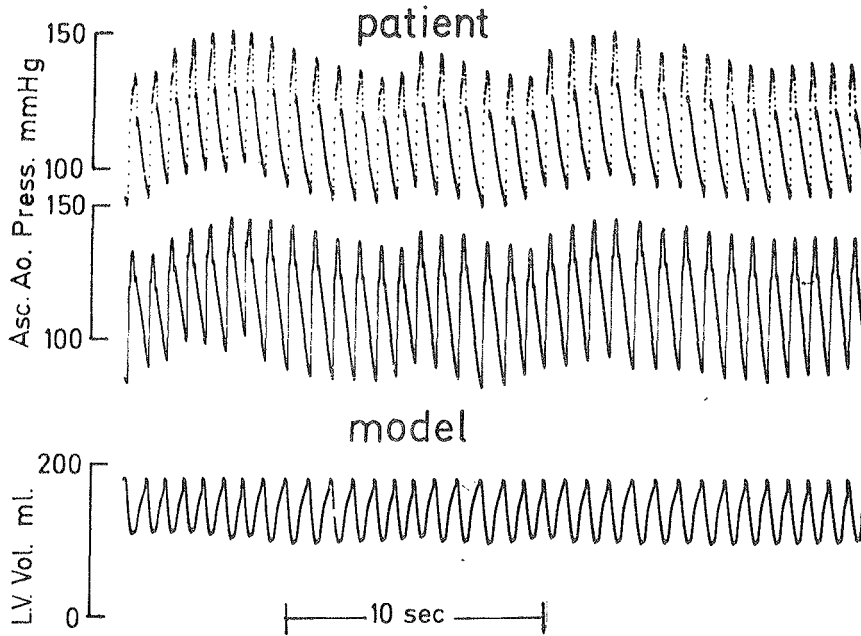


Figure 6.16.

An illustration of the ability of estimator II to follow an aortic pressure curve with strong fluctuations. Approximate parameter values are as on page 124, patient N.N.

These examples and further experience with the system indicates that the dynamic response of the estimator is satisfactory.

An analysis of the sensitivity of the estimates to errors in the measurements and "wrong" assumptions of A and B parameters may be undertaken on a model to model bases. Again, the simulated pressures are recorded on magnetic tape when the model is in the "standard" state.

The recorded variables are used as input to the estimator. Noise and bias may be added to these simulated measurements. Also, we may try different choices of A and B parameters, and study the influence of observer (or operator) errors.

In this section, a parameter is considered not to be significantly affected by any factor which causes the estimate to deviate less than $\pm 10\%$ from the "standard" value. The results of the error analysis are presented in table 6.2. The perturbations are deliberately made quite large in order to get clear reactions.

Stochastic bandpassfiltered (10 - 200Hz) white gaussian noise with mean root square amplitude of 2mmHg does not influence any parameter significantly, neither does a bias of 4mmHg in aortic pressure. If the left ventricular pressure "measurement" is biased 4mmHg, all left ventricular parameters are significantly affected. End diastolic volume and v_{\max} increases to 170 ml and 2.4 sec^{-1} respectively, and σ_{\max} decreases to 8.5 g/mm^2 .

This reaction might be expected, as left ventricular diastolic pressure is used to estimate the degree of filling. The stroke volume and peripheral resistance are not significantly influenced, neither by this nor by any other change in parameters or measurements related to the left ventricle. The result indicates that the estimates of arterial parameters are not critically dependent upon a correct representation of left ventricular phenomenae.

The parameter k_{sac} , relating fibre length and sarcomere length, is decreased from $2.2 \mu\text{m}$ to $2.08 \mu\text{m}$, simulating a dilated ventricle. The end-diastolic volume estimate increases from 150 to 195 ml, and the estimates of v_{max} and σ_{max} are significantly affected.

The left ventricular wall volume V_m , is increased from 230 to 345 ml, simulating a big left ventricle. In this case, the end-diastolic volume estimate is too large (220 ml), and the v_{max} as well as the σ_{max} estimate exhibit significant errors.

A compliant series elastic element is then simulated by decreasing k_{se} from 24 to 16 (normalized values). The end-diastolic volume is correctly estimated, while the v_{max} estimate is too high (4.2 sec^{-1}) and σ_{max} too low (7.5 g/mm^2).

These results demonstrate that errors in the A or B parameters considerably influence the estimates of the left ventricular C parameters. We observe that even if a factor primarily influence the estimate of one parameter, the others are also affected. As an example, decreasing the series elastic element stiffness k_{se} of the model elicits a rise in estimated v_{max} to achieve a similar course in isovolumic pressure buildup. As a consequence of the increased ability to develop shortening velocity, σ_{max} must be decreased to maintain correct aortic pressure waveforms. These considerations stress the need for physiological justification of the model and the A parameters (chapter 8). In order to achieve a reasonable accuracy, the error in the left ventricular diastolic pressure must not exceed 2 mmHg for the "standard" case. This is within the performance of most quality pressure-measurement systems.

The errors in the arterial parameters are also shown in Table 6.2 for different choices of damping T_p , aortic inertance

Disturbance	v_{max} sec ⁻¹	σ_{max} g/mm ²	EDV ml	SV ml	R_p mmHg mlsec ⁻¹	Remarks	
Errors in measurement { Control 2mmHg noise in pressure 4mmHg bias in i.v. pressure	2.2	10.0	150	78	1.0	} Estimator I	
	2.3	9.5	155	78	1.0		
	<u>2.4</u>	<u>8.5</u>	<u>170</u>	78	1.0		
Errors in apriori assumptions { k_{sac} 2.2 → 2.08 V_m 230 → 345 ml k_{se} 24 → 16	<u>2.8</u>	<u>8.5</u>	<u>195</u>	79	1.0		
	<u>2.6</u>	<u>6.5</u>	<u>220</u>	79	1.0		
	<u>4.2</u>	<u>7.5</u>	<u>150</u>	76	1.05		
Errors in measurement { 4mmHg bias in ao. pressure -10msec error in trans. time Errors in apriori ass L_{ao} 1.0 → 0.9 Error in M C_{ao} 0.87 → 0.51 parameters T_p 1.0 → 2.0	2.2	10.5	150	79	1.0	} Estimator II	
	<u>2.4</u>	<u>7.5</u>	150	<u>67</u>	<u>1.15</u>		C_{ao} 0.87 → 0.7
	2.1	<u>11.5</u>	150	<u>86</u>	<u>0.90</u>		C_{ao} 0.87 → 0.97
	<u>2.8</u>	<u>6.0</u>	150	<u>44</u>	<u>1.75</u>		
	2.3	10.0	150	76	1.05		

Enhanced figures denote significant errors. Otherwise see text.

Table 6.2. Errors in the estimates.

correction L_{ao} , and for errors in the aortic transmission time measurement. It is found that the stroke volume estimate error is approximately proportional to the error in the C_{ao} estimate. C_{ao} in turn is dependent upon the accuracy of the pressure wavefront transmission time measurement. An error of 10 msec results in aortic compliance and stroke volume estimates which deviates approximately 15% from the "standard". When the aortic compliance is estimated by the transmission time method, the result is also influenced by the choice of aortic inertance parameters. If L_{ao} , as defined on page is decreased 10%, the compliance and the stroke volume estimates increase by approximately the same relative amount. The accuracy of this method for aortic compliance estimation is therefore critically dependent upon a reasonably constant L_{ao} . This assumption is discussed in chapter 9.

An 100% increase in the peripheral damping, T_p , does not influence the estimates of the other parameters significantly. This indicates that the value chosen for T_p is not critical for the accuracy of the other parameter estimates.

This rather brief error analysis is intended to give a preliminary indication of the accuracy that can be expected. The figures in table 6.2 cannot be relied upon if other parameter sets than the "standard" are used as a basis. The main finding of this analysis is that measurement noise and errors are not the critical determinants of estimation accuracy, whereas unrealistic assumptions can give use to serious errors.

Chapter 7.

METHODS FOR TESTING THE ABILITY OF THE MODEL TO SIMULATE THE LEFT VENTRICLE AND AORTA

Introduction

The model proposed in chapters 2 and 3 can be regarded as a hypothesis of left ventricular and arterial hemodynamic function. It is based on current physiological knowledge as well as on previous models (Beneken 1965, Beneken & de Wit 1967, Snyder & al 1968, de Pater 1966). The exact formulation of this hypothesis has been subject to many changes when comparison with real data demonstrated discrepancies in behaviour. This process will doubt, continue as more detailed and better data become available.

The value of a model or hypothesis is intimately dependent upon how well its ability to represent the real system is documented. The two subsequent chapters are devoted to this aspect. The ambition is to present evidence that the model allows some cardiovascular phenomenae to be simulated with an acceptable fidelity.

The method of "good curvefit"

Pressure and flow waveforms in the cardiovascular system exhibit characteristic waveforms over the heart cycle. A pulsatile model should be able to reproduce these with reasonable accuracy. Some of the measurements are utilized to match the pressure waveforms by means of the methods described in chapter 6. Taking a critical attitude, a good curvefit for these variables indicate only that the model may produce (pressure) waveforms that are realistic. This does not necessarily imply that the model is physiologically interesting or meaningful.

The method of independent measurements

In addition to a comparison with the measurements utilized in the estimation procedure, the model can be tested with regard to its ability to predict the dynamic waveforms of independent flow and pressure measurements. The data used in the subsequent chapters were not available when the model was designed.

If such comparisons are favourable and fairly comprehensive, we are justified to conclude that the model can simulate the relation between these measurements.

The method of perturbations (the experimental method).

Even if the model simulates pressure, flow and volume at many locations with good fidelity, it does not necessarily respond to changes in the cardiovascular state in the same manner as the real system. If the response to a perturbation (such as increased aortic load or increased ventricular filling) is used as a test of the model (hypothesis), it is necessary to assume that certain factors (such as the contractility parameters) are constant. In many cases these assumptions are justifiable, and the perturbation test is a meaningful and tough test of any model.

Choice of comparison criteria

If the timecourse of the model variable deviates from the experimental or clinical data, we shall regard this as an error. Various criteria for the quantification of such errors may be devised. As the limits of what is reasonable, and what is not, are postulated on subjective grounds, it is preferred here to present the raw data and facilitate a visual comparison by superimposing model and patient tracings. Most of the illustrations of time courses presented in this report are photographed directly off a CRT (Tektronix 611) storage display.

Chapter 8.

SIMULATION OF THE LEFT VENTRICLE

Introduction

The behaviour of an actively contracting ventricle is much more complex to formulate in a mathematical description than the phenomena occurring in passive vessels. Most of the reported studies on cardiac muscle mechanics use papillary muscle preparations. It is an interesting subject to use simulation techniques for the analysis of such experiments (Donders & Beneken 1971). The papillary muscle is, however, a simplified "model" of an intact ventricle with many possible sources of error. In as much as the main objective in this study is to simulate the human left ventricle and arterial system, it seems more satisfactory to compare the behaviour of the ventricular model as a whole with its real counterpart.

In the following section the behaviour of the model is compared with findings on the dog heart under various levels of inotropy, filling volume and arterial pressure as reported by various authors. The time courses of the left ventricular model variables are compared with measurements from patients undergoing open-heart surgery at the Surgical Dep. A, Rikshospitalet, Oslo. In the last section, the results are summarized and discussed.

The left ventricular volume-muscle fibre length relation
Comparison with data from the dog heart

As proposed by Rushmer & al (1956) it is possible to monitor continuously distances in the heart by sewing miniature ultrasonic transducers into the myocardium and using the transit time of a sound impulse between these as a measure of the distance. This method has later been used and described by Leraand (1970) and Bugge-Asperheim & al (1969). The distance

measure with this technique may be called myocardial cord length, abbreviated to MCL. (Bugge-Asperheim & al, 1969).

The time course of MCL during a contraction depends upon where the transducers are located in the myocardium. A direct comparison between l_f , the average muscle fibre length in the model, and the MCL as measured by ultrasonic techniques is possible if the crystals are placed in a representative myocardial area, and implanted approximately midway between the outer and inner wall boundaries. The data that are utilized in this and the subsequent sections are taken from published experiments in which this condition seems to be satisfied reasonably well (Lekven & al, 1972). To facilitate a direct comparison between experiment and model, some variables are normalized. MCL is given as percentage of the end-diastolic MCL in the control state. End-diastolic and stroke volumes are likewise normalized with reference to the control state. The pressures are not normalized.

The closed squares in figure 8.1 represent the findings reported by Lekven & al (1972).

By infusing saline at high rates, the left ventricular filling pressure, LVEDP, may be increased in the animals. This leads to a change in other variables associated with the left ventricle; there is a concomitant increase in end-diastolic volume (EDV), stroke volume (SV), end-diastolic MCL (EDMCL) and peak pressure (LVSP).

The starting point for the simulation are the "standard" parameters listed in table 6.1. The left ventricular end-diastolic volume and the peripheral resistance are adjusted manually until the model LVEDP and LVSP are close to the reported values. This procedure is applied to both control and expanded states. The values of the model variables are normalized and plotted as functions of LVEDP in figure 8.1 (circles).

The change in the model variables as a result of the increased blood volume are quite similar to the results of Lekven & al. In particular the correlation is good for EDV and the

EDMCL. It seems that the dogs are increasing their ejection fraction somewhat more than the model as a result of the increased ventricular filling, but the difference is small.

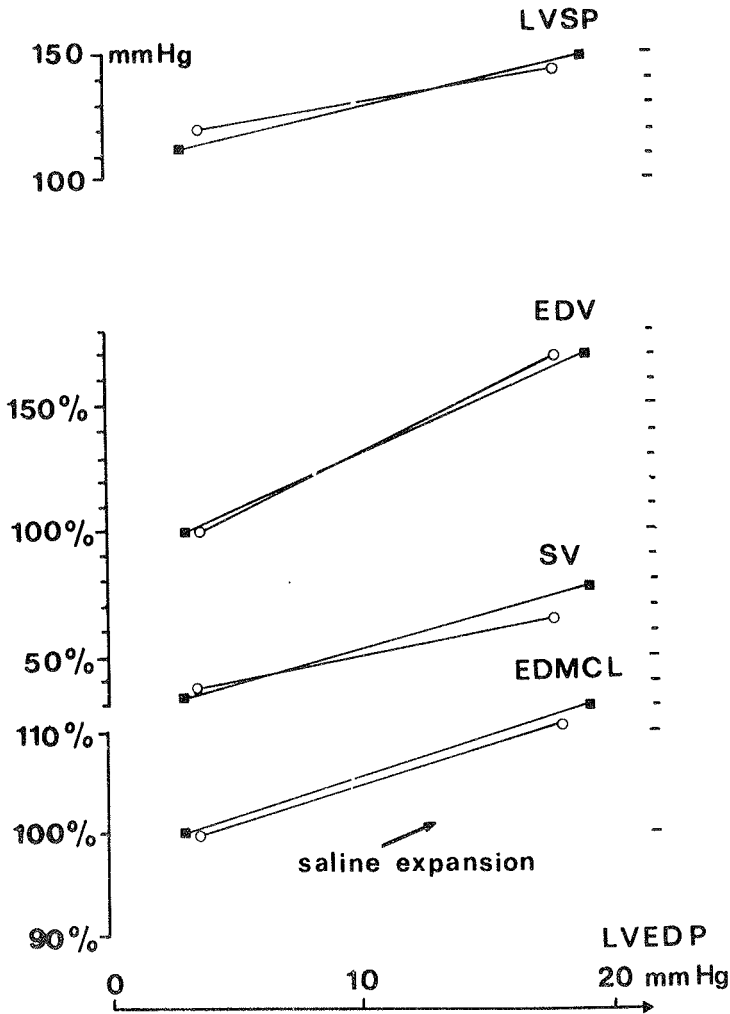


Figure 8.1.

Simulation of a saline infusion experiment reported by Lekven & al 1972.

LVSP - Left ventricular systolic (=peak) pressure.

EDV - Left ventricular end-diastolic volume.

SV - Stroke volume.

EDMCL - End-diastolic myocardial cord length.

LVEDP - Left ventricular end-diastolic pressure.

The following parameters used in this simulation refer to the "human" scaling:

$$v_{max} = 2.1 \text{ sec}^{-1}$$

$$\sigma_{max} = 10 \text{ g/mm}^2$$

$$p_{th} = 0 \text{ mmHg}$$

■ Experiments (Lekven & al.1972, Table 1)

○ Model

Control state: $R_p = 1.65 \frac{\text{mmHg}}{\text{mlsec}^{-1}}$, LVED = 120 ml

Saline expansion: $R_p = 1.30$ -" -", LVED = 200 ml

Otherwise parameters are as in table 6.1.

The response of the left ventricular model to changes in end-diastolic volume and left ventricular peak pressure
Comparison with data from the dog heart

One of the pioneering efforts to quantitate the properties of the ventricular "pump" was reported by Starling (1918). Since then, many investigators have reported on the response of the left ventricle, and in particular its output, the stroke volume, to variations in filling pressure or volume, and impedance to ejection. It is a useful test of a proposed left ventricular model to simulate the conditions of such experiments as faithfully as possible, and compare the output variables of the model with the reported findings. We have chosen the recently published work of Bugge-Asperheim and Kiil (1973) for such a comparison study.

They used clamping of the descending aorta to increase the pressure facing the left ventricle during ejection. In the same preparations they infused saline rapidly to increase ventricular filling. The effects of these perturbations are reported both in a "normal" inotropic state and during infusion of isoproterenol*. The authors measured left ventricular pressure, ECG, aortic flow and distances within the myocardium.

The experiments that we intend to simulate are tabulated in table 2 of Bugge-Asperheim & Kiil (1973), and demonstrates the effects of raising blood pressure before and after saline expansion. The main finding, according to the authors, is that stroke volume diminishes more in response to raised aortic pressure when saline is being infused.

We have to determine the relation between the model variables and the measurements, and obtain estimates of the parameters valid for the experimental situation. Dog heart rates are usually higher than in the human. Since the results will be discussed in terms of stroke volumes, the absolute heart rate is unimportant, and a heart rate of 80 per minute is chosen. The duration of ventricular systole is not known, and we assume $T_{\text{sys}} = 330$ msec.

*Only the normal state is simulated here.

The diastolic pressure-volume relation of the left ventricular model (figure 8.2C) is plotted.

Table 8.1 Summary of findings of Bugge-Asperheim & Kiil (1973) and present simulations.

State	Intervention	LVSP mmHg	LVEDP mmHg	Max. LV dp/dt mmHgsec ⁻¹ .10 ³	SV ml	EDMCL mm
I	Control dogs model	113	1.3	2.1	22	11.2
		115	2.0	2.1	22	11.2
II	Raised pressure dogs model	184	9.6	2.3	20	12.5
		185	8.0	2.3	21	12.5
III	Saline exp dogs model	134	6.7	2.5	37	12.4
		135	7.0	2.3	37	12.4
IV	Saline exp + dogs raised model press.	212	19.9	2.9	23	13.1
		210	15.0	2.6	20	13.1

The myocardial cord length is not an absolute measure of muscle fibre stretch, therefore the end-diastolic pressure is used as a guide for determining the relation between MCL (myocardial cord length) and l_f (model fibre length). The relation: $MCL = 13.6 l_f$ (mm) is found to locate the experimental points II and III quite close to the model pressure-volume relation (figure 8.2). We now add an extra abscissa for MCL in figure 8.2B based upon the $l_f (V_{lvn})$ relation shown in figure 2.2.

In lack of data, C_{ao} , T_p and V_m are assumed to have the values listed in figure 8.2.

The amount of MCL shortening during ejection is not published for the experiments we intend to simulate. We must therefore

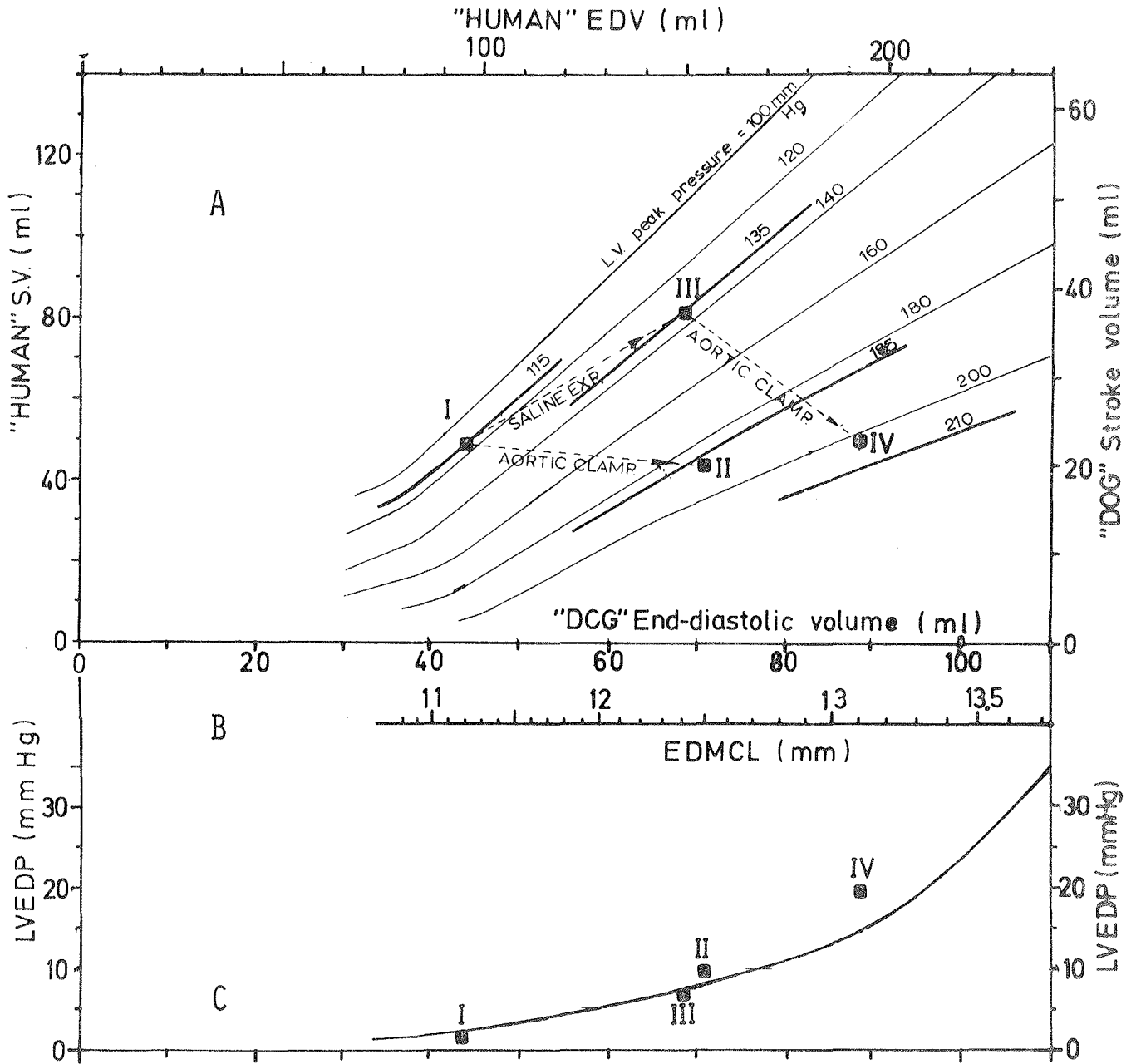


Figure 8.2. A: Left ventricular function curves relating stroke volume (SV) to end-diastolic volume (EDV) and l.v. peak pressure. B: Nonlinear scale relating end-diastolic myocardial cord length (EDMCL) to end-diastolic volume using the relation shown in figure 2.2. C: Passive pressure (LVEDP) - volume relation of left ventricular model.

The filled squares represent the findings of Bugge-Asperheim & Kiel (1973). The following parameters were used in this simulation, and refer to the "dog" volume and flow scaling:

$$v_{max} = 3.0 \text{ sec}^{-1}, \sigma_{max} = 11.5 \text{ g/mm}^2, T_{sys} = 330 \text{ msec},$$

$$V_m = 105 \text{ ml}, C_{ao} = 0.40 \text{ ml/mmHg}, T_p = 1, p_{th} = 0 \text{ mmHg}.$$

LVEDV and R_p are varied.

resort to the data published in table 1 of Bugge-Asperheim & Kiil (1973), in which the experimental procedure is only slightly different. In the control state, the amount of MCL shortening during ejection is 11% of the EDMCL. The setpoint of the LVEDV control system (figure 6.5) is chosen so that $13.6 \times l_f = \text{MCL} = 11.2 \text{ mm}$ (control state). Next, the peripheral resistance, R_p , is controlled so that LVSP is 115 mmHg (as in table 1), regardless of alterations in contractility. σ_{\max} is then adjusted manually until the relative shortening of l_f during a beat is 11%. This occur for $\sigma_{\max} = 11.5 \text{ g/mm}^2$.

Then, attention is given to the maximum derivative of left ventricular pressure, and v_{\max} is adjusted so that $\max \text{ LV } dP/dt$ is $2.15 \cdot 10^3 \text{ mmHg sec}^{-1}$ (table 8.1). This occur when $v_{\max} = 3.0 \text{ sec}^{-1}$. These estimates of σ_{\max} and v_{\max} were found after iterating the procedure until both conditions (correct relative shortening and $\max dP/dt$) were satisfied. We have now obtained estimates of the left ventricular parameters that satisfy the published data for the control state.

It is simple to determine a family of left ventricular function curves for the model. The end-diastolic volume, LVEDV, is kept constant by means of the servo system (chapter 6), the peripheral resistance is varied and the stroke volumes are recorded for peak left ventricular pressures, LVSP, of 100, 120, 140, 160, 180 and 200 mmHg. This procedure is repeated for various levels of LVEDV. The stroke volumes are then plotted as functions of LVEDV in figure 8.2. The stroke volume increases with increasing filling of the left ventricle, according to "Starlings law". The function curves are close to straight lines in the normal physiological range. The model exhibit an inverse relation between stroke volume and peak left ventricular pressure. For an EDV of 150 ml (human scale), the relation between SV and LVSP is replotted in figure 8.3, and is found to be approximately linear.

The upper volume scale in figure 8.2 refer to a "standard" human left ventricle. In order to compare the left ventricular

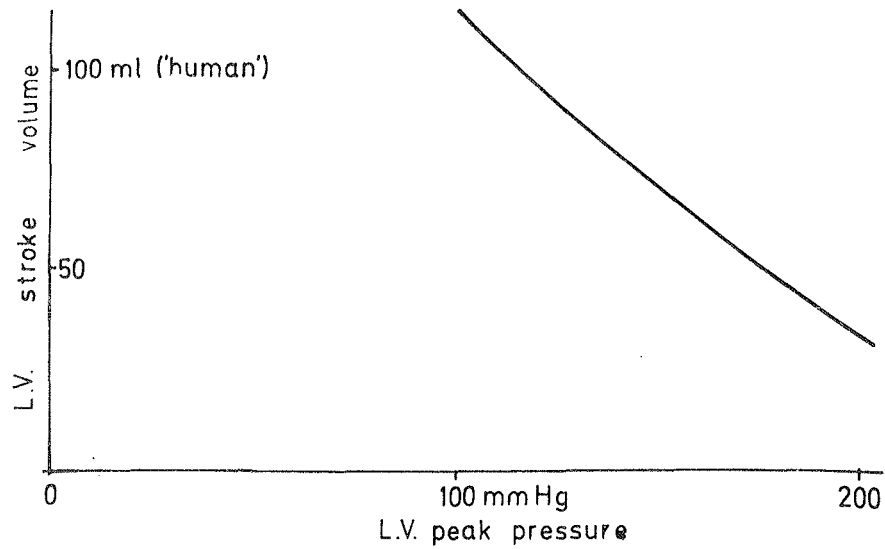


Figure 8.3. The dependency of stroke volume upon left ventricular peak pressure at an LVEDV of 150 ml ("human scale"). Parameters as in figure 8.2.

function curves with the findings of Bugge-Asperheim & Kiil (1973), a rescaling of the volumes (and flows) is necessary. State I (table 8.1) is used to obtain the relation between dog volumes and the "human" model volumes. A piece of function curve for LVSP = 115 mmHg is interpolated between the 100 and the 120 mmHg curve (figure 8.2). The "human SV" is 47 ml for an "human EDV" of 95 ml corresponding to a l_f of 0.825 and a EDMCL of 11.2 mm. The experimental SV was reported to be 22 ml in state I. According to this, the "dog volumes" are given as:

$$(\text{"dog volume"}) = 0.47 (\text{"human volume"})$$

The "dog volume" scales are included in figure 8.2. The experiments of Bugge-Asperheim & Kiil (1973) are plotted (the squares) into the diagram. The appropriate function curves of the model are determined by interpolation, and are indicated by the thick lines in the figure.

State I is the control, and is used for scaling. From state I, the transition to state II is the result of aortic clamping. Both EDMCL and LVSP increase, but the new steady state has a somewhat lower SV than state I. State II is a little off the

function curve predicted by the model, but the difference is small.

From state I, saline expansion causes an increase in EDMCL and a transition to state III. As the increase in LVSP is much smaller than in state II, the result is a large increase in SV. From state III, aortic clamping again results in an increased EDMCL and LVSP, state IV. The SV is now reduced to 23 ml. Again, the function curve predicted by the model is in the neighbourhood of state IV. We observe that an even better prediction would be the result if we use the end-diastolic pressure as a guide for ventricular filling in this state.

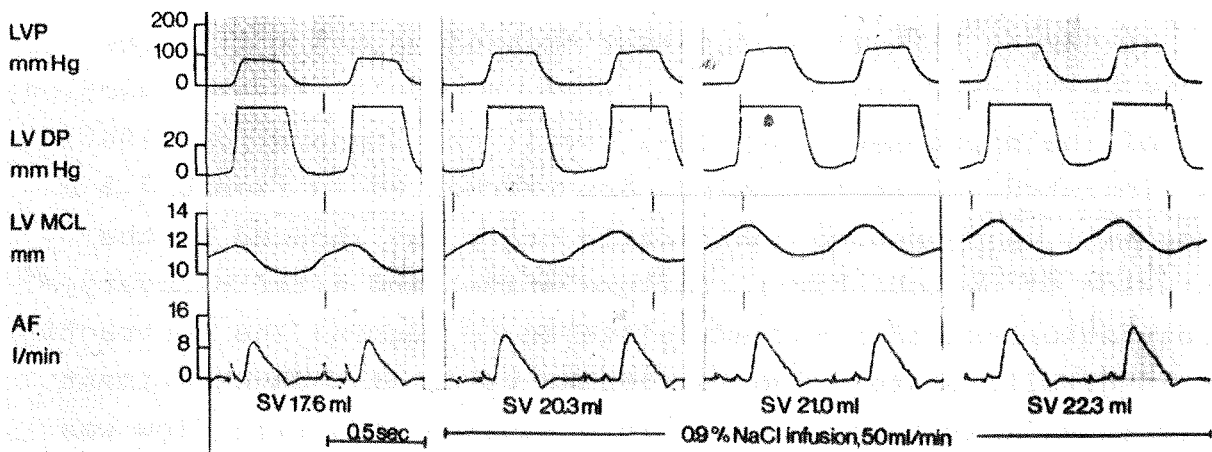
These results suggest that the proposed model may be of value in the analysis of ventricular function.

Based on figure 1 in Bugge-Asperheim & Kiil (1973) we shall simulate the effect of saline expansion in a 18 kg. dog. Their findings are reproduced in figure 8.4 A. By a similar procedure as described above, the parameters relevant to the control state are determined: $v_{\max} = 2.2 \text{ sec}^{-1}$, $\sigma_{\max} = 12 \text{ g/mm}^2$, and $T_{\text{sys}} = 0.32 \text{ sec}$. The heart rate is 104 /min. We find for this dog that:

"dog" stroke volume = $0.26 \times$ "human" stroke volume
and: $\text{MCL} = 13.6 \text{ l}_f$

The peripheral resistance and the setpoint of the l.v. end-diastolic volume control system are chosen so that the end-diastolic fibre length and the peak l.v. pressure are corresponding to the findings of the authors (figure 8.4). The changes in stroke volume represent independent information that is not utilized in the fitting procedure. It is found that these changes in dog and model stroke volumes correlate reasonably well, although the model responds with a somewhat larger increase. Furthermore we observe that the time course of aortic flow is faithfully simulated.

A. Experiment by Bugge Asperheim & Kiil (1973)



B. Simulated experiment.

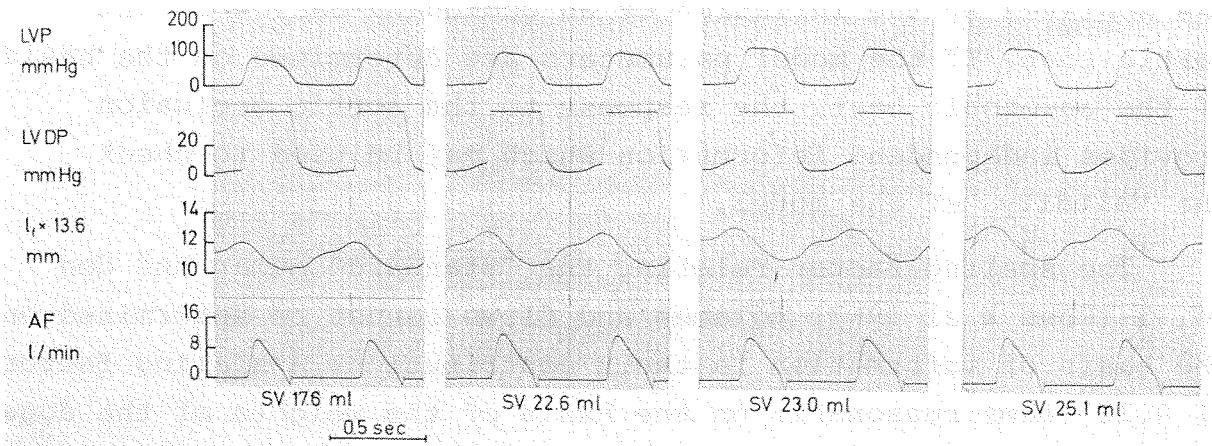


Figure 8.4. Simulation of experiment published by Bugge-Asperheim & Kiil (1973), upper panel. The tracings of dp/dt and an additional MCL recording are omitted from their figure. (Our recorder was only of a 4-channel type). Their experiment demonstrate the effect of saline infusion in a dog.

LVP: left ventricular pressure, LVDP - diastolic LVP.

LVMCL: left ventricular myocardial cord length (base).

AF: aortic blood flow. The lower panel shows the results of the simulations. Here $l_f \times 13.6$ is taken to be representative of LVMCL. The following parameters (referred to "dog" scaling) are kept constant during this simulation:

$v_{max} = 2.2 \text{ sec}^{-1}$, $\sigma_{max} = 12 \text{ g/mm}^2$, $V_m = 60 \text{ ml}$, $C_{ao} = 0.23 \text{ ml/mmHg}$, $T_p = 1$, $p_{th} = 0 \text{ mmHg}$ (openchest). These parameters were varied to simulate experimental conditions: T_{sys} , R_p and LVEDV.

Simulation of changes in the contractile properties of the dog heart

External stimuli or internal mechanisms may modify the contractile properties of the intact ventricle. In this section, one of the experiments by Ross, Covell and Sonnenblick (1967) is simulated. Their recordings are reproduced in figure 8.5 A (dog no.5). A depressed contractile state was induced by the infusion of pentobarbital (failure state) and after recovery, acetylstrophanthidin was administered to augment the contractility (digitalis state). The particular value of this experiment (figure 8.5) is that a sudden interruption of aortic flow was introduced in the second beat shown in each of the panels. This was achieved by the inflation of an occluding ballon in the aortic root. If the model parameters are determined on the basis of the auxotonic beat, the response to the aortic occlusion provides independent information which may be used to check the validity of the model.

The scaling factor relating the "standard" human and dog no. 5 (Ross & al 1967) volumes and flows cannot be determined on the basis of information in their contribution. A scaling factor of 0.25 seems reasonable on the basis of the weights of the dogs. According to this we have:

"dog" stroke volume = 0.25 ("human" model stroke volume)
The term stroke volume will be used for the scaled ("dog") volume for the remainder of this section.

A heart rate of 93 can be found from the published traces. This heart rate is used in the simulation.

The systolic duration, T_{sys} , is adjusted so that the width of the model left ventricular pressure trace is close to the measurements of Ross & al (1967). (Note that this is different in the three states).

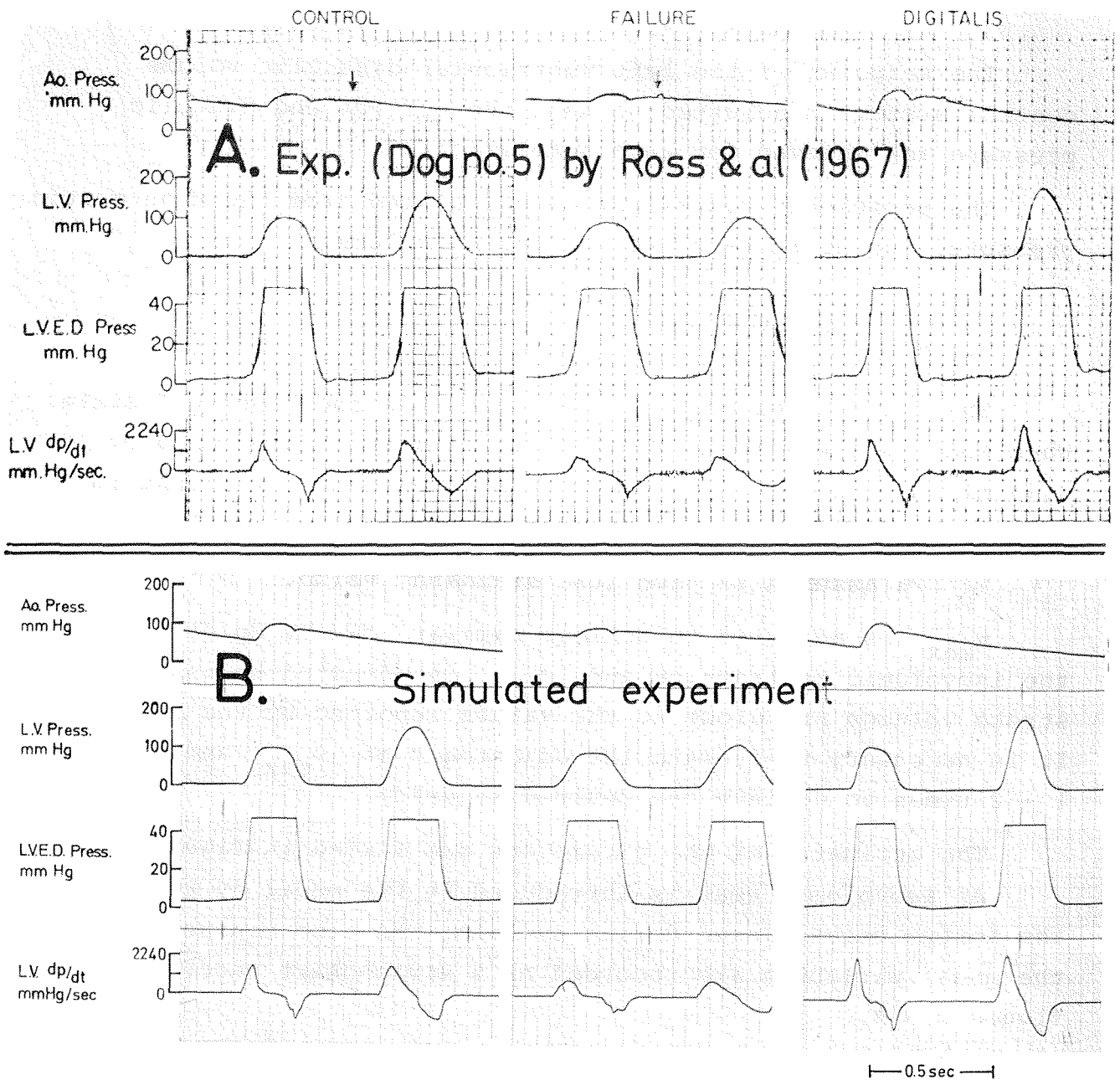


Figure 8.5. Upper panel is reproduction from Ross & al (1967). where the effect of aortic root occlusion are shown for 3 different contractile states. The end-diastolic pressures were controlled. The lower panel is the same experiments simulated on the model. Abbreviations: Ao. press.: Aortic pressure (in the arch), LV. Press.: Left ventricular pressure, L.V.E.D. Press.: LV Diastolic pressure. L.V. dP/dt. The time derivative of L.V. Press. Parameters common to all states are: $C_{ao}=0.15$ ml/mmHg, $V_m=67$ ml, $T_p=1$, $p_{th}=0$ mmHg.

Other parameters:

	Control	Failure	Digitails
v_{max} (sec^{-1})	2.45	1.60	3.50
σ_{max} (g/mm^2)	7.9	5.5	9.5
T_{sys} (msec)	270	330	240
LVEDV (ml)	36	38	37
R_p (mmHg/mlsec $^{-1}$)	3.9	10.5	3.0

The setpoint of the left ventricular diastolic volume control system is adjusted so that the correct end-diastolic pressure is achieved for each simulation.

The peripheral resistance is calculated from the mean aortic pressure, the heart rate and the stroke volume:

$$R_p = \text{MAP}/(\text{SV} \cdot \text{HR})$$

The estimate of C_{ao} is determined in the "control" state. When model stroke volume is 10.5 ml, an aortic compliance of 0.15 ml/mmHg gives an aortic (aar) pressure course that is similar to the published recordings.

T_p is assumed to have its "standard" value.

v_{\max} is adjusted to achieve similar max LV dp/dt as in the isovolumic contraction and σ_{\max} is adjusted so that the stroke volumes are close to the values reported by the authors. It is necessary to iterate the adjustment of v_{\max} and σ_{\max} 1 - 2 times to achieve the desired accuracy.

The estimates of the parameters are listed in figure 8.5.

An isovolumic beat is introduced in the model by keeping the aortic valve closed during systole. The time courses of the model variables are recorded on a strip-chart recorder, figure 8.5 B.

We observe that the model l.v. and aortic pressure in the auxotomic beats follow a slightly different course in systole. This may be due to errors in the model, which is not designed to be representative of the canine cardiovascular system. In particular, the configuration of the arterial system may be different in the dog. The course of the isovolumic beat is, however, closely resembling the measurements by Ross and co-workers.

Let us denote by LVSP the maximum left ventricular pressure during an auxotonic contraction, and by LVIP the maximum during the isovolumic beat. The ratio LVSP/LVIP is 0.67, 0.87 and 0.62 for the control, failure and digitalis

states respectively. The same ratios for the simulations are 0.64, 0.83 and 0.50. These results demonstrate that the model respond to the perturbation (aortic occlusion) in a similar way as dog no. 5.

Moreover, it is interesting to note in figure 8.5 A that isovolumic maximum dp/dt does not increase beyond the auxotonic in the control and failure states, while in the digitalis state, maximum dp/dt is not reached before the start of ejection. The same phenomenon can be seen in the simulated pressure tracings, although not so pronounced.

In the model, it is easy to measure the velocity of the contractile element: Maximum v_{ce} (which is different from v_{max}) is 1.8, 1.3 and 2.5 sec^{-1} for the control, failure and digitalis states respectively.

The maximum v_{ce} was calculated by Ross & coworkers to be 1.72, 1.26 and 1.90. Except for the digitalis state, these results correlate well.

The estimated left ventricular end-diastolic volume, 31 ml, is different from the LVEDV of 15.0 ml determined by the authors using the passive pressure-volume relation of the potassium arrested heart as a basis for their estimate. An ejection fraction of 0.86 (digitalis state) calculated on the basis of their figures is not achieved in the model unless a drastic change in the assumptions.

Simulation of the human left ventricle

The model is designed to simulate the human ventricle, but the data from animal experiments are valuable for testing the model over a wider range in end-diastolic volume and aortic pressure. Thanks to the surgical team of Surgical Department A, Rikshospitalet, Oslo, tape recorded measurements of human left ventricular variables were available. Patient N.K. (figure 8.6) was undergoing coronary bypass operations at the time of measurement. Left ventricular and aortic pressures were recorded together with ascending aortic flow and the ECG. The ventricle was of "normal" size and in reasonably good condition.

Estimator I is used to determine the parameters (listed in table 8.2. During recording of the traces shown in figure 8.6, the estimator is switched off. The two first beats shown are normal auxotonic contractions. The simulated variables are in reasonably good agreement with the measurements. At point A,

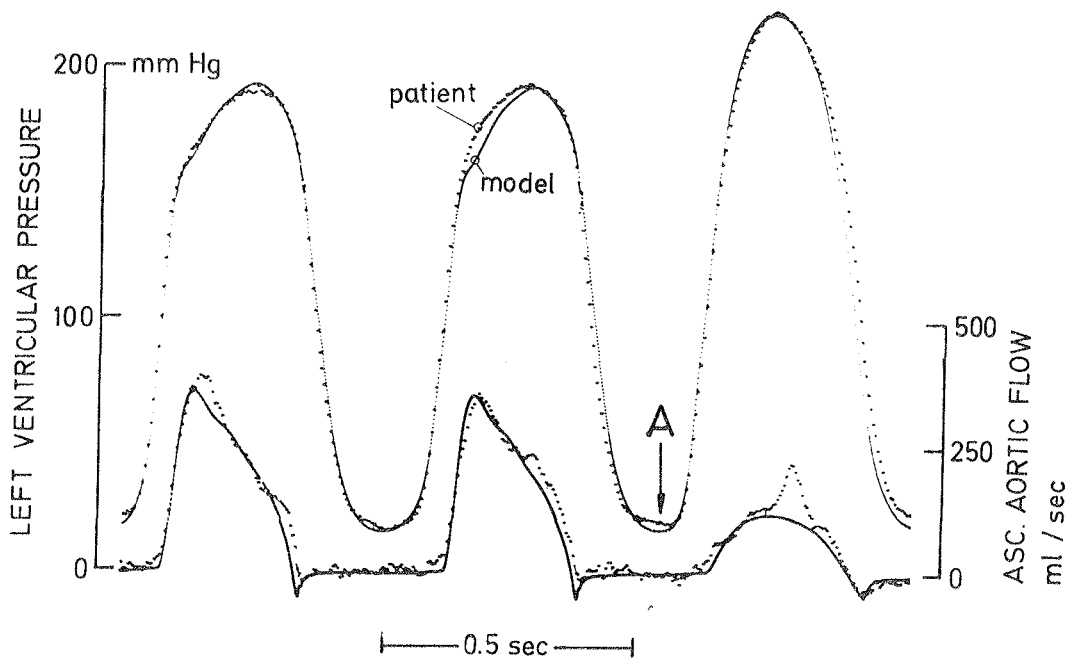


Figure 8.6. Effects of partial clamping of the ascending aorta of patient N.K. during surgery. Parameters as in table 8.2. except $\sigma_{max} = 12 \text{ g/mm}^2$. Clamping resistance = $0.7 \text{ mmHg/mlsec}^{-1}$.

the aorta is partially clamped, resulting in a sudden change in the impedance to ejection. The same maneuver is performed on the model by introducing a high resistance in the aortic valve. The aortic flow pattern is used to select the proper value of this resistance. The response to aortic clamping is an increase in left ventricular peak pressure, and a decrease in peak flow. The response of the model correlates well with the available measurements. The sharp peak in the electromagnetic flow tracing during clamping is not observed in the model, and may be an artifact.

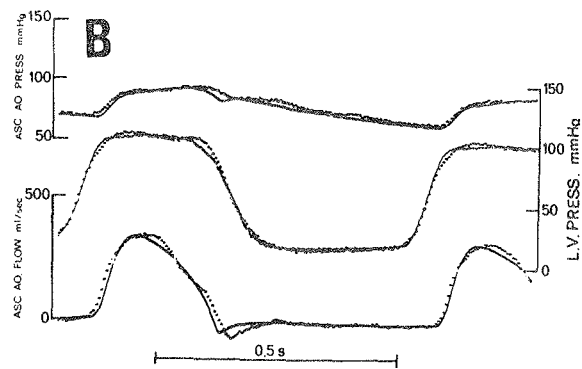
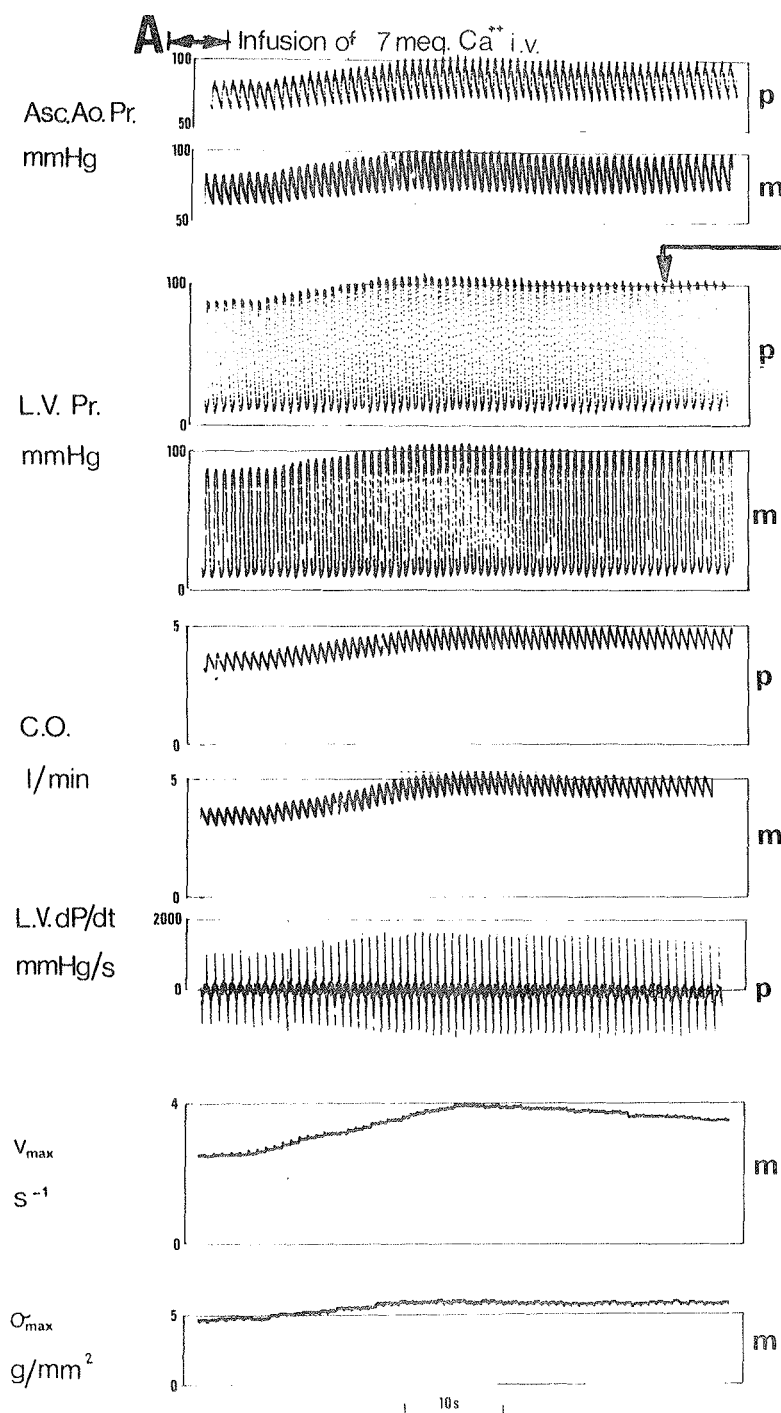


Figure 8.7 B.

Time courses of left ventricular pressure, ascending aortic flow and pressure in patient A.A. (dotted noisy curve) and simulated variables (continuous lines). These tracings are representative of the last portion of the curves in panel A, as indicated by the arrow.

Figure 8.7 A. Effect of infusion of 7 meq. Calicum intravenously in patient A.A. during surgery. Tracings marked by p are from the patient and those marked by m are from the model. Asc.Ao.Pr.: Ascending aortic pressure, L.V.Pr.: Left ventricular pressure, C.O.: Cardiac output obtained by filtering the asc. aortic flow signals with a 1. order time constant, L.V. dP/dt: Time derivative of left ventricular pressure (in patient), v_{max} : max. velocity and σ_{max} : max. tension of contractile element as estimated from the σ_{max} measurement using the approach described in chapter 6 (Esimator I). Parameters as in table 8.2.

Left ventricular pressure of patient R.H. undergoing a similar operation is shown in figure 6.15. The aortic pressure and flow of patient R.H. and N.K. are shown in figure 9.2.

One recording of a change of inotropy in the human heart became available before finishing this report. Patient A.A. was undergoing surgery for mitral valve replacement due to combined stenosis and insufficiency of this valve. His ventricle was in a reasonable good condition, and had only slight signs of dilatation and hypertrophy. The measurements shown in figure 8.7 A were taken approximately 20 minutes after termination of cardio-pulmonary bypass. To the left of this recording the cardiac output was 3.45 l/min and max. left ventricular dp/dt was 1000 mmHg/sec. The operating team decided to infuse calcium to improve ventricular contractility and increase the cardiac output. The effect of this is shown in the figure. Cardiac output rose to 4.5 l/min and max l.v. dp/dt to 1700 mmHg/sec.

The patient is simulated, using estimator I. Cardiac output in the control state (before infusion) is used as a basis for estimating C_{aO} . In this simulation, reasonably good curve-fits are obtained, as shown in the figure 8.7 B where patient and model tracing are superimposed. The estimate of cardiac output, based upon the pressure recordings is shown in figure 8.7 A. The model appears to overestimate slightly the increase as it predicts 4.75 l/min after the effect of calcium (compared to 4.5 l/min by electromagnetic flowmetry). The reason for this is probably the increase in arterial pressure causing a decrease in aortic compliance because of nonlinear effects.

The estimates of the contractility parameters change after infusion of calcium as can be seen in the two lower tracings of figure 8.7 A. v_{max} increases from 2.5 sec^{-1} to 4.0 sec^{-1} and σ_{max} increases from 4.8 g/mm^2 to 6.2 g/mm^2 .

We also observe that the l.v. end-diastolic pressure is relatively constant during the intervention.

10 patients undergoing operations for aortic valve replacement are simulated. 5 of these also had their mitral valve replaced. The pivoting disc valve prothesis represent a restriction to ventricular outflow. We found that the instantaneous pressure gradient across the valve was approximately proportional to the square of the flow through the valve as measured by an electromagnetic flowmeter (Aaslid & al 1974). The viscous term of the aac flow submodel was replaced by a quadratic term: $(q_{aac}/k_{av})^2$, where k_{av} is a parameter dependent upon valve type and size. The value of k_{av} was determined individually from the measurements as:

$$k_{av} = q_{max} / \sqrt{\Delta p_{qmax}}$$

q_{max} is peak ascending aortic flow and Δp_{qmax} is the difference between l.v. and ascending aortic pressure at the instant of peak flow.

Some of these patients had indications of dilated and/or hypertrophied ventricles. On the bases of chest x-rays and angiographic procedures a value of V_m was assumed.

The recordings of pressure and flow were taken after termination of cardio-pulmonary by-pass and before closing the chest. We observes an abnormally wide QRS-complex in the ECG of some of these patients. This indicates a considerable delay from the activation of the first left ventricular muscle fibre until the entire myocardium is activated. We may expect that the rise of isovolumic l.v. pressure will be slower due to this. This effect may be simulated by assuming an abnormally compliant series elastic element in these patients. We use the relation:

$$k_{se} = 24 \cdot 80/T_{QRS}$$

k_{se} is series elastic element stiffness (normally 24/unit muscle length) and T_{QRS} is the width of the QRS complex (normally 80 msec).

Estimator I is used and aortic compliance is estimated by the cardiac output method (Chapter 6). The results are summarized

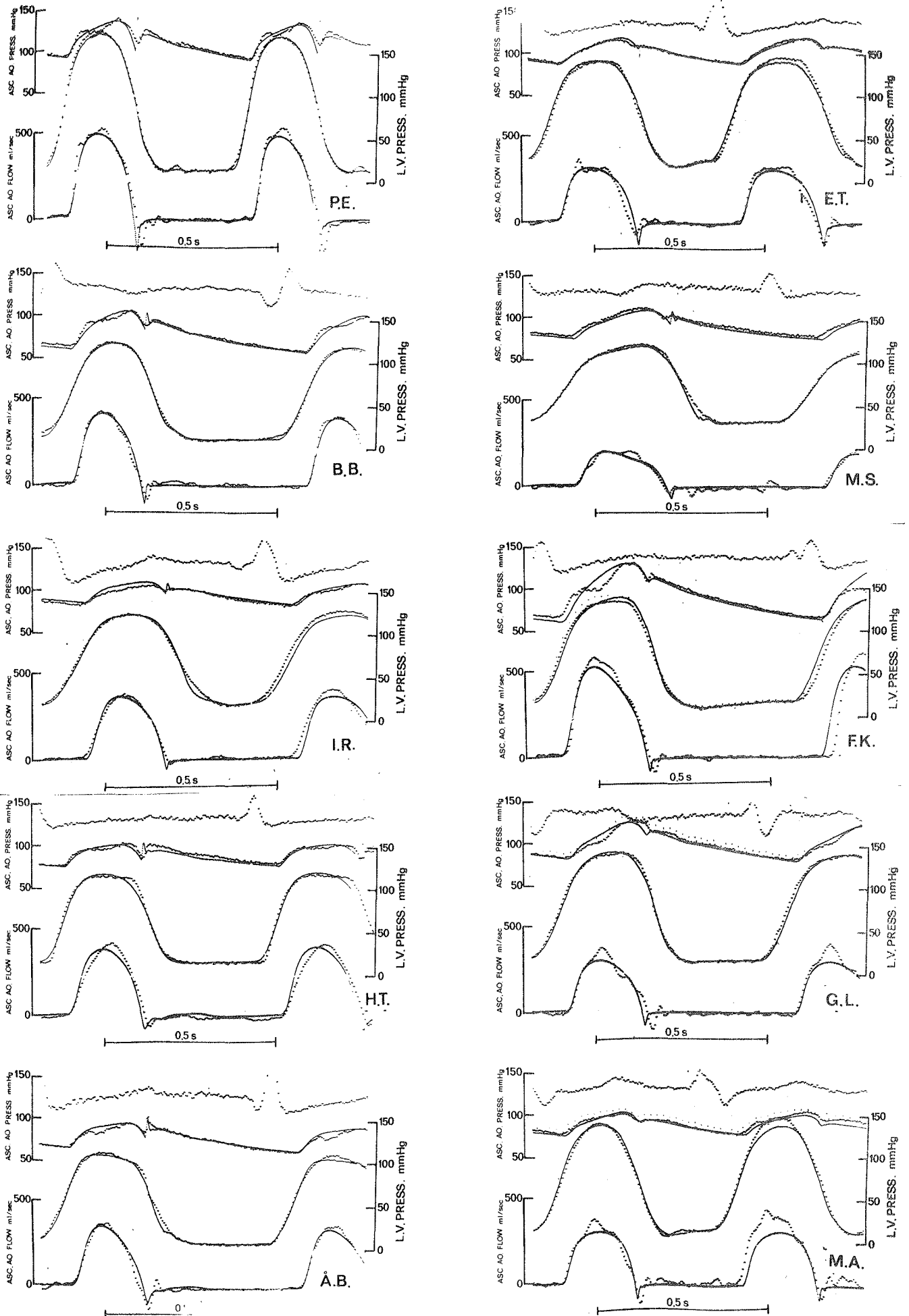


Figure 8.8. Superimposed patient (slightly noisy) and model pressure and flow tracings. Parameters are listed in table 8.2. The upper tracing is the ECG.

Table 8.2. Results from simulation of patients undergoing open-heart surgery.

Patient	Age	Operation	MAP mmHg	C.O. l/min	v_{\max_1} sec ⁻¹	σ_{\max_2} g/mm ²	T_{sys} msec	R_p $\frac{\text{mmHg}}{\text{mlsec}}^{-1}$	C_{ao} $\frac{\text{ml}}{\text{mmHg}}$	T_p (norm)	V_m ml	k_{se} (norm)	k_{av} $\frac{\text{mlsec}^{-1}}{(\text{mmHg})^{1/2}}$	
R.H.	53	CB	113	3.55	1.4	10.5	505	1.85	0.53	2.0	230	24	330	
N.K.	55	CB	169	5.8	2.2	13.0	460	1.7	0.25	1.4	230	24	330	
P.E. (2)	53	AO+MI	112	6.6	3.6	11.0	320	1.05	0.63	1.4	300	24	95	
B.B.	52	AO+MI	80	4.8	2.2	9.5	420	1.05	0.53	1.4	350	14	120	
I.R.	43	AO	95	5.0	1.8	8.0	460	1.40	0.89	1.4	320	15	130	
H.T.	51	AO	89	5.8(1)	2.7	7.0	390	0.90	1.08	2.0	400	24	130	
Å.B.	55	AO	78	5.0(1)	1.7	10.0	390	0.95	0.87	2.0	300	17	135	
E.T.	64	AO	101	5.2	2.3	8.0	400	1.20	0.90	1.4	300	17	73	
M.S.	60	AO+MI	90	3.2	1.25	6.5	500	1.80	0.45	1.4	260	17	78	
F.K.		AO+MI	95	2.1	2.1	10.0	435	0.85	0.51	1.4	320	14	140	
G.L.	63	AO	104	4.3	1.9	9.0	430	1.50	0.53	2.8	300	15	72	
M.A.	44	AO+MI	88	5.5	2.5	8.0	380	1.20	0.88	1.4	320	16	58	
A.A.	45	MI	see figure 8.7							1.00	1.4	230	24	220

(1) - Flow measured in aar on model

(2) - ECG not shown

CB - Coronary bypass measured before cardio-pulm. bypass

AO - Aortic valve replacement measured after cardio-pulm bypass

MI - Mitral valve replacement measured after cardio-pulm. bypass

AO+MI - Aortic and Mitral valve replacement measured after cardio-pulm. bypass

MAP - Mean aortic pressure, otherwise abbreviations as in table 6.1 and chapters 2 and 3.

For all: $T_1 = 5$ msec, $T_2 = 5$ msec. (Flowmeter time constants)

in table 8.2 and the ECG, the ascending aortic flow and pressure, as well as l.v. pressure for these patients are shown in figure 8.8.

Discussion

The left ventricle may be envisaged in systole as a pressure, volume and time-dependent flow generator:

$$q_{av} = f_{qlv}(p_{aac}, V_{lv}, t)$$

and in diastole as a passive nonlinear volume compliance:

$$p_{lv} = f_d(V_{lv})$$

The functions f_{qlv} and f_d are defined by the assumed model structure and the various nonlinear functions described in chapter 2, as well as the parameters V_m , v_{max} , σ_{max} and T_{sys} that can be varied to simulate changes in ventricular size and contractile state. With many nonlinear functions involved, it is somewhat surprising to find that the function curves obtained on the model are nearly linear (figure 8.2).

Unfortunately, a thoroughly documented study on such function curves with sufficient information to simulate the experiments has not been found in the literature.

A family of function curves, such as shown in figure 8.2 is a simplified expression of the function f_{qlv} . For any end-diastolic volume (fibre length or pressure) and peak systolic pressure, the stroke volume is given by the appropriate point on the curve. If a certain disturbance changes both LVEDV and LVSP, the result of this change on the stroke volume can be predicted from such curves - under the condition that the contractile state does not change.

The function curves in figure 8.2 are essentially determined on the basis of the control state (I) only. This diagram is

found to be quite accurate in the prediction of the response to increased MCL and LVSP. Even if the verification of 4 points in this diagram is no definite proof that the family of function curves is valid, this evidence nevertheless supports the proposed model.

The almost linear inverse relation between LVSP and SV at a constant LVEDV is different from the results of Sagawa (1967) and Sarnoff & al (1960). These authors found that the SV was almost independent of mean arterial pressure below a certain threshold pressure (assuming constant mean left atrial pressure). A mechanism called homeometric autoregulation was postulated (Sarnoff & al 1962) to account for the increased vigour of contraction in response to raised aortic pressure. No evidence for such a mechanism is found in the results of Bugge-Asperheim & Kiil (1973).

Let us assume a constant end-diastolic volume of the ventricle. The maximum pressure, LVIP, is reached during an isovolumic contraction. If the aortic obstruction is only partial or absent, the peak systolic pressure LVSP is less than LVIP. Two factors contribute to this phenomena:

- 1) The volume effect: When ejection starts, the muscle fibres shorten, thus for sarcomere lengths below the optimum ($\sim 2.2\mu$), the potential of developing tension decreases. This effect may partially be compensated by an increased shape factor when the left ventricular volume decreases ("Laplaces law").
- 2) The velocity effect: According to the force-velocity relation of heart muscle (figure 2.11 and Sonnenblick 1962), the shortening velocity affects the tension developed; if the velocity increases during the auxotonic beat, developed force diminishes.

The stroke volumes are practically identical in model and experiment. In light of the findings presented in the section on simulation of the effects of saline expansion and aortic clamping, it seems justifiable to infer that the volume effect (1) is reasonably realistic in the model.

The findings of Ross & al demonstrate that the heart with an increased contractility, implying an increase in stroke volume and velocity of fibre shortening exhibit an increased LVIP, while the failing heart develops a LVIP which is close to LVSP.

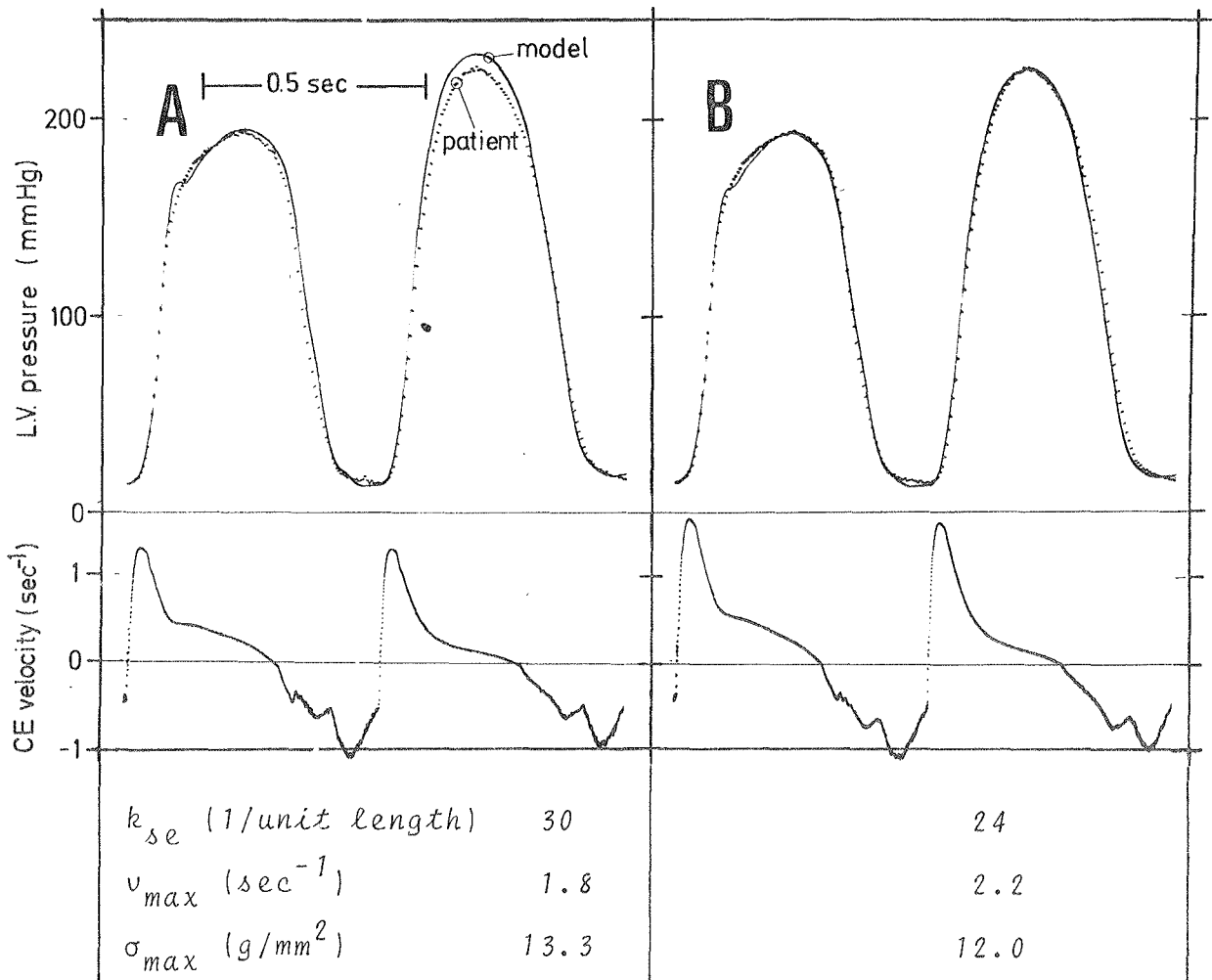
The simulations shown in figure 8.5 demonstrates that the model is capable of predicting this effect of aortic constriction under different levels of inotropy. This result may be interpreted as indirect evidence that the velocity effects (2) are similar in dog and model, implying that the force-velocity relation of the muscle model is reasonably realistic for the loads encountered during ejection.

When a somewhat "milder" occlusion is applied to the human ventricle during surgery, the model predicts the effect of this perturbation on the pressure course.

A relevant question at this stage is: If we base the model upon different assumptions, can a similar ability to predict real ventricular behaviour be demonstrated? The available recordings and data do not allow a thorough investigation of all assumptions, but we may take one example based upon the recording from patient N.K.

The rate of pressure buildup during isovolumic contraction in the model is determined by the interaction between the compliance of the series elastic element and the force-velocity relation of the contractile element. Let us assume a somewhat stiffer SE, $k_{se} = 30$, than the "standard". In order to achieve a "correct" rate of isovolumic pressure buildup in the model, the estimator reduces v_{max} from 2.2 sec^{-1} to 1.8 sec^{-1} . The result of this is that the ability to eject the stroke volume, which is determined by the capabilities of the fibres to shorten, is diminished, and the estimator compensates for this by increasing σ_{max} from 12.0 g/mm^2 to 13.3 g/mm^2 . As shown in figure 8.9 A the parameters based upon an assumed k_{se} of 30 also give rise to an auxotonic pressure tracing that is closely resembling the real. But the response to aortic clamping is

different, the model reaches a higher peak pressure than the real ventricle. This is indirect evidence that a series element stiffness of $k_{se} = 24$ is a reasonable assumption; as shown in figure 8.9 B we then achieve a faithful simulation of the left ventricular pressure course in both beats. But the results are also influenced by other assumptions as the shape and curvature of the force-velocity curve and the course of active state.



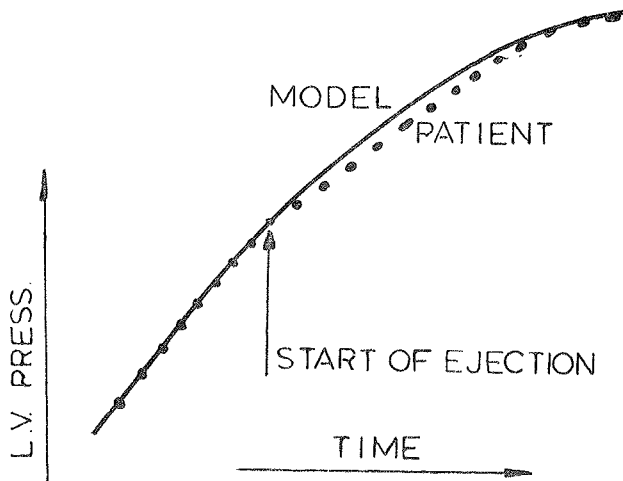
Other parameters as listed in table 8.2. (Patient N.K.)

Figure 8.9. Effects of partial clamping of the ascending aorta for two assumptions of series elastic element stiffness. CE velocity: Shortening velocity of contractile element.

The lower tracing in both panels represent the velocity of the contractile element. It is seen that a considerable amount of CE shortening occur before ejection. The maximum v_{ce} of 1.6 sec^{-1} is reached early in isovolumic contraction. The maximum v_{ce} during ejection is 0.47 sec^{-1} , or 21% of v_{max} .

The simulation of 10 patients undergoing open-heart surgery demonstrates that the model may generate reasonably realistic left ventricular pressure and outflow waveforms for the human heart, and that the adjustment of parameters allow the individual case to be simulated.

If we regard this material closely, we find noticeable aberrations for most of the simulations. The slope of the left ventricular pressure tracings change rather abruptly just after onset of ejection in the patient. This phenomena is most pronounced in patients I.R., H.T., F.K. and G.L., but is also seen in the others. The tracing from the model change its slope more gradually. A schematic illustration of this phenomenon is shown in figure



8.10. The single 3-element muscle model appearantly does not represent the transition from isovolumic contraction to ejection accurately. The causes of this discrepancy are not clear.

Figure 8.10
Course of patient and model left ventricular pressures at onset of ejection (Schematic).

Also we note that the course of patient and model ventricular pressures in late ejection and isovolumic relaxation are different for some patients (particularly H.T. and Å.B.) while others are simulated quite well (P.E. and B.B.). It is possible that non-synchronous repolarisation of different muscle fibres influence this part of the pressure curve. Presently we have included no

description of such phenomena, and the course of isovolumic relaxation is determined by the decline of active state as shown in figure 2.14. The estimation scheme is based upon the assumption that the rate of rise of l.v. pressure during the isovolumic contraction period reflect a velocity contractile property of the myocardium. The l.v. dp/dt is also influenced by the end-diastolic volume and the maximum tension that can be developed. Using the proposed estimation scheme, we should have the same influence of these factors in the model, - under the assumptions that it is reasonably realistic. The estimate(s) of v_{max} (and σ_{max}) should then ideally be independent of left ventricular filling. The simulations of the experiments on dogs (figure 8.1 and 8.2) are a preliminary indication of this. The dependency of the estimates on changes in l.v. filling remains to be investigated for the human ventricle (and further confirmed for the dog ventricle).

Increasing the inotropy of the human heart by calcium reflects itself in an increase in v_{max} and σ_{max} (figure 8.7). This result is in accordance with the findings of Sonnenblick (1962) on papillary muscle. He found that both the maximum velocity and the isometric tension rose as a result of an increased calcium concentration in the perfusion bath.

In a ventricle, the muscle fibres are depolarized in sequence, and a considerable time may pass from the activation of the endocardial fibres until the last muscle of the epicardium is activated. The width of the QRS-complex is a rough measure of the time required for the spread of electrical (and mechanical) activation in the myocardium. It is quite obvious that the time required for the spread of activation also influences the course of isovolumic pressure buildup. In the present simulations we have chosen to modify the SE-compliance to account for this effect. Given a fixed v_{max} , the rate of rise of isovolumic tension is dependent upon the value of k_{se} . Further investigations on this problem are necessary to find out if this is a realistic choice.

In dilated and/or hypertrophied ventricles (to a less extent in normal) we may expect that muscle fibres situated at different depths of the myocardium work in different regions of their

length-tension relationships. Also, in abnormal ventricles, the passive pressure-volume relation of the chamber may be significantly different from the "normal". It remains to be investigated if and how a single "average muscle fibre" model should be modified to account for these situations. The end-diastolic volume and the muscle fibre stretch are estimated on the basis of the end-diastolic pressure. This approach is probably quite inaccurate especially at lower levels of filling, and better means of evaluating these variables should be considered.

The 10-layer model recently proposed by Hanna (1973) gives insight into the distribution of stress, length and velocity within different layers in the myocardium. A comparison between some of the parameters assumed by Hanna (1973) and the "standard" parameters of the model developed in the present study (table 8.3) demonstrates a good correlation except for σ_{\max} .

Although not explicitly formulated by Hanna (1973) one gains

Table 8.3

	v_{\max}	σ_{\max}	LVEDV	SV	V_m
Hanna 1973	4.8 u/sec = 2.4 sec ⁻¹	16.5 g/mm ²	150 ml	75 ml	225 ml
Present study	2.1 sec ⁻¹	10 g/mm ²	150 ml	70 ml	230 ml

the impression that such a complex model is necessary to simulate the left ventricle. His argument is based upon a comparison with the model of Beneken & de Wit (1967). The left ventricular variables pressure and flow of their model did not compare favourably with time courses found in a real ventricle. The present model is essentially based upon the same approach as the model of Beneken & de Wit (1967), but with some modifications. The results presented in the previous sections suggest that the normal left ventricular behaviour may be simulated quite faithfully by this approach. This does not imply that the muscle model is "correct". But the results indicate that it may be used as a conceptual tool for the interpretation of ventricular dynamics.

Chapter 9.

SIMULATION OF THE ARTERIAL SYSTEM

Introduction

The arterial model as presented in chapter 3 is intended to represent a realistic load or impedance on the ejection from the left ventricle, and it should also reproduce the pressure and flow pulse propagation along the aorta, the carotid and the iliac-femoral arteries.

First a comparison in the frequency domain is presented. Then the model pressure and flow waveform patterns are compared with measurements from patients undergoing open-heart surgery at the Surgical Dep. A, Rikshospitalet. A number of aortic pressure recordings from the catheterizations at the Section of Cardiology, the Central Hospital, Trondheim were also available for comparison studies. Two of these are selected here. They both have reasonably good catheter-manometer frequency responses and the patients' arterial systems are essentially normal. Data from the rest of this patient group are presented in another section of this chapter.

Frequency domain comparisons

The hydraulic (or hemodynamic) impedance:

$$Z(j\omega) = p(j\omega)/q(j\omega)$$

as defined in chapter 3 is an intrinsic property of the vascular system, and is independent of the input signal if the system is linear. If non-linear effects do not become prominent, the impedance is a convenient concept to express the pressure-flow relation.

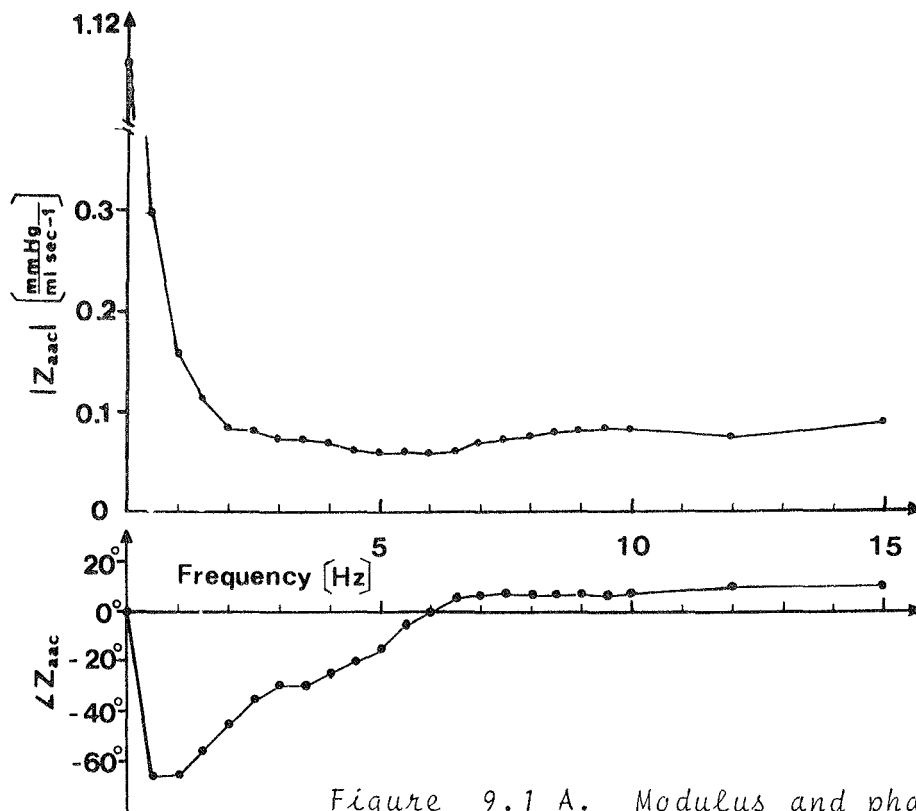


Figure 9.1 A. Modulus and phase of the impedance of the model aorta.

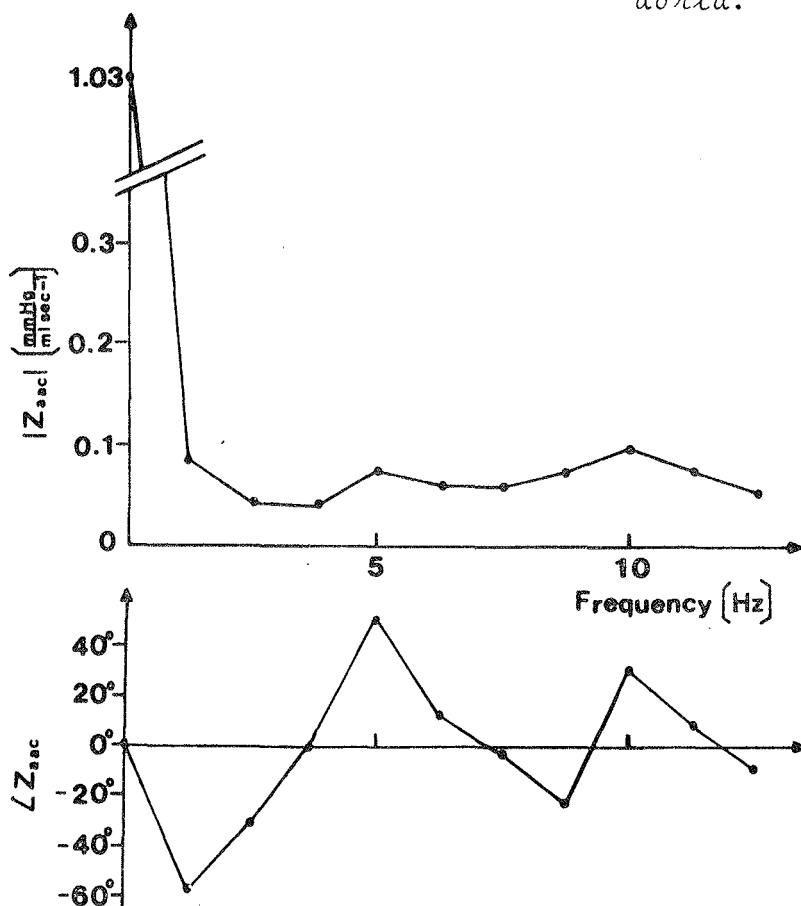


Figure 9.1 B. Modulus and phase of the impedance of patient C.H. as reported by Patel & al (1965).

It is simple to excite the arterial model with a sinusoidal input flow, and measure the amplitude and phase of the pressure and flow signals for the segments.

Figure 9.1 A illustrates the frequency dependence of the impedance modulus and phase for the ascending aorta as measured on the model with "standard" parameters as in table 6.1. Both frequency and modulus are plotted linearly, following the usual convention established in physiological literature.

These plots demonstrate clearly that the impedance to ejection is much lower in the frequency range of 1 - 10 Hz than the total peripheral resistance. The reason for this is the volume storage effects of the elastic arterial and aortic walls.

It is not advisable to measure the impedance in the human cardiovascular system by forcing a sinusoidal flow into the aorta. Only by harmonic analysis of naturally occurring pressure and flow pulses is a determination of impedance possible. This method is connected with considerable error sources due to noise, measurement artifacts, and the dynamic and static distortion of the signal in the measurement and recording system. The Fourier transform also imposes its own truncation errors on the results. As the impedance is an indirect way of expressing the pressure-flow relation, any errors in the results are not immediately attributable to the original data.

Probably because of the difficulties experienced when trying to obtain high-fidelity measurements in a clinical situation, the published data on the impedance of the human arterial system are scarce.

In figure 9.1 B the impedance calculated by Patel & al (1965) for the patient C. H. is redrawn.

Even if the main patterns of the model impedance are similar to the published calculations, some deviations are seen, especially in the phase angles. If we examine Patel's data more closely, we will however, find even greater variations in the impedance modulus and phase from one patient to another. These data is therefore not ideal for testing the validity of the model.

Time domain comparisons

Simultaneously recorded pressure and flow waveforms contain information to compute a more or less accurate (depending upon the noise level) estimate of the impedance. If the simulated variables exhibit time courses that are closely resembling recordings from the human arterial system, the impedance may also be assumed correlate well for the frequencies present in the waveforms. It therefore seems unnecessary to use impedance comparisons if the model is able to reproduce sufficiently well the measured timecourses. A direct comparison of the timecourses is, however, only proper if the input signals are similar. This might be achieved by driving the model with one measured variable (for example flow), as demonstrated by Spencer & al (1961). In the following simulations, this approach has not been judged necessary since the model is able to generate realistic input signals to the arterial model.

During coronary by-pass operations, high quality measurements of ascending aortic pressure and flow are possible. The circulatory system behaves essentially normal in these patients.

The slightly noisy and sampled tracings shown in figure 9.2 are obtained from patients N.K. and R.H. just after exposure of heart. Estimator I is used to obtain pressure curvefit. The aortic compliance is estimated on the basis of the mean aortic flow (cardiac output) amounting to 3.55 l/min for R.H. and 5.8 l/min for N.K. The simulated pressure waveforms are in good agreement with the measurements.

The present data cannot be used for a verification of the mean ascending aortic flow estimate as this information is used in the estimation procedure. The dynamic flow course, however, represent independent information. The simulated flow-patterns are in good agreement with the measurements, in fact the curvefit seems to be even better than for the pressure waveforms. We notice that patient N.K. has a high blood pressure and stiff aorta while R.H. is closer to the "standard". The parameters are listed in table 8.2.

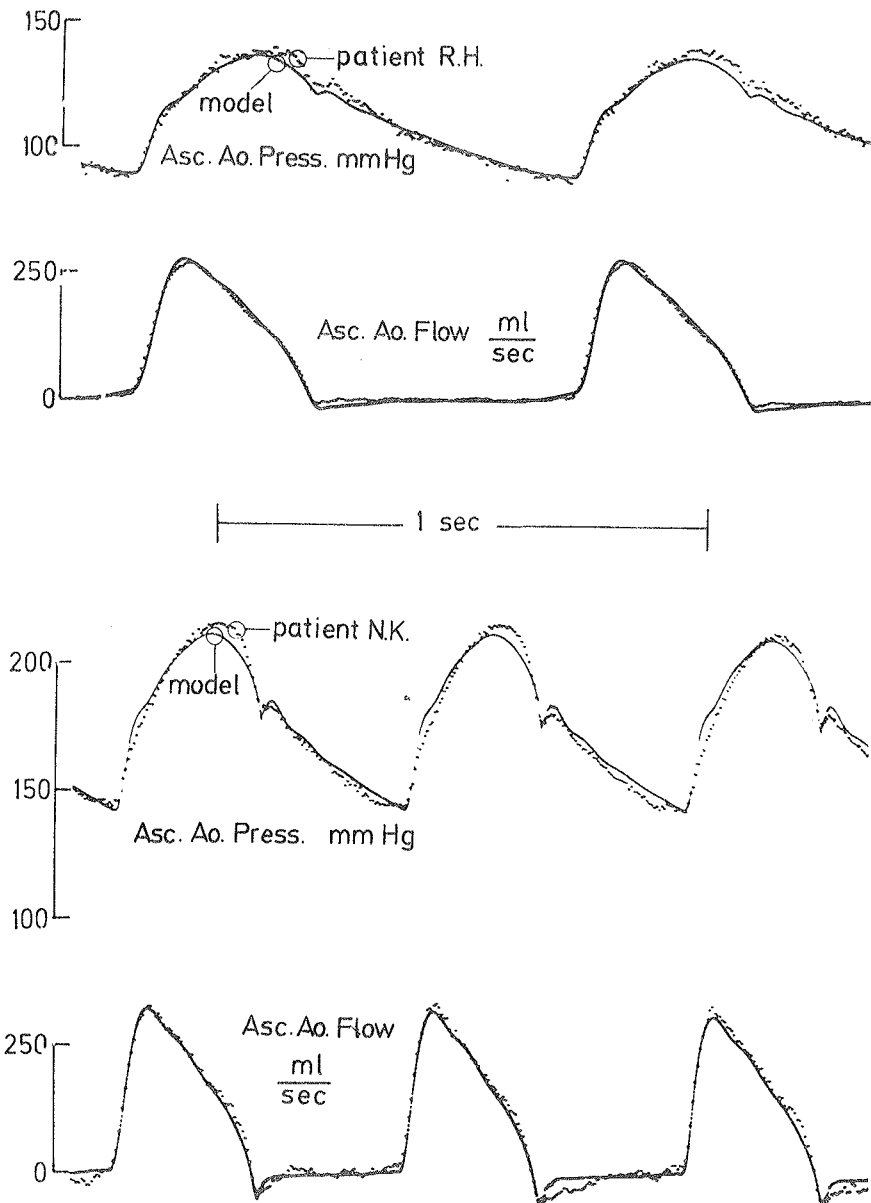


Figure 9.2. Ascending aortic pressure and flow in patients R.H. and N.K. during surgery. Simulated tracings superimposed. Parameters in table 8.2.

Simultaneous recordings of pressures and flows at other locations in the aorta have not been available. During catheterization, however, the opening of the pressure lumen may be positioned at practically any location in the aorta. Data for two patients, B.L. and N.N. are shown in figure 9.3. Estimator II is used and aortic compliance is estimated from the pulse transmission time.

B.L. has a "standard" aortic compliance and a cardiac output of 3.8 l/min by Fick's method whereas the simulation gave 4.0 l/min. The arterial blood pressure is fairly low - 100/55 in the ascending aorta.

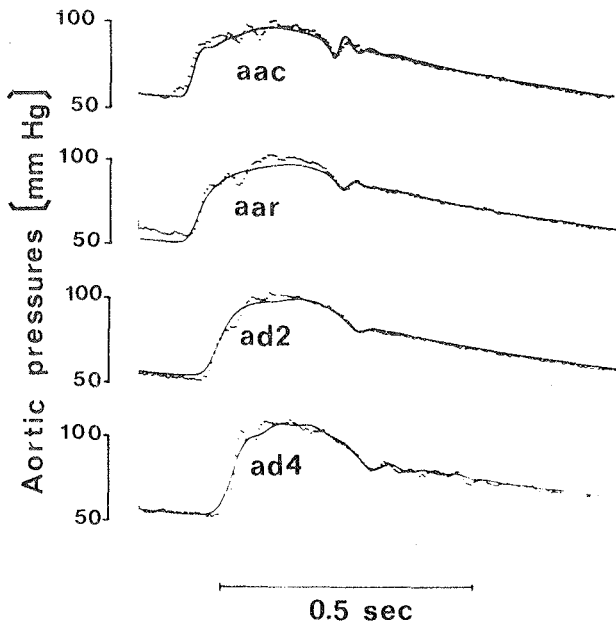


Figure 9.3 A. Aortic pressures from patient B.L. and superimposed model pressures.

Parameter table		
Patient	B.L.	N.N.
v_{max} (sec^{-1})	1.9	2.0
σ_{max} (g/mm^2)	8.5	13.0
T_{sys} (msec)	500	520
LDV (ml)	150	180
V_m (ml)	230	230
C_{ao} (ml/mmHg)	0.87	0.72
T_p (dim. less)	1	1
R_p (mmHg/mlsec $^{-1}$)	1.10	1.25
p_{th} (mmHg)	-4	-4
δ_0 (Hz)	24	12
ξ (dim. less)	0.2	0.3

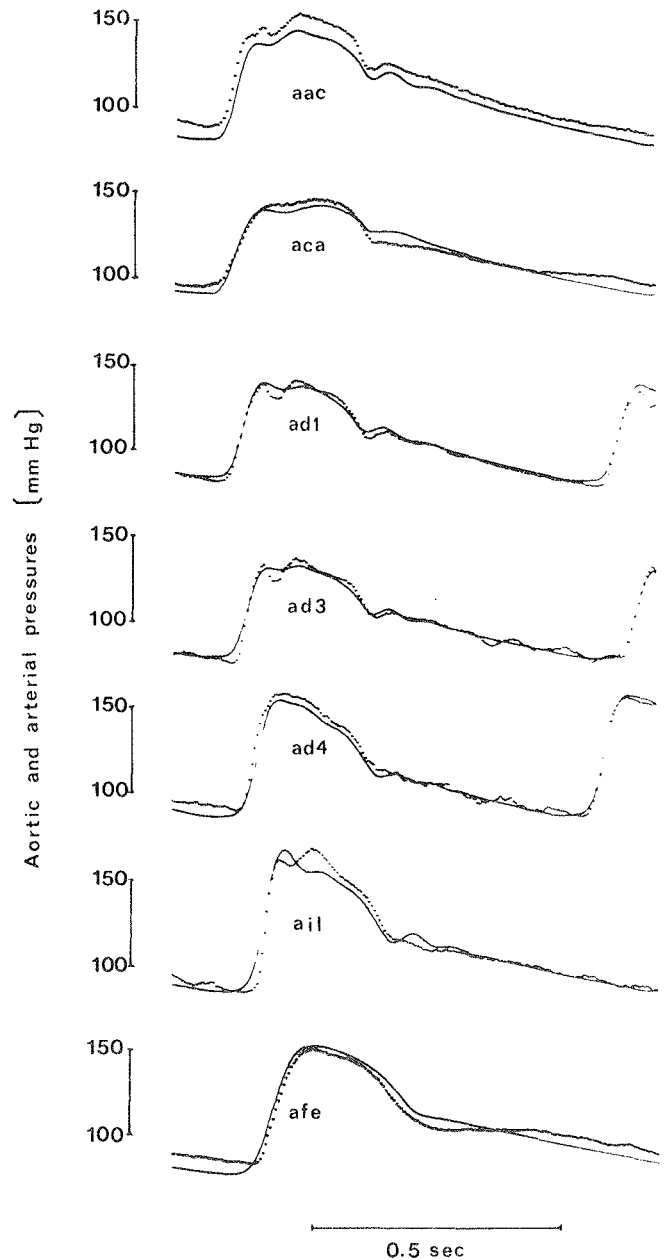


Figure 9.3 B. Aortic pressure from patient N.N. Model pressures superimposed. See figure 3.9. and table 3.2 for abbreviations. (p. 50 and p. 54).

The other patient, N.N., has a slightly stiffer aorta (1.2 x "standard"), the cardiac output was not measured, and the ascending aortic pressure was somewhat high (150/90). The patient tracings *aca* and *afe* are obtained by external pulse transducers (Aaslid & Brubakk 1971) on the carotid and femoral artery respectively.

The tracings demonstrate how the pressure waveshape is dependent on the position in the arterial system. The systolic pattern changes from being relatively flattopped into a more triangular shape, and both the initial upstroke and the peak pressure increase as the catheter is withdrawn from the ascending aorta to the iliac artery. The delay line effects of the aorta are also apparent in the tracings, which start simultaneously with the R-wave of the ECG. The superimposed curves from the model are in good agreement with the measurements, except for the diastolic portion of the pulse tracings (*afe* and *aca*). These external measurements cannot be expected to correlate too well with intravascular recordings, and they are scaled in amplitude to correspond to the model.

Simulation of a group of 24 patients

In cooperation with dr. A.O. Brubakk, a pilot investigation on the aortic dynamics in the human was undertaken, using the proposed model and estimation method.

A group of patients undergoing catheterization at the Central Hospital, Trondheim (22 patients) and at St. Thomas Hospital, London (2 patients) were simulated. With permission of dr. A.O. Brubakk and dr. R.D. Bradley this material is included in the present thesis.

Aortic and arterial pressures were measured through catheters connected to the pressure transducers. The site of measurement was the ascending aorta in 6 patients, the aortic arch just distal to the left carotid artery in 16 patients and the iliac artery in 2 patients. In 22 of the patients, the catheter was withdrawn gradually to determine the propagation delay through the aorta. Femoral and carotid artery pulse tracings were obtained using a

system described previously (Aaslid & Brubakk 1971). ECG and heart sounds were recorded together with the pressures on magnetic tape.

For simulation of these patients, the estimator II was used as described in chapter 6. The setpoint of the l.v. end-diastolic volume control system was adjusted to give a reasonable end-diastolic volume. The model was able to simulate the pressure recordings with acceptable accuracy. We also tried the estimator for 5 patients with atrial fibrillation, but the dynamic response was not satisfactory and these are excluded from the material. The aortic compliance was estimated on the basis of the pressure pulse transmission time. Both withdrawal data as well as the external pulse measurements were used. To minimize "observer-bias" the results of the cardiac output determinations were not known to the operator.

Cardiac output was determined in 12 patients using Fick's principle. Blood samples were drawn from the pulmonary artery and the aorta. In 8 patients dye dilution was used, injecting Cardiogreen in the superior vena cava and sampling in the aorta. In the remaining 4 patients thermodilution was used. Room temperature saline was injected in the superior vena cava and the temperature in the pulmonary artery was recorded. The cardiac outputs ranged from 1.7 to 9.7 l/min.

The results of this investigation are presented in table 9.1. The factor $L_{ao} = C_{ao}(\text{pulse})/C_{ao}(\text{C.O.})$, is relevant for the comparison of the two independent methods for estimation of aortic compliance. We find that L_{ao} has a mean of 0.96 and a mean absolute deviation of 0.08. The maximum deviations are -0.20 (patient 21) and +0.19 (patient 14).

Patient no.	Sex	Age years	Height cm	Weight kg	HR min ⁻¹	MAP mmHg	C.O. l/min	C _{ao} (pulse) ml/mmHg	C _{ao} (C.O.) ml/mmHg	C _{ao} (pulse)	Diagnosis
										C _{ao} (C.O.)	
1	M	16	181	76	102	95	7.0	1.01	1.18	0.86	Systolic murmur
2	M	20	181	91	58	113	4.9	1.01	1.01	1.00	H.T.(Hypertension)
3	M	27	173	68	77	123	4.4	0.87	0.89	0.98	H.T.
4	M	32	176	75	66	135	5.0	0.53	0.64	0.83	H.T.
5	M	36	190	75	60	78	3.8	0.87	0.81	1.07	Kidney cyst
6	M	41	173	78	58	110	4.1	0.61	0.71	0.86	H.T.
7	M	46	177	76	80	145	5.4	0.49	0.53	0.92	H.T.
8	M	47	170	74	68	143	8.3	0.47	0.56	0.84	Uremia
9	M	47	164	67	108	103	4.5	0.55	0.58	0.95	Cardiomyopathy
10	M	48	182	79	85		5.9	0.64	0.58	1.10	H.T.
11	M	57	166	86	71	95	5.4	0.81	0.89	0.91	Mitral insuff.
12	M	58	174	88	59	128	5.1	0.51	0.54	0.94	A.P. (Angina Pectoris)
13	M	58	169	79	75	98	2.8	0.20	0.21	0.95	A.P.
14	M	59	170	70	67	90	3.1	0.68	0.59	1.15	H.T.
15	M	59	177	85	66	103	4.2	0.55	0.61	0.90	A.P.
16	M	60	163	82	62	125	5.2	0.45	0.45	1.00	A.P. + H.T.
17	M	60	171	69	69	113	4.3	0.43	0.46	0.96	A.P.
18	M	64	170	65	78	100	3.4	0.47	0.50	0.94	Myocard. infarction
"					75	100	3.0	0.47	0.52	0.90	
"					79	100	2.7	0.47	0.45	1.04	
19	M	66	170	69	100	100	3.4	0.32	0.29	1.10	Myocard. infarction
"					85	88	2.8	0.32	0.32	1.10	
"					84	83	2.5	0.32	0.30	1.07	
"					115	75	1.7	0.44	0.51	0.88	
20	M	78	171	73	65	113	3.7	0.41	0.32	1.08	Pulm. Hypertension
"					65	105	5.1	0.41	0.50	0.82	
21	F	18	165	59	34	65	5.8	1.52	1.96	0.76	Cong. A-V. block
"					56	93	9.7	1.52	1.62	0.96	
22	F	40	168	53	98	153	6.2	0.47	0.43	1.09	H.T.
23	F	51	160	55	83	75	3.6	0.45	0.44	1.02	Myocard. infarction
"					75	83	3.3	0.45	0.50	0.90	
24	F	66	165	54	62	108	4.3	0.34	0.32	1.06	Renal tuberculosis

Table 9.1. Results from simulation of 24 patients. 6 of these are measured in different cardiovascular states. HR-heart rate, MAP-mean arterial pressure, C.O. cardiac output, C_{ao} (pulse)- Aortic compliance as estimated by pulse transm time. C_{ao} (C.O.) Aortic compliance as estimated by cardiac output-pulse pressure method (Chapter 6).

Discussion

The model of the arterial system proposed in chapter 3 is less detailed than the comprehensive models of de Pater (1966) and Noordergraf (1963). It also has fewer segments than the analog computer model of Snyder & al (1968), but otherwise this is quite similar. Since different segmentation strategies are used (equal volume vs. equal bandwidth segments) the models are not, however, directly comparable.

The authors mentioned above, and other modelbuilders of the arterial system have not published extensive reports on how their models compare with physiological or clinical measurements. It is therefore difficult to compare the performance of the present model with the approaches of other authors.

It is clear that the results presented in this chapter are too scarce to justify all the assumptions introduced in chapter 3. Some main aspects of the model can, however, be given evidence.

Compared with the calculations of Patel & al (figure 9.1), the input impedance of the model seems reasonable, although deviations in phase are seen. These may be caused by errors and noise in the measurements.

The peripheral resistance R_p determines the impedance level at 0 Hz. As patient and model have identical mean arterial pressures and cardiac outputs, the estimate of this parameter can be regarded as representative within the errors inherent in the measurements techniques. The influence of R_p on the impedance modulus for frequencies higher than 1 Hz is normally small.

The compliance of the aorta is a chief determinant of the input impedance in the range from 0.5 Hz and up. A considerable part of the stroke volume is stored in the aorta during diastole. The "aortic compliance" may be estimated matching the model stroke volume and the aortic pressure time course with the measurements from the patients (chapter 6). It is then found that the simulated flow (and pressure) is closely resembling the real (figure 9.2). Furthermore (as discussion in a subsequent section), the transmission characteristics of the model aorta are reasonable, and the compliance estimate based on the pulse transmission time C_{ao} (pulse) is quite close to C_{ao} (C.O.).

This evidence indicate that the C_{ao} estimates are physiologically relevant. It might then be of interest to compare the findings listed in table 9.1 with data found in the literature. Reports on the "in vivo" human aorta volume distensibility have not been found (for quite obvious reasons). Careful "in vitro" studies on the excised human thoracic aorta have been reported by Wagner & Kapal (1953). For the age group of 15 - 30 years (3 examples) and the blood pressure range of 80 - 120 mmHg we may calculate a mean volume distensibility of 0.375 ml/mmHg from the data published in figure 2 B (Wager & Kapal 1952). 3 of the patients listed in table 9.1 are within this range of age and mean blood pressure.

The mean C_{ao} (C.O.) for this group is 0.89 ml/mmHg. Of this aortic compliance estimate, 0.52 ml/mmHg is shared by the segments aar, ad 1 and ad 2, corresponding to the aortic segment used in the "in vitro" measurement. These figures seem to correlate reasonably well.

The input impedance of the model is also much influenced by reflections of wave energy from points of elastic and geometrical changes and from the terminating segments. The assumed taper of the aorta, and the peripheral input impedances (table 2.1) give rise to a realistic input pressure-flow relationship in most patients studied.

For some of the patients with aortic valve prothesis (figure 8.9) we observe considerable deviations in the aortic pressure tracings. In particular B.B., P.E., F.K. and G.L. have a more pronounced "plateau" during the first and middle phase of ejection. This phenomenon may be caused by altered ascending aortic flow dynamics due to the pivoting disc prothesis, but is more likely caused by errors in the assumptions in the model. We also note an aberration in the simulated flow tracing of patient A.A. (figure 8.7) with a presumably normal aortic valve. The descending slope is more wavy in the patient. In the model, a curve of this shape may be produced by changing the tapering assumptions in segments ad 1, ad 2 and ad 3 so that a more abrupt change of characteristic impedance occur in the thoracic descending aorta. By such modifications it is also possible to produce more pronounced "plateaus"

in ascending aortic pressure. An investigation of these effects is not undertaken in the present pilot study.

The aortic pressure waveshape is also influenced (figure 6.22) by the peripheral impedance approximations through reflected wave energy originating from the terminating segments. The achievement of approximately correct input pressure-flow relationship and pulse transmission properties necessitates that the reflected waves occurring in the model are of a similar phase and amplitude as in the real aorta. Again, this is only indirect evidence that the peripheral impedance assumptions are reasonable. These are, however, not in the main focus of the present study, and may be regarded as a convenient way of terminating the central arterial model. As long as the parameters in the terminating segments give rise to approximately correct aortic waveshapes, we are content here.

The tracings presented in figure 9.3 indicate that the model exhibit pressure transmission properties that are close to those found in the two patients examined. These results indicate that 6 lumped L-C-R segments may be used to simulate the aorta without serious losses in accuracy. Furthermore, it seems justifiable to conclude that the linearized version of the model may give acceptable results in these two patients. If pulse pressures are large, as for patient N.K. (210/130, figure 9.2), we might suspect that the negligence of nonlinear effects would cause noticeable errors. We observe that the flow patterns are almost identical, but some deviations are found in the pressure courses. The slight "shoulder" on the pressure occur earlier in the patient tracing, which also climb to a slightly higher systolic peak pressure. These discrepancies may perhaps be ascribed to the nonlinear pressure-volume relation of a real aorta, being relatively compliant near the diastolic pressure, and increasing its stiffness as the transmural pressure increases.

We shall now consider two sources of errors in the estimates of aortic compliance.

- 1) The pulse transmission time as used in the present scheme is primarily dependent upon the arterial compliance around the diastolic pressure. In patients with considerable

pulse pressures and nonlinear aortas we may expect that this value is not representative of the aortic compliance as determined by the cardiac output method. The latter is most sensitive to the compliance around the mean pressure range as this determines the pulse pressure. Thus, in patients with aged arterial systems and high blood pressures (where we may expect the most pronounced nonlinearities) we may expect that the aorta is considered more elastic by the transmission time estimate than by the cardiac output-pulse pressure estimate. In fact we find that the ratio $C_{ao}(\text{pulse})/C_{ao}(\text{C.O.})$ correlate with blood pressure ($r = 0.49$).

- 2) We have assumed constant aortic inertances in the present study. This assumption implies a constant ratio between the length and the cross-sectional area of the aorta.

As the $C_{ao}(\text{pulse})/C_{ao}(\text{C.O.})$ ratio does not correlate with height ($r = 0.09$) and weight ($r = 0.13$) we may consider this assumption reasonable for subjects of varying size. However, we may expect the aorta to dilate with increasing age and blood pressure. Then the assumption of a constant area/length ratio is questionable. An increased aortic radius (with fixed length) implies a decrease in the inertance parameters as predicted by the equation $L = 1.1p\Delta Z/\pi r^2$. As the wave velocity is dependent upon the product $L \cdot C$, where C is the compliance, we shall expect that the pulse-transmission time method will result in an estimate of aortic compliance that is too stiff (C is low).

Thus, in patients with mildly dilated aortas, caused by age or increased blood pressure, we consider two sources of errors (1) due to a nonlinear compliance and (2) due to changes in geometry. These draw in opposite directions and may tend to cancel under favourable conditions. This may be the reason that the relatively simple linear model with constant inertances gives a good correlation between the two independent estimates of aortic compliance.

The aortic inertance parameters listed in table 3.2 should be multiplied with 0.96 to achieve a better correspondence between the $C_{ao}(\text{C.O.})$ and $C_{ao}(\text{pulse})$ estimates.

The available data suggest that the model may be used to obtain continuous estimates of cardiac output and stroke volume from the aortic pressure. The deviation of the estimates from the other methods as Fick, dye- or thermodilution should be of the same magnitude as the deviations in the compliance estimates. The simulation of the 24 patients therefore suggest a mean absolute error of $\pm 8\%$ and a maximum error of $\pm 20\%$ for the cardiac output estimates. As the errors may partly be ascribed to the control method, the errors seem to be within acceptable limits for clinical use.

Chapter 10.

CONCLUSIONS AND SUMMARY

The emphasis in the present study has been on the investigation of the left ventricular-arterial model proposed in chapters 2 and 3. Available physiological knowledge as well as the results of previous model builders have been incorporated in the present model, which is realized in electronic circuits as a special-purpose analog computer.

It was found that the dynamic time courses of pressure and flow were simulated with good fidelity. Moreover, the responses of the model to perturbations such as increased left ventricular filling and/or increased aortic pressure were similar to findings reported in the literature. Also the effects of changing the contractile state of the myocardium can be simulated with good quantitative agreement. Moreover it was found that the model was able to predict the course of left ventricular pressure during partial and total occlusion of the aortic root.

The arterial part of the model was found to impose a realistic impedance on the left ventricle, and the transmission properties of the aorta were in good agreement with the available measurements.

At the present stage it seems justifiable to conclude that these results are encouraging for the further work along these lines, and we have an indication that the left ventricular-arterial system may be simulated with a model that is quite simple, at least compared to the overwhelming complexity of the real system.

Claude Bernard (1865) states: "After carrying out an analysis of phenomena, we must therefore reconstruct our physiological synthesis, so as to see the joint action of all parts we have isolated". The usefulness of a model in research is briefly illustrated by the figures 8.2, 8.4 and 8.5 where the experimental conditions reported by various authors are simulated. Thus the data can be regarded not only in the special context

which the authors appearantly intend, but with reference to a more complete concept of the system under study. For example: Simulating the experiments reported by Bugge-Asperheim & Kiil (1973) (figures 8.2 and 8.4), we may use their data to demonstrate that the response of the left ventricle to increased filling and/or arterial pressure as found by these authors is qualitatively and quantitatively consistent with the properties of heart muscle and the left ventricular geometry.

When a physiological hypothesis gains evidence, it may be used in medicine to improve diagnosis and therapy. A clinical study with these technique also reported in Aaslid & Brubakk (1974) was centered on the properties of the aorta, and in particular its compliance. This compliance was estimated by two independent methods which were in good agreement.

As demonstrated in chapters 6 and 8 the estimation techniques allow a determination of the time-varying parameters on almost a beat to beat basis. These parameters may provide a sensitive measure of the state of the individual cardiovascular system, facilitating diagnosis and the evaluation of the particular therapy.

In conclusion it seems justified to state that the model is a synthesis of available physiological knowledge that shows promise to be of value in the interpretation and evaluation of events in the individual left ventricular-central arterial system.

R E F E R E N C E S

- [1] Aaslid, R. and Brubakk, A.O. (1974):
"Aortic compliance in man".
Submitted for publication.
- [2] Aaslid, R. and Brubakk, A.O. (1971):
"A measuring and recording system for cardiovascular data".
Proceedings of II. Nordic Meeting on Medical and Biological
Eng. Oslo.
- [2a] Aaslid, R., Frøysaker, T., Ringdal, R., Skagseth, E.
and Hall, K.V.: (1974):
In situ pressure gradient-flow relationship of the aortic
pivoting disc valve prosthesis".
XXIII Congress European Society of Cardiovascular Surgery,
Oslo 1974.
- [3] Abbot, B.C. and Mommaerts, W.F.H.M. (1959):
"Study of inotropic mechanisms in the papillary muscle
preparation".
J. Gen Physiol, 42, 533 - 551.
- [4] Anliker, M., Rockwell, R.L. and Ogden, E. (1970):
" Theoretical Analysis of Nonlinear Phenomena Affecting the
Pressure and Flow Pulse in Arteries".
In: Fluid Dynamics of Blood Circulation and Respiratory Flow.
Preprint of AGARD Conference Proc. (No 65) Naples.
- [5] Baker, D.W. (1973):
"Pulse doppler techniques in cardiology and peripheral
vascular disease".
2nd World Congress on Ultrasound in Medicine, Rotterdam.
- [6] Beneken, J.E.W. (1965):
"A mathematical approach to cardiovascular function".
Ph. D. Thesis, Institute of Medical Physics, Utrecht.
- [7] Beneken, J.E.W. (1972):
"Some computer models in cardiovascular research".
In: Cardiovascular fluid Dynamics, Ed. Bergel. Academic
Press, London.
- [8] Beneken, J.E.W. and de Wit, B. (1967):
"A Physical Approach to Hemodynamic Aspects of the Human
Cardiovascular System".
In: Physical Bases of Circulatory Transport, Ed. Reeve
& Guyton. Saunders Philadelphia.

- [9] Bergel, D.H. (1961):
"The Dynamic Elastic Properties of the Arterial Wall".
J.Physiol. 156, 458 - 469.
- [10] Bergel, D.H., Clark, C., Schultz, D.L. and Tunstall Pedoe,
D.S. (1970):
"The Measurement of Instantaneous Blood Velocity and a
Calculation of Total Mechanical Energy Expenditure in
Ventricular Pumping".
In: Fluid Dynamics of Blood Circulation and Respiratory
Flow. Preprint of AGARD Conference Proceedings (No 65),
Naples.
- [11] Bernard, C. (1865):
"An Introduction to the study of experimental medicine".
Translated by H.C. Green.
Dover Publications Inc., New York.
- [12] Brady, A.J. (1971):
"A measurement of the active state in heart muscle".
Cardiovascular Research, Supplement 1, 11 - 17.
- [13] Braunwald, E., Ross, J. and Sonnenblick, E.H. (1967):
"Mechanics of Contraction of the Normal and Failing
Heart".
Little, Brown & Co., Boston.
- [14] Brusaert, D.L. and Sonnenblick, E.H. (1969):
"Force-velocity-length-time relations of contractile
elements in heart muscle of the cat".
Circulation Research, 24, 137 - 149.
- [15] Brusaert, D.L., Parmley, W.W. and Sonnenblick, E.H. (1970):
"Effects of Various Inotropic Interventions on the Dynamic
Properties of the Contractile Elements in Heart Muscle of
the Cat".
Circulation Research, Vol 27, 513 - 522.

- [16] Brusaert, D.L. and Sonnenblick, E.H. (1971):
"Nature of the force-velocity relation in heart muscle".
Cardiovascular Research, Supplement 1, 18 - 33.
- [17] Brusaert, D.L., Claes, V.A. and Donders, J.J.H. (1972):
"Effects of controlling the velocity of shortening on force-
velocity-length and time relations in cat papillary muscle".
Circulation Research, 30, 310 - 315.
- [18] Bugge-Asperheim, B. and Kiil, F. (1973):
"Preload, contractility, and afterload as determinants of
stroke volume during elevation of aortic blood pressure
in dogs".
Cardiovascular Research, 7, 528 - 541.
- [19] Bugge-Asperheim, B., Leraand, S. and Kiil, F.: (1969):
"Local Dimensional Changes of the Myocardium Measured by
Ultrasonic Technique".
Scand. J. clin. Lab. Invest., 24, 361 - 371. (1969).
- [20] Chang, P.P. (1973):
"Model-based Parameter Estimation of Canine Systemic
Circulation System".
Ph.D. Thesis, University of Wisconsin.
- [21] de Pater, L. (1966):
"An Electrical Analogue of the Human Circulatory System".
Thesis University of Groningen.
- [22] Donders, J.J.H. and Beneken, J.E.W. (1970):
"Myocardial force-velocity parameters as a function of the
active state".
VI. World Congress of Cardiology, London.
- [23] Donders, J.J.H. and Beneken, J.E.W. (1971):
"Computer model of cardiac muscle mechanics".
Cardiovascular Research, Supplement 1, 34 - 50.

- [24] Donders, J.J.H., Zuiderwaard, J.C., Robijn, J.P. and Beneken, J.E.W. (1973):
"Estimation of Heartfunction Parameters by Hybrid Optimization Techniques".
3rd IFAC Symposium on Identification and Parameter Estimation, Haag.
- [25] Dyken, J.G. (1970):
"Analog Computer Simulation of Left Heart and its Load".
Report E-170. Norwegian Defence Research Establishment, Kjeller, Norway.
- [26] Edman, K.A.P. and Nilsson, E. (1971):
"Time course of the active state in relation to muscle length and movement: a comparative study on skeletal muscle and myocardium".
Cardiovascular Research, Supplement 1, 3 - 10.
- [27] Frank, O. (1899):
"Die Grundform des arteriellen Pulses".
Z. Biol., 37, 483 - 526.
- [28] Fry, D.L. (1959):
"Measurement of pulsatile blood flow by the computed pressure-gradient technique".
IEEE Trans. Biom. Eng. BME 6, 259 - 264.
- [29] Fry, D.L., Griggs, D.M. and Greenfield, J.C. (1964):
"Myocardial Mechanics, tension-velocity-length relationship of heart muscle".
Circulation Research, 14, 73 - 85.
- [30] Gaasch, W.H., Battle, W.E., Oboler, A.A., Banas, J.S. and Levine, H.J. (1972):
"Left ventricular Stress and Compliance in Man".
Circulation 45, 746 - 761.

- [31] Gabe, I.T. (1972):
"Pressure Measurement in Experimental Physiology".
In: Cardiovascular Fluid Dynamics, Vol. 1. Ed. by D.H. Bergel, Academic Press., London.
- [32] Gasser, H.S. and Hill, A.V. (1924):
"The dynamics of muscular contraction".
Proc. Roy. Soc. (London). Biol. 96, 398 - 437.
- [33] Green, H.D., Rapela, C.E. and Conrad, M.C. (1963):
"Resistance (conductance) and capacitance phenomena in terminal vascular beds".
In: Handbook of Physiology, sect. 2, Circulation, vol. 2, 935 - 960. Washington.
- [34] Greenfield, J.C., Cox, R.L., Hernandez, R.R., Thomas, C. and Schoonmaker, F.W. (1967):
"Pressure-Flow Studies in Man During the Valsalva Maneuver with Observations on the Mechanical Properties of the Ascending Aorta".
Circulation, 35, 653 - 661.
- [35] Grewe, L.A., Neustedter, P.F., Rideout, V.C. and Rukavina, D.M. (1969):
"Cardiovascular Modeling using Integrated Circuit Op-Amps".
SIMULATION.
- [36] Grodins, F.S. and Buoncristiani, J.F. (1967):
"General Formulation of the Cardiovascular Control Problem".
In: Physical Bases of Circ. Transport. Ed. Reeve & Guyton. Saunders, Philadelphia.
- [37] Guyton, A.C. and Coleman, T.G. (1967):
"Long-term regulation of the circulation: Interrelationships with body fluid volumes".
In: Physical Bases of Circulatory Transport. Ed. Reeve & Guyton. Saunders, Philadelphia.

- [38] Hanna, W.T. (1973):
"A simulation of human heart function".
Biophysical Journal, 13, 603 - 621.
- [39] Hill, A.V. (1938):
"The heat of shortening and the dynamic constants of muscle".
Proc. Roy. Soc., 126, 136.
- [40] Hill, A.V. (1970):
"First and last experiments in Muscle Mechanics".
Cambridge University Press.
- [41] Huxley, A.F. (1957):
"Muscle structure and theories of contraction".
In: Progress in Biophysics and Biophysical Chemistry,
7, 157 - 318.
- [42] Huxley, A.F. and Niedergerke, R. (1954):
"Structural changes in muscle during contraction. Interference
microscopy of living muscle fibres".
Nature, 173, 971 - 972.
- [43] Huxley, H.E. and Hanson, J. (1954):
"Changes in cross-striations of muscle during contraction
and stretch and their structural interpretation".
Nature, 173, 973 - 976.
- [44] Lekven, J., Bugge-Asperheim, B. and Kiil, F. (1972):
"Relationship between local myocardial dimensions and left
ventricular volume in dogs".
Scand. J. clin. Lab. Invest. 29, 5 - 14.
- [45] Leraand, S. (1970):
"An ultrasonic technique for in vivo distance measurements".
In: Proceedings of the I. Nordic Meeting on Medical and
Biological Eng. Otaniemi, Finland.

- [46] Levine, J.L. and Britman, N.A. (1964):
"Force-Velocity Relations in the Intact Dog Heart".
J. of Clinical Invest. 43, 1383 - 1396.
- [47] Light, H. and Cross, G. (1972):
"Cardiovascular Data by Transcutaneous Aortavelography".
In: Blood flow Measurement. Ed. C.Roberts. Sector Publ.
ltd. London.
- [48] Mc Donald, I.G. (1970):
"The shape and Movement of the Human Left Ventricle during
Systole".
The Am. J. of Cardiology, 26, 221 - 230.
- [49] Mc Hale, P.A. and Greenfield, J.C. jr. (1973):
"Evaluation of Several Geometric Models for Estimation of
Left Ventricular Circumferential Wall Stress".
Circulation Research, 33, 303 - 312.
- [50] Mills, C.J., Gabe, I.T., Gault, I.H., Mason, D.T., Ross, J. jr.,
Braunwald, E. and Shillingford, I.P. (1970):
"Pressure-flow relationships and vascular impedance in man".
Cardiovascular Research, 4, 405 - 417.
- [51] Nilsson, E. (1972):
"Influence of Muscle Length on the Mechanical Parameters of
Myocardial Contraction".
Acta physiol. scand., 85, 1 - 23.
- [52] Noble, M.I.M. and Else, W. (1972):
"Reexamination of the Applicability of the Hill Model of
Muscle to Cat Myocardium".
Circulation Research, 31, 580 - 589.
- [53] Noordergraf, A. (1963):
"Development of an analog computer for the human systemic
circulatory system".
In: Circulatory Analog Computers, 29 - 44. Ed. A. Noordergraf,
G.M. Jager and N. Westerhof. North-Holland Publ. Comp.
Amsterdam.

- [54] Noordergraf, A. (1969):
"Hemodynamics".
In: Biological Engineering, 391 - 545. Ed. H.P. Schwan.
Mc Graw-Hill, New York.
- [55] Parmley, W.W. and Sonnenblick, E.H. (1967):
"Series Elasticity in Heart Muscle".
Circulation Research, 20, 112 - 123.
- [56] Patel, D.J., Greenfield, J.C. jr., Austen, W.G., Morrow, A.G.
and Fry, D.G. (1965):
"Pressure-flow relationships in the ascending aorta and
femoral artery of man".
J. Appl. Physiol., 20, 459 - 463.
- [57] Pollack, G.H. (1968):
"Analysis of the Cardiovascular System: Pulmonary Arterial
Hemodynamics and Cardiac Muscle Mechanics".
Ph.D. Thesis, University of Pennsylvania.
- [58] Pollack, G.H. (1970):
"Maximum velocity as an index of contractility in cardiac
muscle".
Circulation Research, 26, 111 - 127.
- [59] Pollack, G.H., Huntsman, L.L. and Verdugo, P. (1972):
"Cardiac Muscle Models. An overext. of series elasticity?"
Circulation Research, 31, 569 - 579.
- [60] Remington, J.W. (1962):
"Pressure-diameter relations of the in vivo aorta".
Am. J. Physiol., 203, 440 - 448.
- [61] Rideout, V.C. and Dick, D.E. (1967):
"Difference-differential equations for fluid flow in
distensible tubes".
IEEE Trans. Bio-Medical Eng. BME-14, 171 - 177.

- [62] Robinson, D.A. (1965):
"Quantitative analysis of the control of cardiac output in the isolated ventricle".
Circulation Research, 17, 207 - 221.
- [63] Ross, J., Covell, J.W. and Sonnenblick, E.H. (1967):
"The Mechanics of left Ventricular Contraction in the Acute Experimental Cardiac Failure".
J. of Clinical Invest, 46, 299 - 311.
- [64] Rothe, C.F. and Nash, F.D. (1968):
"Renal arterial compliance and conductance measurement using on-line self adaptive analog computation of model parameters".
Med. Biol. Eng., 6, 53 - 59.
- [65] Rushmer, R.F., Franklin, D.L. and Ellis, R.M. (1956):
"Left ventricular dimensions recorded by sonocardiometry".
Circulation Research, 4, 684.
- [66] Sagawa, K. (1967).
"Analysis of the ventricular pumping capacity as a function of input and output pressure loads".
In: Physical Bases of Circulatory Transport. Ed. Reeve & Guyton. Saunders, Philadelphia.
- [67] Sarnoff, S.J., Mitchell, J.H., Gilmore, J.P. and Remensnyder, J.P. (1960):
"Homeometric autoregulation in the heart".
Circulation Research, 8, 1077.
- [68] Sandler, H. and Dodge, H.T. (1963):
"Left Ventricular Tension and Stress in Man".
Circulation Research, 13, 91 - 104.
- [69] Sims, J.B. (1970):
"A hybrid-computer aided study of parameter estimation in the systemic circulation".
Ph.D. Thesis, University of Wisconsin.

- [70] Snyder, M.F., Rideout, V.C. and Hillestad, R.J. (1968):
"Computer modeling of the human systemic arterial tree".
J. Biomechanics, 1, 341 - 353.
- [71] Snyder, M.F. and Rideout, V.C. (1969):
"Computer Simulation Studies of the Venous Circulation".
IEEE trans on Bio-Medical Eng., BME - 16, 325 - 334.
- [72] Sonnenblick, E.H. (1962):
"Force-velocity relations in mammalian heart muscle".
Am. J. Physiol., 202, 931 - 939.
- [73] Sonnenblick, E.H. (1965):
"Determinants of active state in heart muscle: force,
velocity, instantaneous muscle length, time".
Federation Proc., 24, 1396.
- [74] Spencer, M.P. and Greiss, F.C. (1962):
"Dynamics of Ventricular Ejection".
Circulation Research, 10, 274 - 279.
- [75] Spencer, M.P., Okino, H., Denison, A.B. and Berry, R.L. (1961):
"Electronic and Mathematical Models of the Circulatory
System".
Digest of the 4th Int. Conf. on Med. Electronics, 144,
New York.
- [76] Starling, E.H. (1918):
"The Linacre Lecture on the Law of the Heart".
Longmans, London.
- [77] Szücs, B., Monos, E. and Szutrély, J. (1973):
"Comparison of Identification Methods in the Cardiovascular
System".
3rd IFAC Symposium on Identif. and System Parameter
Estimation, Haag.

- [78] Vadot, L. (1963):
"Application d'une analogie électrique à l'étude des corrections des malformations cardiaques combinées".
In: Medical Electronics. Ed. F Bostem, Desoers, Brussel.
- [79] Wagner, R. and Kapal, E. (1951):
"Über Eigenschaften des Aorten Windkessels"
Zeitschrift für Biologie, 104, 169 - 202.
- [80] Wagner, R. and Kapal, E. (1952):
"Über Eigenschaften des Aorten Windkessels"
Zeitschrift für Biologie, 105, 263 - 292.
- [81] Warner, H.R. (1959):
"The use of analog computer for analysis of control mechanisms in the circulation".
Proc. I.R.E., 47, 1913 - 1916.
- [82] Wesseling, K.H., de Wit, B. and Beneken, J.E.W. (1973):
"Arm arterial parameters derived from non-invasively recorded pulsewaves using parameter estimation".
Med. & Biol. Eng., 11, 724 - 731.
- [83] Wetterer, E. and Kenner, T.H. (1968):
"Grundlagen der Dynamik des Arterienpulses".
Springer-Verlag, Berlin.

APPENDIX 1.

THE VENOUS SYSTEM, THE RIGHT HEART, THE
PULMONARY CIRCULATION AND THE LEFT ATRIUM

Introduction

The venous system collects the blood from the capillaries and passes it to the right heart. The venous system also act as the main volume reservoir in the circulation. It is a low-pressure system. The right atrium and the right ventricle act as low pressure pumps into the pulmonary arteries. The resistance of the pulmonary circulation is low so that the systolic right ventricular pressure is in order of 20 - 25 mmHg. The oxygenated blood from the lung capillaries is collected by the pulmonary veins leading to the left atrium.

The structure of the model presented here is based upon previous work of Snyder & Rideout (1969) although some modifications are made.

The models of the venous system, the atria and the pulmonary circulation

The model of the venous system and right atrium is illustrated in figure A 1.1. Flow from the capillaries cha (head and arms), cpo (portal), crn (renal) and clg (legs) enters the venous capacitance vessels vha, vpo, vrn and vlg. These are represented by nonlinear pressure-volume relations as shown in figure A 1.2.

These functions are characterized by the following parameters:

- V_u - the "unstressed" volume (nonactivated)
- p_0 - the pressure at "0" volume (nonactivated)
- $p_{1.5}$ - the pressure at $1.5 V_u$ (nonactivated)
- p_a - max actively developed pressure by smooth muscle
- a - degree of activation, $a = 0$ means that "passive" curve is used, $a = 1$ means an "unstressed" volume of 0.

The venous pressure submodel is shown in figure A 1.3.

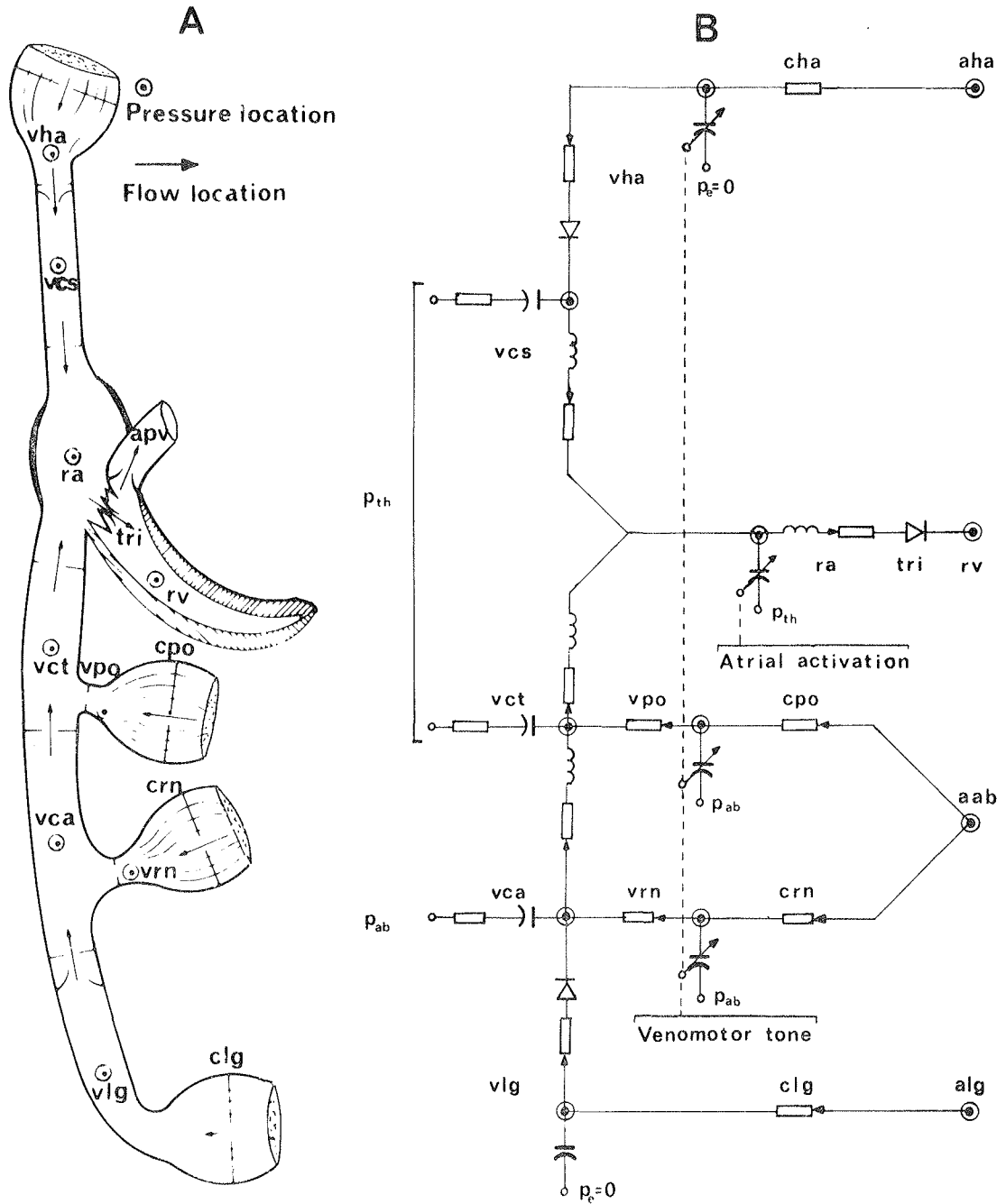


Figure A.1. The venous system model. Abbreviations as in table A1.

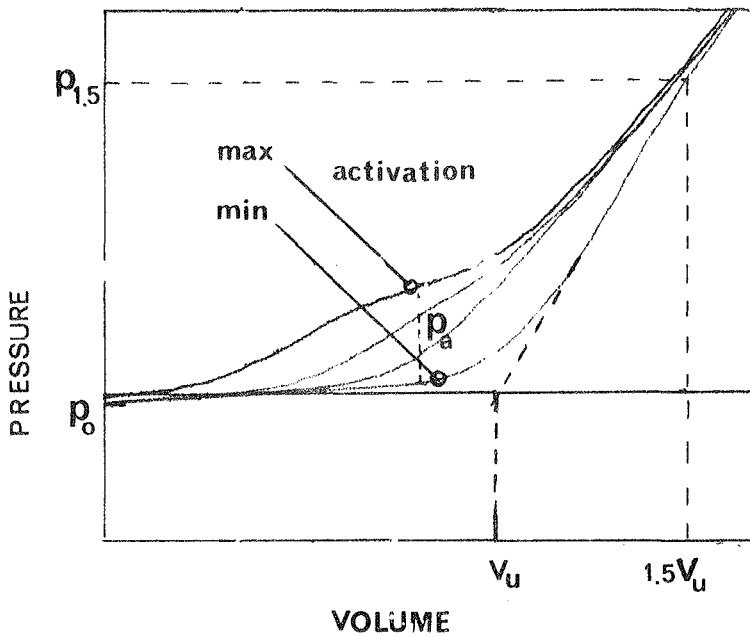


Figure A1.2. Pressure-volume relation of a venous segment in the model with varying degree of venomotor tone.

The capacitor symbol $\frac{1}{C}$ used in figure A 1.1 signifies such a nonlinear compliance. The venomotor tone, a_{ven} , is assumed to operate on all small veins in parallel. By changing this parameter, the venous filling pressure and the venous return may be changed.

The flow from the smaller veins into the vena cava is assumed resistive (no inertance effects). Perfect valves are assumed in the arm veins and the leg veins. These are symbolized by diodes. The vena cava is divided in 3, vcs representing the superior part, vct, the thoracic and vca the abdominal sections. Inertance effects are included in this vessel. The pressure-volume relation is nonlinear as shown in figure A 1.2, but without activation.

The right atrium is assumed to have a pressure-volume relation as defined by figure A 1.2, but this is activated by a time dependent activation factor $a_{at}(t)$ as shown in figure A 1.4.

The valves tri (tricuspidal valve) ap (pulmonary artery valve) and mi (mitral valve) are assumed to be nonleaking "diodes". Resistance and inertance effects are thought to be present when these valves are open.

The pulmonary circulation and left atrial models are illustrated in figure A 1.5. The arteries are represented by one linear

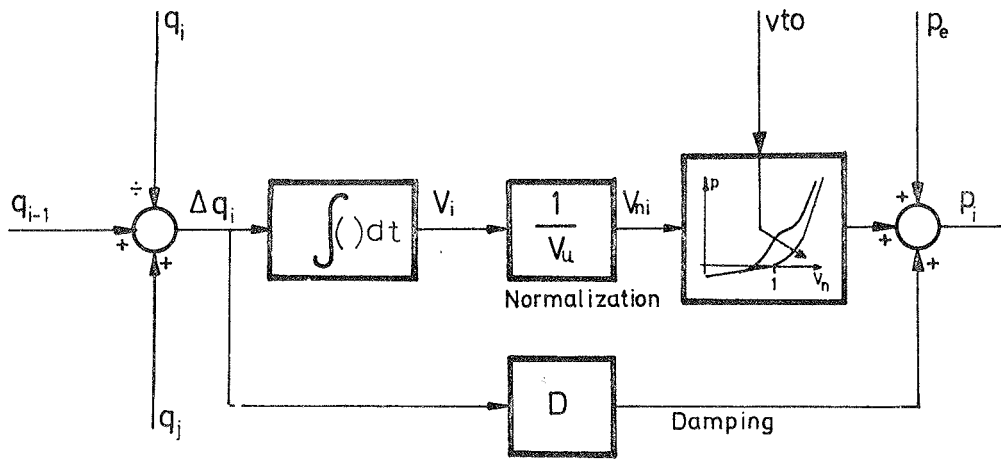


Figure A1.3. Pressure "submodel" of a venous segment. Symbols as defined in text and in chapter 3.

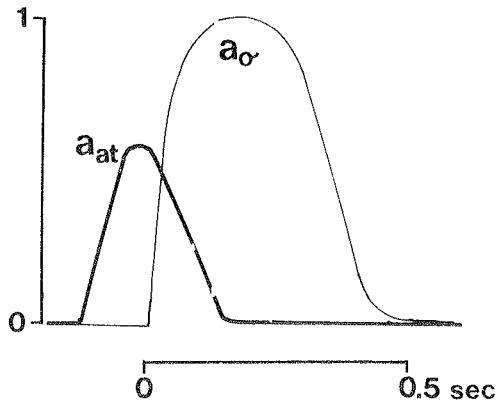


Figure A1.4. Time-dependent activation factor of the atria.

segment. The capillaries are assumed to exhibit linear pressure-flow relations. The pulmonary veins are joined in one segment similar to that used for the systemic veins. The left atrial pumping is simulated by a time dependent activation factor (figure A 1.4) influencing the pressure-volume relation as indicated in figure A 1.2. The parameters involved in the venous, pulmonary and atrial models are summarized in table A 1 below.

	V_u Unstr. volume ml	P_o "0" pressure mmHg	$P_{1.5}$ Press. at $V_u \cdot 1.5$ mmHg	P_a Max act. press. mmHg	a Activation	R Resistance $\frac{\text{mmHg}}{\text{mlsec}^{-1}}$	L Inertance $10^{-3} \frac{\text{mmHg}}{\text{mlsec}^{-2}}$	Damping timeconst. msec.		P_e Ext. press.
vha	400	-10	50	50	} a_{ven}	0.4	} 200	head & arm veins	0	
vlg	500	-10	50	50		1.0		leg veins	0	
vpo	1000	-10	50	50		0.3		portal veins	} P_{ab}	
vrn	200	-10	50	50		0.35		renal veins		
vca	100	-4	75			0.001		5.0		abdominal vena cava
vct	100	-4	75		0.001	2.5	100	thoracic vena cava	} P_{th}	
vcs	80	-4	75		0.001	1.5	50	superior vena cava		
ra+tri	90	-4	50	12	a_{at}	0.0005	0.3	right atrium+tricuspi-	} P_{th}	
apu	$C_{apu} = 4 \cdot C_{ao}$	-	-	-	-	0.001	0.4	dal valve		
cpu	-	-	-	-	-	0.05	-	pulmonary arteries		
vpu	1200	-4	50	-	-	0.01	1.0	200		pulmonary capillaries
la+mi	100	-4	50	25	a_{at}	0.0005	0.3	50		pulmonary veins
rv:	$P_{rvp} = 10 \text{ mmHg}, V_o = 230 \text{ ml}, p_{max} = 50 \text{ mmHg}, q_{max} = 1000 \frac{\text{ml}}{\text{sec}}$								right ventricle	P_{th}

Table A1.

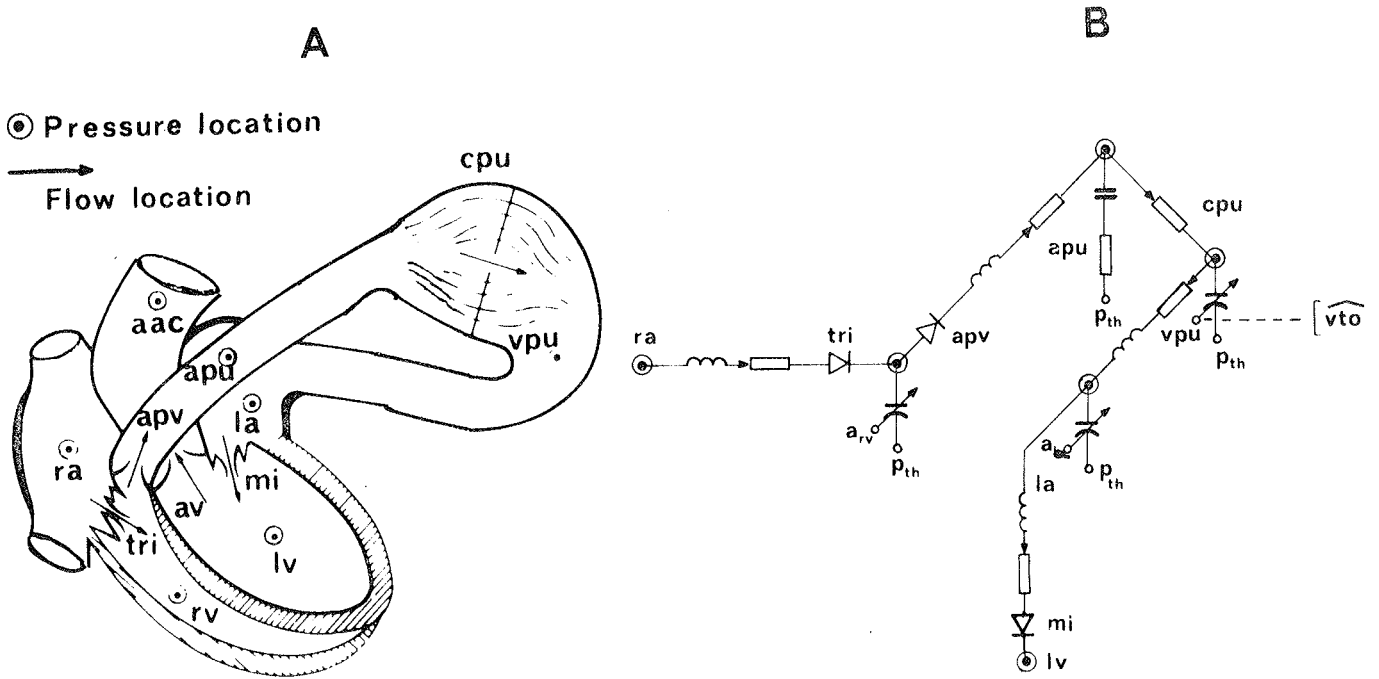


Figure A1.5. The model of the pulmonary circulation. Abbreviations as in table A1.

The right ventricle model

The right ventricle is modelled according to the block diagram of figure A 1.6.

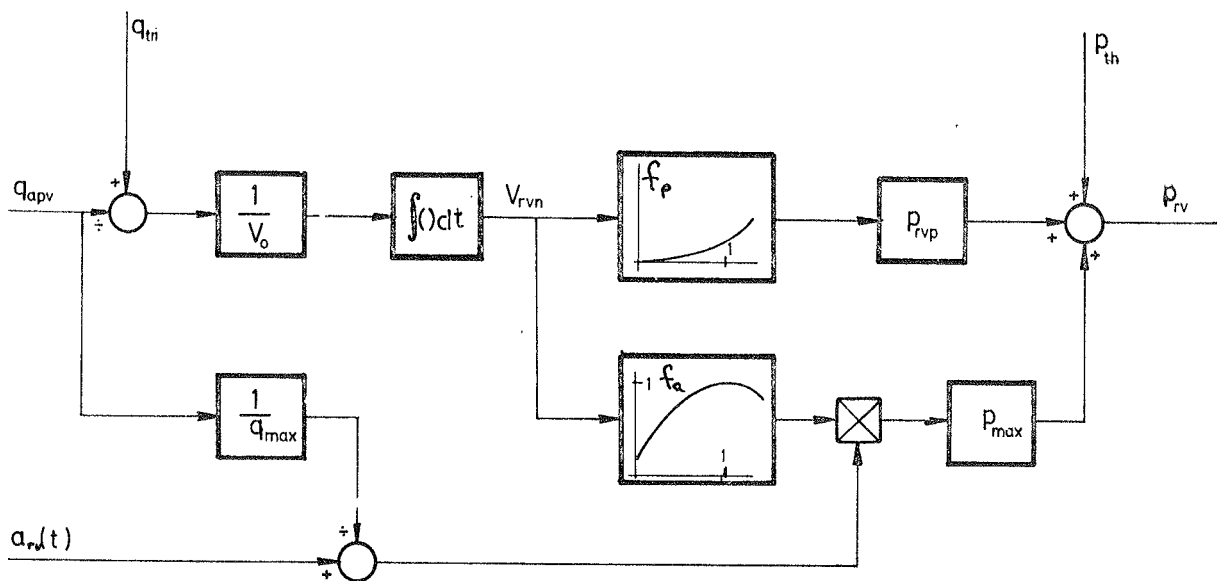


Figure A1.6. Block diagram of the model of the right ventricle.

Expressed in mathematical terms we have for the right ventricular pressure:

$$p_{rv} = p_{th} + p_{rvp} \cdot f_p \left(\frac{V_{rv}}{V_0} \right) + \left(a_{rv}(t) - \frac{q_{apv}}{q_{max}} \right) \cdot p \cdot f_a \left(\frac{V_{rv}}{V_0} \right)$$

The right ventricular pressure is a sum of the thoracic pressure (p_{th}), the "passive" pressure determined by the relation f_p shown in figure A 1.7, lower curve ($p_{rvp} = 10$ mmHg) and actively generated pressure determined by the right hand term of the equation. Here $a_{rv}(t)$ is a normalized activation factor shown in figure A 1.8. From this is subtracted a term q_{apv}/q_{max} which is an approximation to a linear force-velocity relation (or rather a pressure-flow relation or output impedance).

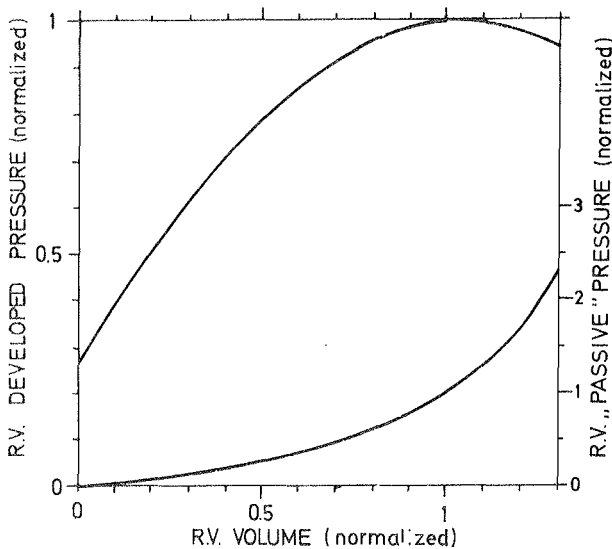


Figure A1.7. Passive and active pressure-volume relations of the right ventricle.

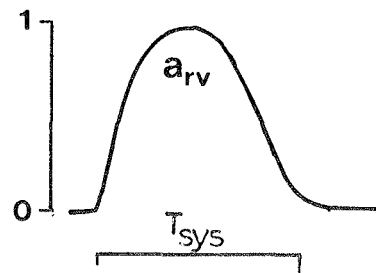


Figure A1.8. Activation factor for the model of the right ventricle.

p_{max} signifies maximum developable pressure and f_a is the "Starling" curve shown in figure A 1.7 (upper). The right ventricular volume is normalized with respect to V_0 , and we assume that $V_0 = V_m$ (page 10).

This description of the right ventricle appears to be somewhat more realistic than the simple timevarying compliance.

Finally in this appendix we reproduce some time courses relevant to the description in this appendix, as recorded from a "standard" model (figure A 1.9). During estimation p_{max} is always checked so that the right ventricle operates properly (central venous pressure of 0 - 5 mmHg).

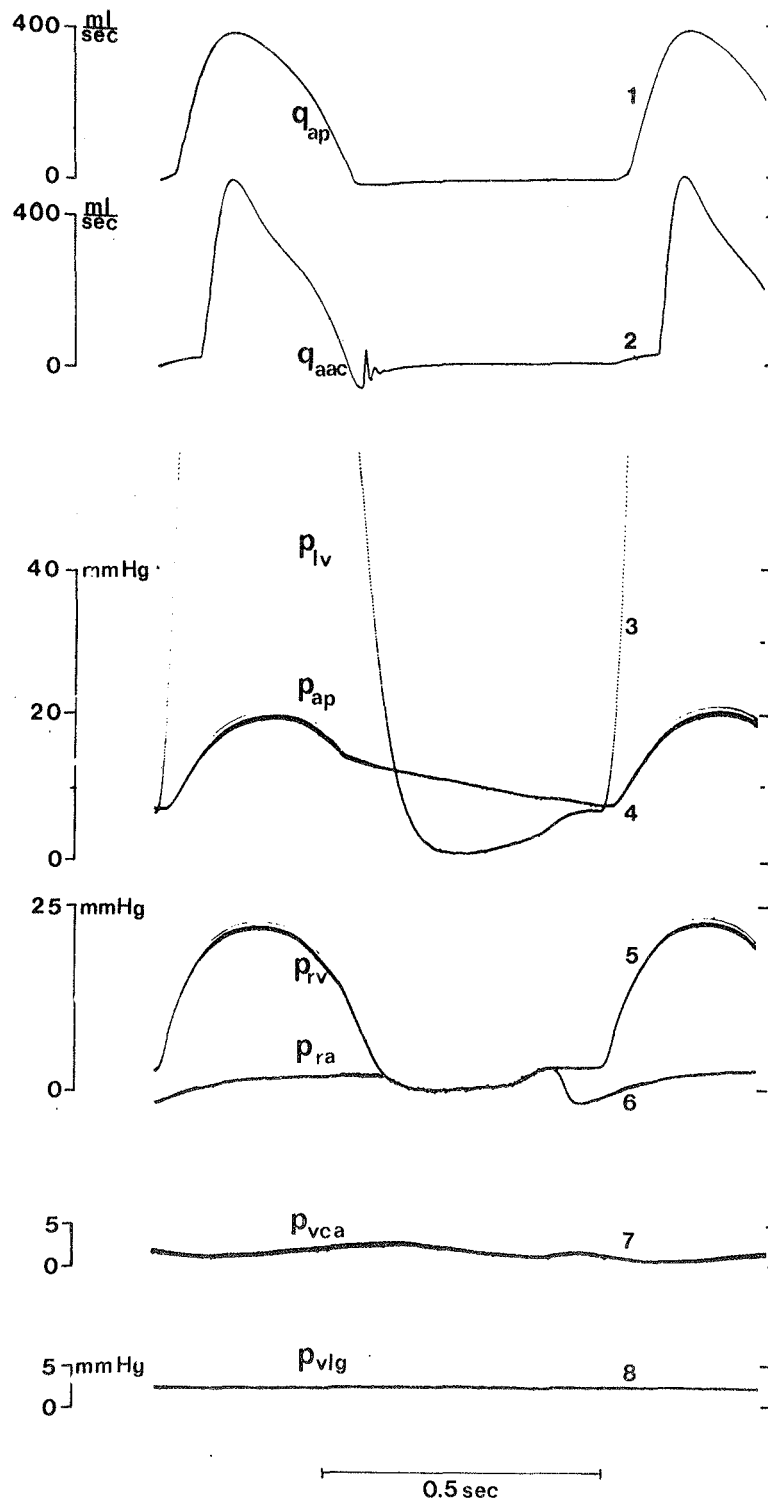


Figure A1.9. Time course of q_{ap} (flow in arteria pulmonalis), q_{aac} (asc. aorta), p_{lv} (l.v. pressure), p_{ap} (pulm. art. pressure), p_{rv} (right ventricular pressure), p_{ra} (right atrial pressure), p_{vca} (pressure in vera cava) and p_{vlg} (pressure in leg veins).

APPENDIX 2

DIAGRAMS OF THE MODEL

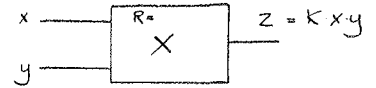
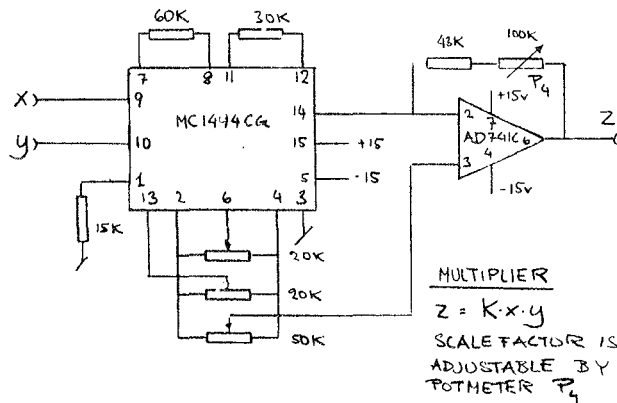
The following schematics are based upon the block diagrams in the various chapters. To simplify these drawings a shorthand notation for analog multiplication, for an operational amplifier and for an analog digital multiplier is adopted as defined on page 155. The circuit designs presented later are of conventional types, and brief explanations are included in the drawings. These are not intended to be complete. Rather they present the general design of this model. For detailed explanations, I refer to the technical manual of the commercial version of this model as produced by AUTRONICA A/S, 7000 TRONDHEIM, NORWAY.

Contents of Diagrams:

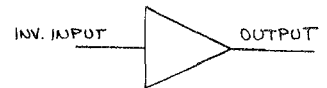
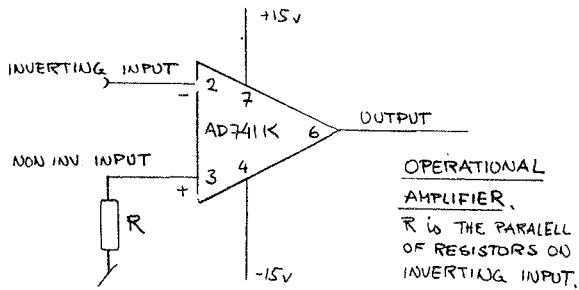
- A2.2 Left ventricular model
 - SE_o - external series elastic element
 - Sarcomere length-tension relation
- A2.3 SE, PE - series and parallel elastic elements
 - Force-velocity relationship of contractile element
- A2.4 Active state synthetizer
 - Model of arterial segment
 - Model of capillaries
- A2.5 Model of aortic valve
 - Model of catheter-manometer dynamics
 - System for scaling of pulse measurements
- A2.6 ECG trigger
 - Estimator circuits

SHORTHAND NOTATION.

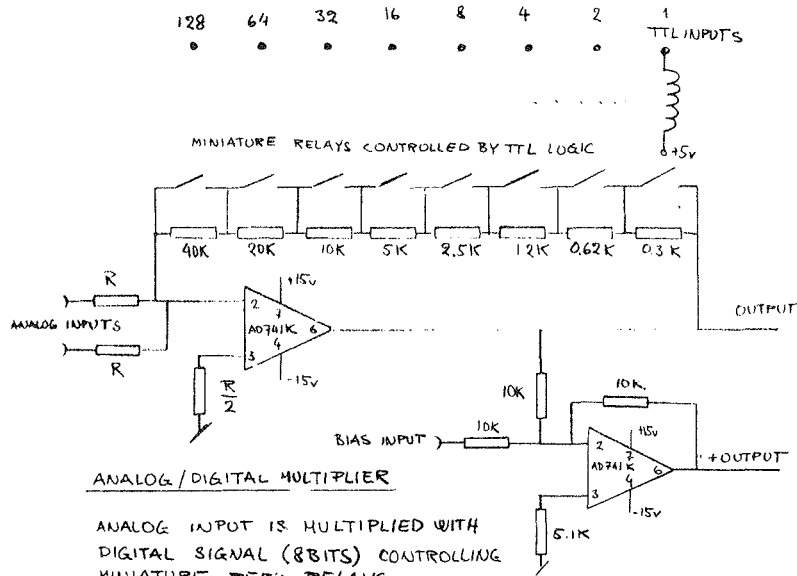
A 2.1



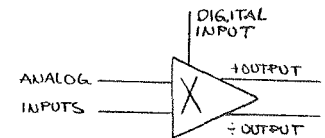
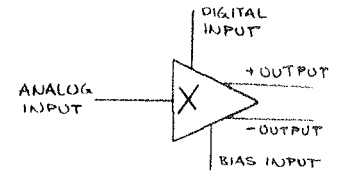
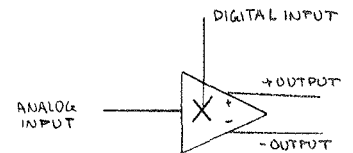
SHORTHAND NOTATION FOR MULTIPLIER



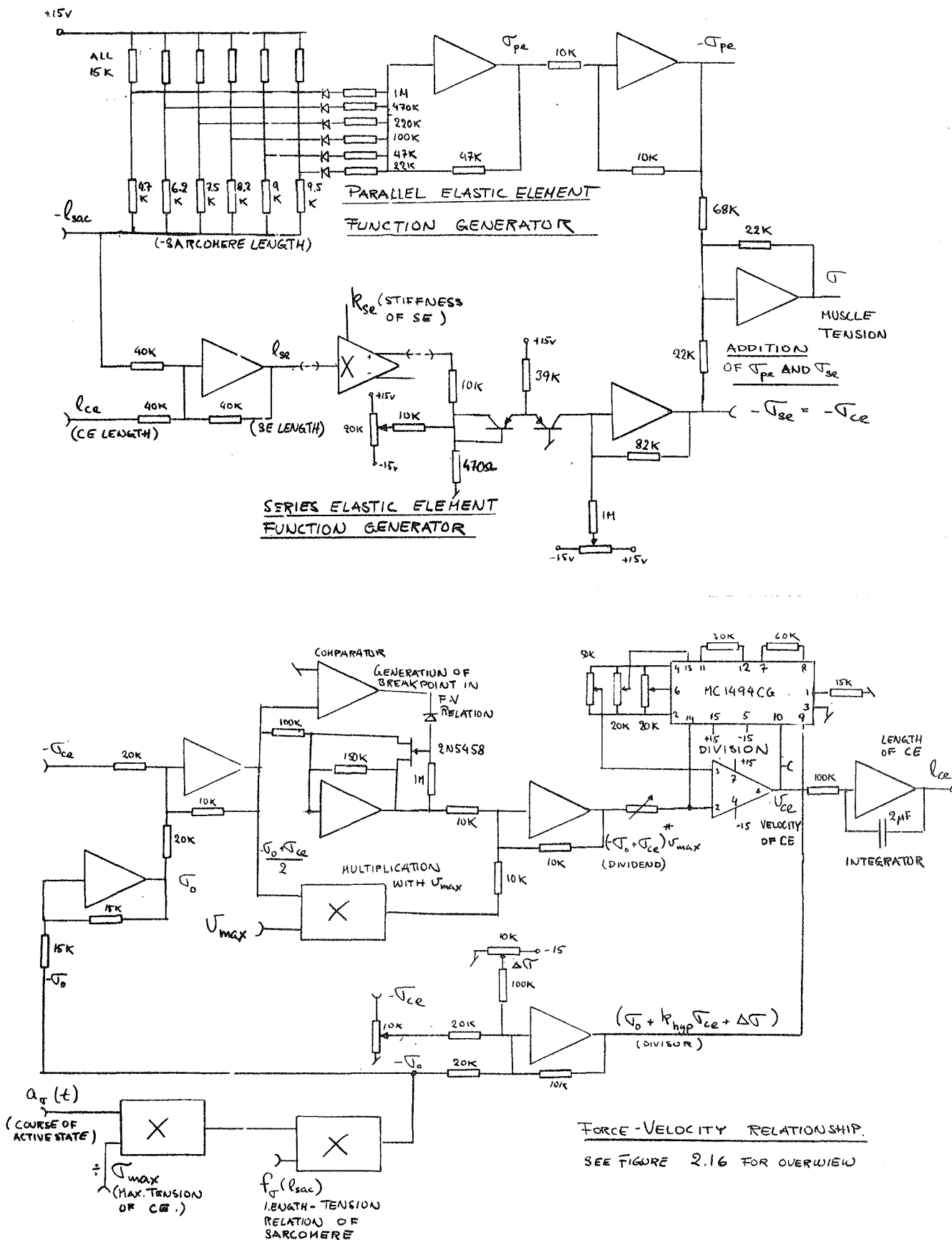
SHORTHAND NOTATION FOR OP. AMP. (WITHOUT FEEDBACK)



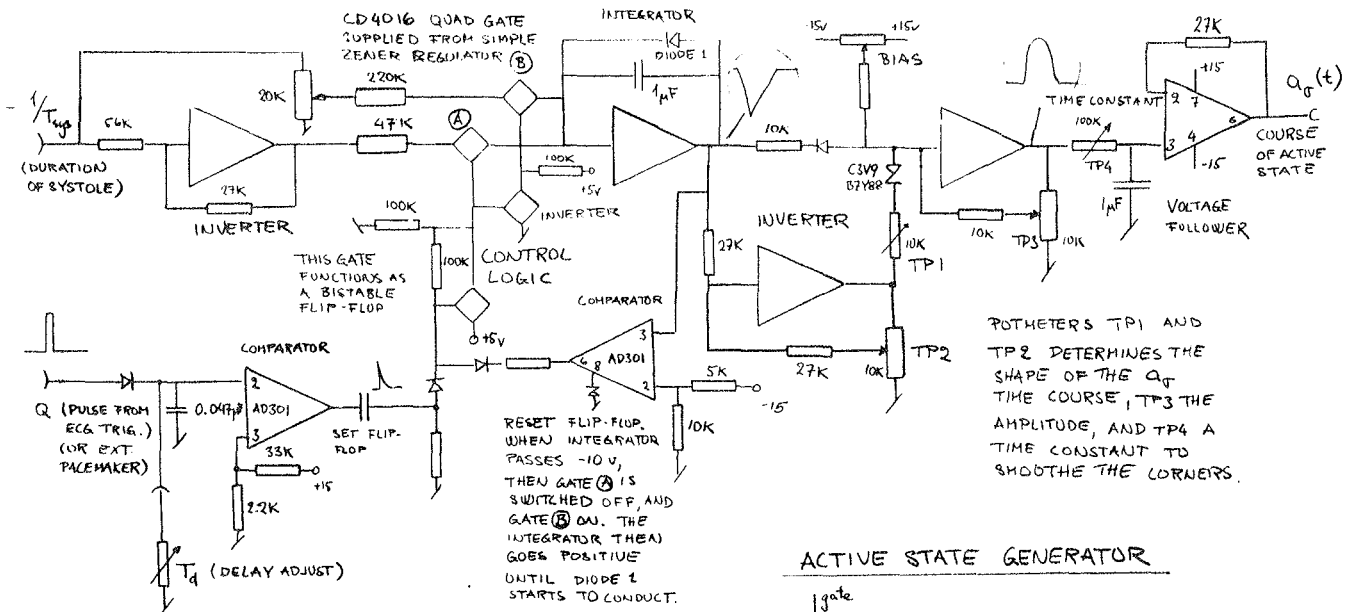
+ OUTPUT = - BIAS INPUT + (SUM OF ANALOG INPUTS) X DIGITAL INPUT



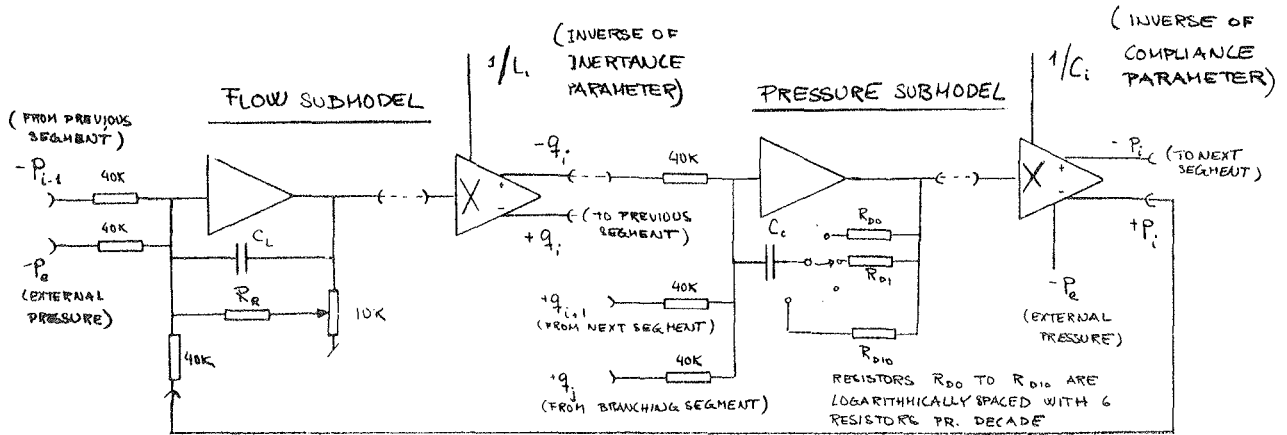
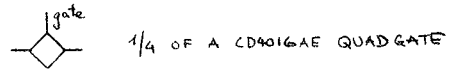
SHORTHAND NOTATIONS FOR ANALOG/DIGITAL MULTIPLIERS



A2.4

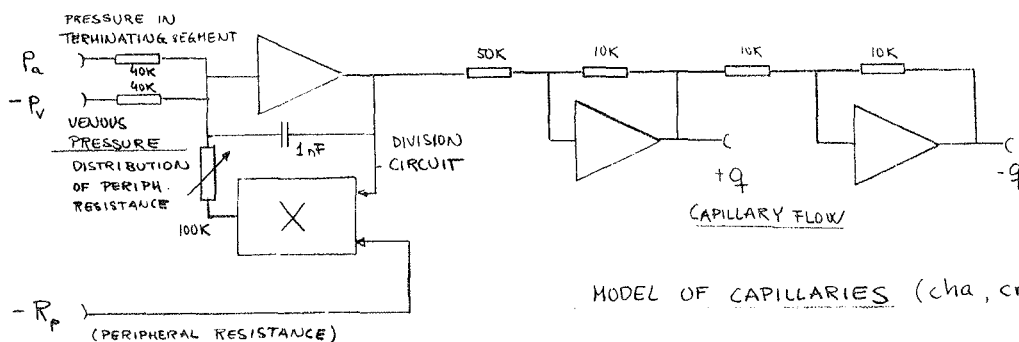


ACTIVE STATE GENERATOR

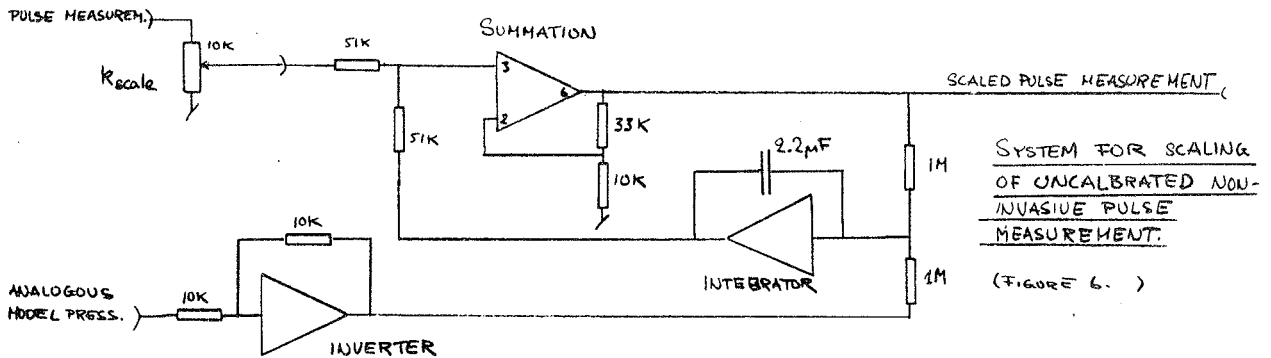
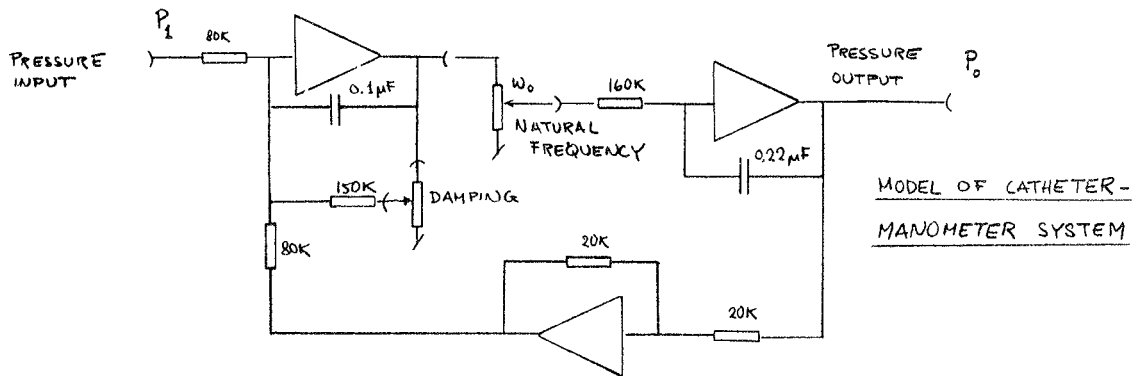
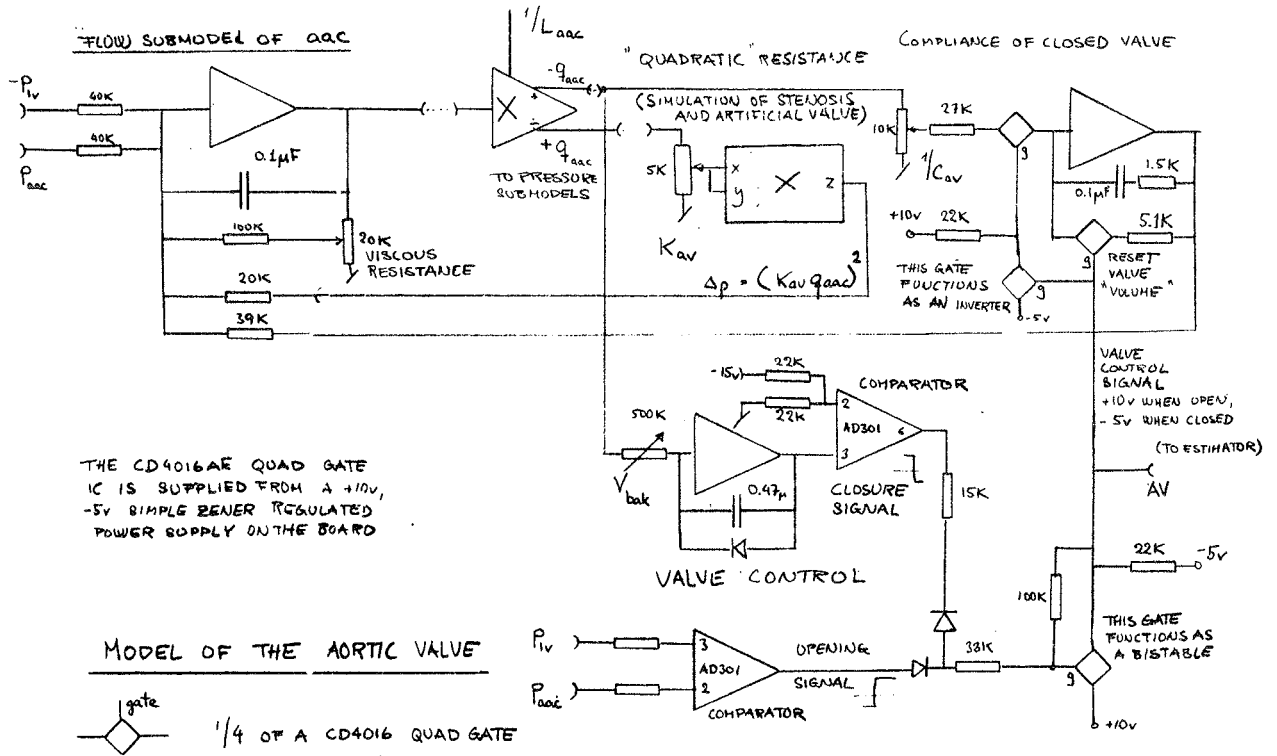


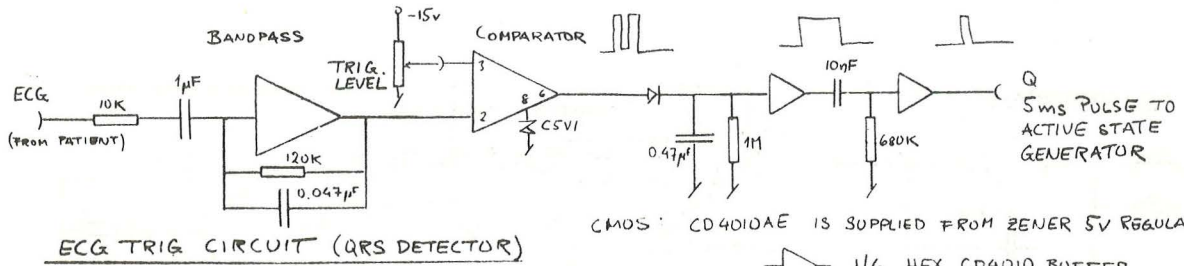
MODEL OF ARTERIAL SEGMENT

COMPARE WITH BLOCK DIAGRAM, FIGURE 3.



A.25





- 1/6 HEX CD4010 BUFFER
- 1/4 QUAD CD4016 GATE.

